TIME - DEPENDENT QUANTUM MECHANICAL APPROACH TO REACTIVE SCATTERING

A Thesis Submitted
in Partial Fulfilment of the Requirements
for the Degree of

DOCTOR OF PHILOSOPHY

by

V. MOHAN

to the

DEPARTMENT OF CHEMISTRY
INDIAN INSTITUTE OF TECHNOLOGY KANPUR
MAY, 1986

TO MY PARENTS

STATEMENT

I hereby declare that the matter embodied in this thesis is the result of investigations carried out by me in the Department of Chemistry, Indian Institute of Technology, Kanpur, India under the supervision of Professor N. Sathyamurthy.

In keeping with the general practice of reporting scientific observations, due acknowledgement has been made wherever the work described is based on the findings of other investigators.

V. MOHAN
Candidate

Kanpur:
May 2, 1986

DEPARTMENT OF CHEMISTRY
INDIAN INSTITUTE OF TECHNOLOGY KANPUR, INDIA

CERTIFICATE I

This is to certify that Mr. V. Mohan has satisfactorily completed all the courses required for the Ph.D. Degree program. These courses include:

Phy 432	Quantum Mechanics I
Chm 505	Principles of Organic Chemistry
Chm 521	Chemical Binding
Chm 524	Modern Physical Methods in Chemistry
Chm 525	Principles of Physical Chemistry
Chm 545	Principles of Inorganic Chemistry
Chm 600	Basic Course in Mathematics II
Chm 622	Chemical Kinetics
Chm 800	General Seminar
Chm 801	Graduate Seminar
Chm 900	Research

Mr. V. Mohan was admitted to the candidacy of the Ph.D. Degree in January 1984 after he successfully completed the written and oral qualifying examinations.

P.T. Narasimhan

(P.T. Narasimhan)
Head,
Department of Chemistry
IIT-KANPUR

P. C. Nigam
May 2, 19

(P.C. Nigam)
Convener,
Departmental Post-Graduate
Committee
Department of Chemistry,
IIT-Kanpur

CERTIFICATE II

Certified that the work contained in this thesis entitled: "TIME-DEPENDENT QUANTUM MECHANICAL APPROACH TO REACTIVE SCATTERING", has been carried out by Mr. V. Mohan under my supervision and that the same has not been submitted elsewhere for a degree.

N. Sathyamurthy

(N. Sathyamurthy)
Thesis Supervisor
Professor of Chemistry
IIT-KANPUR

Kanpur:
May 2, 1986

ACKNOWLEDGEMENTS

I wish to thank Professor N. Sathyamurthy for his constant and enthusiastic guidance throughout the course of this study. I might add that even though his knowledge of Chemistry is superb, his knowledge of people is even more spectacular. I treasure my association with him.

I wish to record my deep gratitude to my teachers, especially to Professors K. Ganapathy & T. Rangarajan at Annamalai University for encouraging me to pursue research as a career.

Particular thanks should go to my friend K. Raghavan for many helpful and stimulating discussions. I am indebted to Dr. Tomi Joseph and Dr. K. Banerjee for lively discussions and consultations. I am grateful to Dr. P.M. Agrawal of Vikram University for his collaboration in the initial stages of this work.

I wish to express my gratitude to my friends, Messrs V. Muruganandam, V. Palaniappan, G. Kumaravel, Sajan P. Joseph, B.S. Rajan and K. Mohan Rao, all of whom had been a constant source of encouragement.

I thank Mrs. Sathyamurthy, Mrs. and Mr. Rajagopalan, Mrs. Muruganandam and Mrs. Raghavan for having provided me a congenial and homely atmosphere during my period of stay here.

The extensive computations that went into the production of this thesis was possible only because of the generous amount of computer time made available on the DEC-1090 of our Computer Centre.

V. MOHAN

ABSTRACT

There has been a renewed interest in the time-dependent quantum mechanical (TDQM) approach to reactive scattering in the last few years. The different computational methods and applications that have created such an interest have been reviewed in Chapter 1 of the thesis. A comparative study of the efficacy of 3-point, 5-point and 7-point finite difference formulae and fast-fourier-transform algorithm to compute the Laplacian operator in the Hamiltonian of the Schrödinger equation has been made and the results are reported.

The absorption spectrum of the transition state (TS) configurations for the collinear reaction

$$H + H_2 \longrightarrow H_3^{\neq} \longrightarrow H_2 + H \qquad (R1)$$

has been predicted by solving the time-dependent Schrödinger equation for the nuclear motion on the chemically accurate Siegbahn-Liu-Truhlar-Horowitz (SLTH) potential-energy surface (PES) in Chapter 2. The wings to the Lyman-α line have been interpreted in terms of the build up of the probability density function in the inner repulsive wall of the PES. Effects of varying relative translational energy of the reactants and the vibrational state of the molecule under attack have been investigated. Transition state spectra have also been computed for thermal distributions of $H + H_2$, at 300 and 1000 K. Our results are in agreement with those obtained by using the time-independent quantum mechanical approach as well as the quasiclassical trajectory (QCT) method.

Dynamics on the H_3^* PES that correlates with H^* (2p) + H_2 has also been carried out using the TDQM approach and the results are reported in Chapter 3. The emission spectrum of the TS configurations for the collinear reaction (R1) has also been computed and it is shown to be complementary to the absorption spectrum results reported in Chapter 2.

Results of a detailed investigation of the collision-induced dissociation process in the collinear H + H_2 collisions on the SLTH surface, using the TDQM approach are given in Chapter 4 The exchange and the dissociation probabilities have been computed over a wide range of relative translational energies (0.5 - 10.0 eV) The dynamical threshold for dissociation ($\sim$ 8-10 eV) has been found to be nearly two times the energetic threshold ($\sim$ 4.5 eV). This is in contrast to the results of three dimensional QCT calculations carried out elsewhere (J. Dove et al.) for the same system wherein the dynamical threshold was comparable to the energetic threshold. But, our results compare well with the earlier reported TDQM results for collinear H_3 collisions on a model PES. Therefore, we have concluded that the difference in the dynamical and energetic threshold arises mainly from the constraint that the three nuclei lie along a straight line. For v = 1 of H_2 molecule, the nodal structure in the initial wave function has been found to be retained, even after the collision was over. In addition, more nodal structures in the wavepacket densities became apparent suggesting that this collisional process is governed by a propensity rule of $\Delta v = 2$ for vibrational excitation.

A summary of our findings is presented in Chapter 5.

CONTENTS

...

LIST OF ABBREVIATIONS AND SYMBOLS

CID - Collision-induced dissociation

DIM - Diatomics-in-molecules

E_{th}^{dy} - Dynamical threshold

E_{th}^{en} - Energetic threshold

E_{tr} - Translational energy

$\langle E_{tr} \rangle$ - Average translational energy

FD - Finite difference

FT - Fourier transform

FFT - Fast Fourier transform

HM - Heller's method

LEPS - London-Eyring-Polanyi-Sato

k - Rate coefficient

MW - McCullough Wyatt

p^D - Dissociation probability

p^R - Reaction probability (for the exchange reaction)

$\langle p^R \rangle$ - Average reaction probability

PE - Potential-energy

PES - Potential-energy surface

QCT - Quasiclassical trajectory

QM - Quantum mechanical

S - Entropy

SC - Semiclassical

...contd.

SLTH - Siegbahn-Liu-Truhlar-Horowitz

T - Temperature (Kelvin)

TDSE - Time-dependent Schrödinger equation

TDQM - Time-dependent quantum mechanical

WP - Wavepacket

μ - Reduced mass

1D - One dimension(al)

3D - Three dimension(s)(al)

PDF - Probability density function

TS - Transition state

CHAPTER 1

INTRODUCTION

1.1 Introduction

Although it was realised more than fifty years ago that, in principle, any chemical problem could be solved by an appropriate formulation of it in quantum mechanical terms,[1] in practice, developments in that direction had to await the arrival of modern electronic computers. In the early seventies one could calculate reaction probabilities (P^R) readily for exchange reactions of the type

$$A + BC \longrightarrow AB + C \qquad (R1)$$

in collinear geometries by solving the time-independent Schrödinger equation for the nuclear motion, given the electronic energy (for example, see ref. 2). That exact (converged)

solutions to the problem in three dimensions (3D) also could be obtained was demonstrated in 1975 when Kuppermann and Schatz[3a,b] and Elkowitz and Wyatt[3c] published their results for the reaction

$$H + H_2 \longrightarrow H_2 + H \qquad (R2)$$

at low energies, making full use of the symmetry of the system. There has not been any report of results of similar accuracy for any other reactive system in the past ten years. Even for the reaction (R2), some converged results have become available[4] only recently on the chemically accurate Siegbahn-Liu-Truhlar-Horowitz[5] (SLTH) potential-energy surface (PES) for the ground and the first excited vibrational states ($v = 0, 1$) of the reactant. While some progress can be expected in the next few years, thanks to the supercomputers/parallel processors becoming available, the enormity of the problem remains.

A viable alternative is a semiclassical (SC) approach. "For any system with a classical analogue, a state for which the classical description is valid as an approximation, is represented in quantum mechanics by a wave packet. The wave packet should move according to the laws of classical dynamics" (P.A.M. Dirac).[6] Equations of motion were derived by Dirac, assuming $\hbar$ to be very small as in the limit $\hbar \to 0$, the classical dynamics corresponds to the quantum dynamics. Heller has

taken a slightly different viewpoint in the series of papers he has published.[7-18] He has exploited[7] the correspondence between the classical dynamics and the quantum dynamics of localised wave packets (WP) on smooth PESs. He assumed that if the wavefunction is represented by a sum of Gaussians, we can propagate each Gaussian independently and that in the process, the width of each Gaussian is smaller than the length over which the potential changes. He has applied successfully his semi-classical method in the study of photodissociation,[8-11] photo-absorption,[12] molecular spectroscopy,[13] stochastic processes,[14] investigation of local modes and dynamical tunneling[15,16] and atom diffraction by surfaces.[17,18] His studies have also stimulated elegant experiments.[19,20]

Coalson and Karplus[21] have extended the Heller's method (HM) to provide a theory of quantum mechanical (QM) motion for multidimensional anharmonic systems. It has also been extended[22] for systems for which the generalised Liouville equation is applicable. Its description of the atom diffraction from surfaces[17,18] has recently been improved by Jackson and Metiu[22b] in a way that would enhance the prospects of its contribution to surface science.

It has been shown recently[23,24] that the HM is valid only for systems which deal with short-time dynamics of quantal degrees of freedom and for high-energy processes. Recent calculations by Skodje and Truhlar[25] and Heather et al.[26] indicate

that the HM fails to give correct values for the time evolution of the states of the Morse oscillator. They have shown that because of the anharmonicity of the oscillator potential in the asymptotic region, error in the time evolution accumulates and this causes large inaccuracies in the transition probabilities especially for low-energy collisions, which require a long time to establish the asymptotic conditions.

For many elementary systems, it has been possible for sometime to solve the time-dependent Schrödinger equation (TDSE) directly (numerically) by time-evolving a WP and thereby obtain a QM description analogous to the classical picture. In their pioneering work, Mazur and Rubin[27] solved the TDSE for a reaction of the type (R1) using a model potential based on Harmuth's integration scheme.[28] McCullough and Wyatt[29] (MW) did an elaborate study in which they solved the TDSE for the reaction (R2) in collinear geometries using a realistic PES.[30] Unfortunately their approach could not be used readily for many systems as (i) the computer memory and the time requirement were large, (ii) the resolution of the state-to-state P^R information was poor and (iii) there was very little hope of the method being extended to 3D. In the last few years, however, the situation has changed dramatically. Newer methods[31,32] of solving the TDSE have become available and they are an order of magnitude faster than that used by MW.[29] Feit et al.[33] have proposed another method of

solving the TDSE, based on the spectral properties of it, for cases which deal with bound state problems. Thus, there is a renewed hope of studying 3D atom-diatom exchange reactions quantum mechanically. Also, Kulander[34] and Leforestier[35] have shown that it is possible to deconvolute the average reaction probabilities ($<P^R>$) that result from a time-dependent quantum mechanical (TDQM) study. They have also shown that the TDQM approach can be used successfully in solving collision-induced dissociation (CID) processes - an area where the time-independent approach has been carried out successfully only for a few model systems.[36] There are also other advantages offered by the time-dependent approach. It is analogous to classical trajectories in that a pictorical representation of the chemical reaction is possible-giving us a "feel" for the molecular collision. It has been shown[29] that flux patterns could be obtained for a chemical reaction on a PES and the whirlpools in the resulting picture can provide insight into reactive scattering resonances. Very recently, we have also shown[37] that by solving the TDSE, we can construct the probability density function and predict the absorption spectrum for the transition state (TS) of the collinear reaction (R2). We have also predicted the emission spectrum for the TS of the same reaction on an excited state PES. Gas-surface scattering problems have also been shown[38] to be amenable to solution via the TDSE.

The TDQM methods have been applied to different collinear triatomic systems. The only exception is the study of Jackson and Wyatt[39] who studied the time evolution of a planar H_3 system. The speed of the explicit method gives us the hope of extending it to atom-diatom exchange reactions in three-dimensions in the very near future. The existing methodology and applications of the TDQM approach to a study of reactive scattering processes are reviewed below.

1.2 Methodology

Mazur and Rubin[27] solved the TDSE

$$i\hbar \partial \Psi(\vec{r},t)/\partial t = H\Psi(\vec{r},t) \qquad .. (1)$$

where $$H = -\frac{\hbar^2}{2m} \vec{\nabla}^2 + V(\vec{r}) \qquad .. (2)$$

with $\vec{\nabla}^2$ the Laplacian operator and $V(\vec{r})$ the potential energy, by separating the real and imaginary parts in Ψ. Letting $\Psi = u + iv$, Eq. (1) becomes

$$Hu = -\hbar \frac{\partial v}{\partial t}$$

$$Hv = \hbar \frac{\partial u}{\partial t} \qquad .. (3)$$

The spatial and the temporal derivatives were approximated by second order and first order finite differences (FD), respectively.

With the advent of high speed computers, later workers could deal with the complex wavefunction directly. The time evolution of the wavefunction can be represented as

$$\Psi(t) = U\Psi(t_o) \qquad .. (4)$$

$$\text{with } U = \exp\left[-i\Delta t H/\hbar\right],\ \Delta t = t - t_o \qquad .. (5)$$

$\Psi(t)$ is the wavefunction at any desired time t and $\Psi(t_o)$ is the initial wavefunction at time t_o. For computational reasons, the (exponential) evolution operator in Eq. (5) has to be truncated, but at the same time the unitarity of the operator has to be preserved. Therefore, MW[29] represented it as

$$U = \left[1 - i\Delta t H/\hbar\right] / \left[1 + i\Delta t H/\hbar\right] \qquad .. (6)$$

When time evolution is carried out in steps, Ψ at the n and $n \pm 1$ steps are related as

$$\Psi^{n+1} = U\Psi^n \qquad .. (7)$$

$$\text{and } \Psi^{n-1} = U^{\dagger}\Psi^n \qquad .. (8)$$

Eliminating Ψ^n between Eq. (7) and (8) gives

$$U^{\dagger}\Psi^{n+1} = U\Psi^{n-1} \qquad .. (9)$$

Thus,

$$\frac{[1+i\Delta tH/\hbar]}{[1-i\Delta tH/\hbar]}\,\Psi^{n+1} = \frac{[1-i\Delta tH/\hbar]}{[1+i\Delta tH/\hbar]}\,\Psi^{n-1} \qquad .. (10)$$

Employing a 3-point FD scheme for the second order spatial derivative of Ψ in one dimension gives:

$$H\Psi_j^{n\pm1} = -\frac{\hbar^2}{2m}\,(\Psi_{j+1}^{n\pm1} + \Psi_{j-1}^{n\pm1} - 2\Psi_j^{n\pm1})/\Delta x^2 + V_j\Psi_j^{n\pm1} \qquad .. (11)$$

where j refers to the value of Ψ at the location x_j, that is,

$$\Psi_j^{n} = \Psi(x_j,\ t_n) \qquad .. (12)$$

Substituting for $H\Psi^{n\pm1}$ in Eq. (10), we get

$$[1 + i(2\alpha + V_j\Delta t)]\ \Psi_j^{n+1} + i\alpha(\Psi_{j+1}^{n+1} + \Psi_{j-1}^{n+1}) =$$

$$[1-i(2\alpha + V_j\Delta t)]\ \Psi_j^{n-1} + i\alpha(\Psi_{j+1}^{n-1} + \Psi_{j-1}^{n-1}) \qquad .. (13)$$

where $\alpha = \hbar\Delta t/2m(\Delta x)^2$ .. (14)

Defining $\Psi^{n\pm1}$ as a vector with components $\Psi_j^{n\pm1}$, Eq. (13) becomes

$$\underline{A}\,\Psi^{n+1} = \underline{B}\,\Psi^{n-1} \qquad .. (15)$$

where $\underline{B} = \underline{A}^*$ and the elements of $\underline{A}$ and $\underline{B}$ are easily deduced

from Eq. (13). The above method is referred to as an implicit method and is computationally expensive. It requires a large computer memory as well. As a result, it has been applied to a few systems only.[40-42]

Askar and Cakmak[31] have proposed an integration scheme for solving the TDSE in which U is truncated after the linear term. By combining the forward and backward evolution operators, they could devise an algorithm which is an order of magnitude faster than the implicit method of MW.[29]

Subtracting (8) from (7), we get

$$\Psi^{n+1} - \Psi^{n-1} = [\exp\{-i\Delta t H/\hbar\} - \exp\{i\Delta t H/\hbar\}]\Psi^{n} \qquad .. (16)$$

Expanding $\exp[\pm i\Delta t H/\hbar]$ into a Taylor series and keeping only the linear terms, we obtain

$$\Psi^{n+1} = -\frac{2i\Delta t H}{\hbar}\Psi^{n} + \Psi^{n-1} \qquad .. (17)$$

The second order spatial derivative of Ψ for an equally spaced mesh in x, using the 3-point FD formula, is

$$\left.\frac{d^2\Psi}{dx^2}\right|_j^n = \frac{\Psi_{j+1}^{n} + \Psi_{j-1}^{n} - 2\Psi_{j}^{n}}{\Delta x^2} \qquad .. (18)$$

Substituting Eq. (18) into Eq. (17), we get

$$\Psi_j^{n+1} = -2i[(2\alpha + V_j\Delta t/\hbar)\Psi_j^n - \alpha(\Psi_{j+1}^n + \Psi_{j-1}^n)] + \Psi_j^{n-1} \quad .. (19)$$

This can be written as

$$\underline{\Psi}^{n+1} = \underline{A}.\underline{\Psi}^n + \underline{\Psi}^{n-1} \quad .. (20)$$

This method is referred to as an explicit method, as the state of the system at any time step $(n+1)$ is directly calculated in terms of the states at past times without the need to invert a matrix.

In two dimensions, Eq. (19) becomes

$$\Psi_{j,k}^{n+1} = \Psi_{j,k}^{n-1} - 2i[\{2(\alpha_1 + \alpha_2) + V_{j,k}\Delta t/\hbar\}\Psi_{j+1,k}^n$$

$$. \quad -\alpha_1(\Psi_{j+1,k}^n + \Psi_{j-1,k}^n) - \alpha_2(\Psi_{j,k+1}^n + \Psi_{j,k-1}^n)]$$

$$.. (21)$$

It turns out that the above first order explicit method is identical to a second order explicit method. Therefore, the errors are of third order in Δt. As a matter of fact it can be shown readily that the turncation upto any odd order in time is equivalent to the truncation upto the next higher order.

Truncating the forward evolution operator upto the second order term gives

$$U(\Delta t) = [1 - i\Delta tH/\hbar + (i\Delta tH/\hbar)^2/2!] \quad .. (22)$$

Truncating the backward evolution operator upto the second order term gives

$$U(\Delta t) = [1 + i\Delta tH/\hbar + (i\Delta tH/\hbar)^2/2!] \quad .. (23)$$

Substituting for the forward and backward evolution operators from Eqs. (22) and (23) in Eq. (16), we obtain

$$\Psi^{n+1} - \Psi^{n-1} = [-2i\Delta tH/\hbar]\ \Psi^n \quad .. (24)$$

which is identical to (17).

TDQM studies[34,35] have also been carried out using either a 5-point FD or a 7-point FD scheme instead of the 3-point FD scheme [Eq.(18)] to compute the Laplacian operator in the Hamiltonian. We have carried out a comparative study of the accuracy of the 3, 5 and 7-point FD schemes for evaluating the second derivative of a function using a Gaussian, $\exp[-(x-x_o)^2]$ as a test case. The rms deviation is plotted as a function of the mesh size Δx, in Fig. 1. It is clear that the 3-point FD can yield reliable results if Δx is

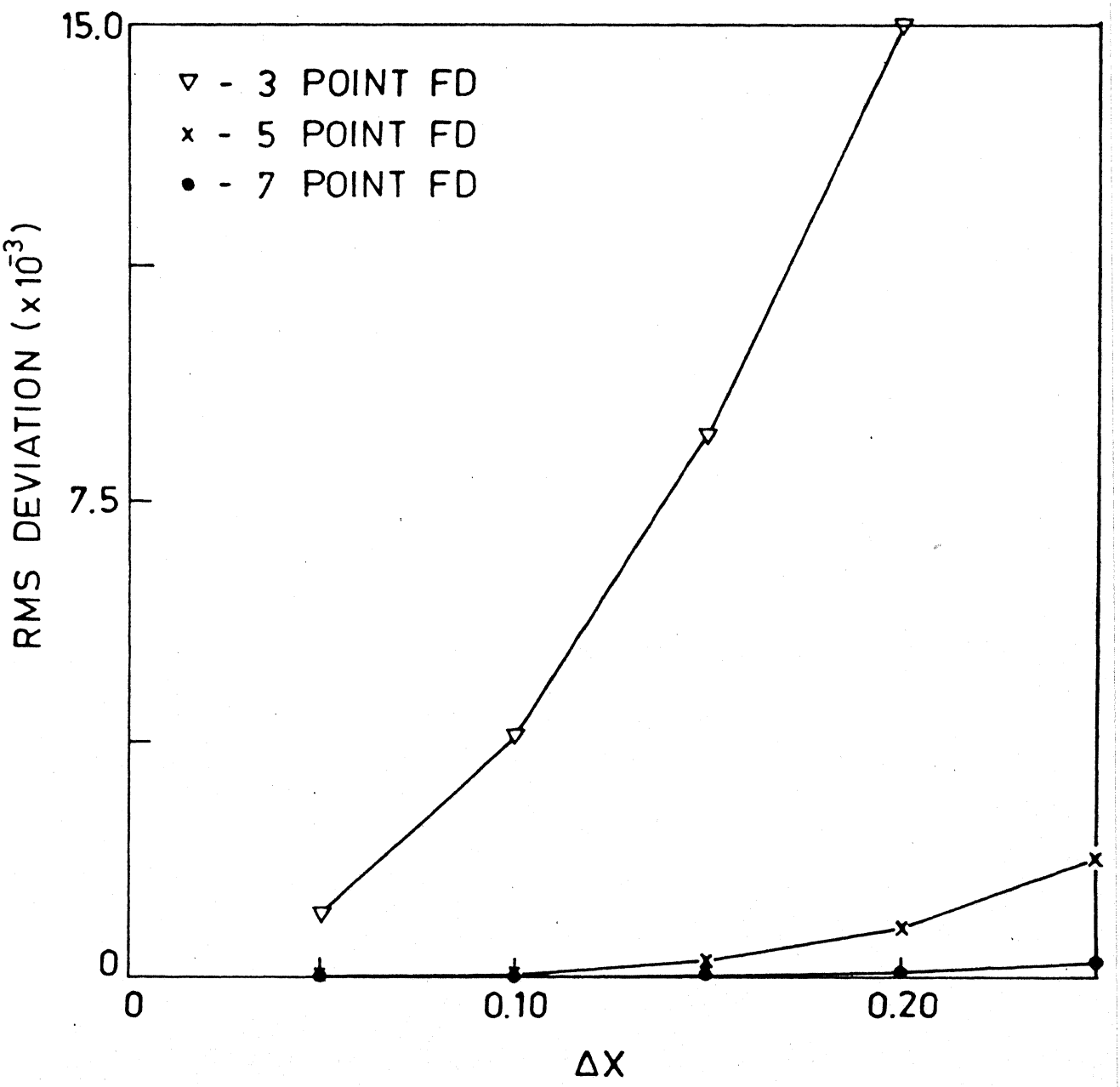

Fig. 1. RMS deviation of the second derivative of the function $\exp[-(x-x_o)^2]$ plotted as a function of the mesh size for different FD schemes. In all the cases, $0 \leq x \leq 6.3$, with $x_o = 3.15$

sufficiently small. On the other hand, the higher order FD methods allow the use of successively larger Δx for obtaining results of the same accuracy. Results of our comparative study of these methods for the reaction (R2) are presented in Chapter 2.

Recently, Kosloff and Kosloff[32] have proposed a Fourier transform (FT) method to obtain the kinetic energy term. They make use of the property of the Fourier transform that a derivative in the spatial domain becomes a multiplication by iK_{i_1} in the frequency domain, where K_{i_1} is the wave number, corresponding to the 1-spatial coordinate. The Laplacian in Eq. (2) is thus obtained by performing a 2-dimensional Fourier transform on Ψ^n, multiplying the result by $-(K_{i_1}^2 + K_{i_2}^2)$ and performing an inverse Fourier transform back to the spatial domain. In practice, the readily available, fast Fourier transform (FFT) algorithms[43] are made use of.

Kosloff and Kosloff[32] approximated the temporal derivative of Ψ by the second order FD scheme

$$\frac{\partial \Psi^n}{\partial t} = \frac{\Psi^{n+1} - \Psi^{n-1}}{2\Delta t} \qquad .. (25)$$

which is equivalent to the first order explicit method[31] for the time evolution.

Substituting Eq. (25) in Eq. (1), we obtain

$$i\hbar \frac{\Psi^{n+1} - \Psi^{n-1}}{2\Delta t} = H\Psi^n \qquad .. (26)$$

Rearranging the above equation, we get

$$\Psi^{n+1} = - \frac{2i\Delta t H\Psi^n}{\hbar} + \Psi^{n-1} \qquad .. (27)$$

which is the same as Eq. (17).

Therefore, the FT method[32] and the explicit method[31] differ from each other only in the way in which the kinetic energy term is computed. The disadvantage of using the FD method is its low accuracy and slow rate of convergence, due to the semilocal approximation to the kinetic energy. Because the FT method uses a nonlocal function expansion, the number of operations per grid point is higher than for the FD method. But, by using the FFT algorithm,[43] the numerical efficiency can be considerably improved. Since the FT method is completely vectorisable, its efficiency can be improved using array processors.

We have also made use of the FT method to solve the TDSE for the reaction (R2), the results of which are reported in Chapter 2. We have checked our computer code by computing second derivatives of the function $\exp[-(x^2+y^2)]$ where $-5 \leq x \leq 5$ and $-5 \leq y \leq 5$, with a mesh size of $\Delta x = \Delta y = 0.125$.

We obtained an rms deviation of 3.8×10^{-4} in contrast to the value of 2.0×10^{-3} obtained by the 7-point FD scheme. Therefore, we see that the FT method is an order of magnitude more accurate than the FD scheme for the same mesh size. The function and its Laplacian are shown in Figs. 2 and 3, respectively. Because of the greater accuracy of the FT method, we can afford to use a larger mesh size, when compared to the FD scheme. This would result in considerable reduction of the number of grid points to be used for each spatial dimension. The above fact would play an important role in carrying out 3D quantal calculations.

The FT method has generated a lot of interest in the time-dependent approach to reactive scattering.[44-49] Tal-Ezer and Kosloff[45] have proposed a new propagator scheme for solving the TDSE in which the evolution operator has been represented in terms of a Chebyschev series:

$$\exp\left[-i\Delta t H/\hbar\right] = \sum_{n=0}^{N} a_n \Phi_n \left(-i\Delta t H/\hbar\right) \qquad .. (28)$$

where a_n are the expansion coefficients and Φ_n are the complex Chebyschev polynomials. This new method for the time evolution combined with the FT method for the evaluation of the Laplacian seems to have an error determined only by hardware considerations.[45]

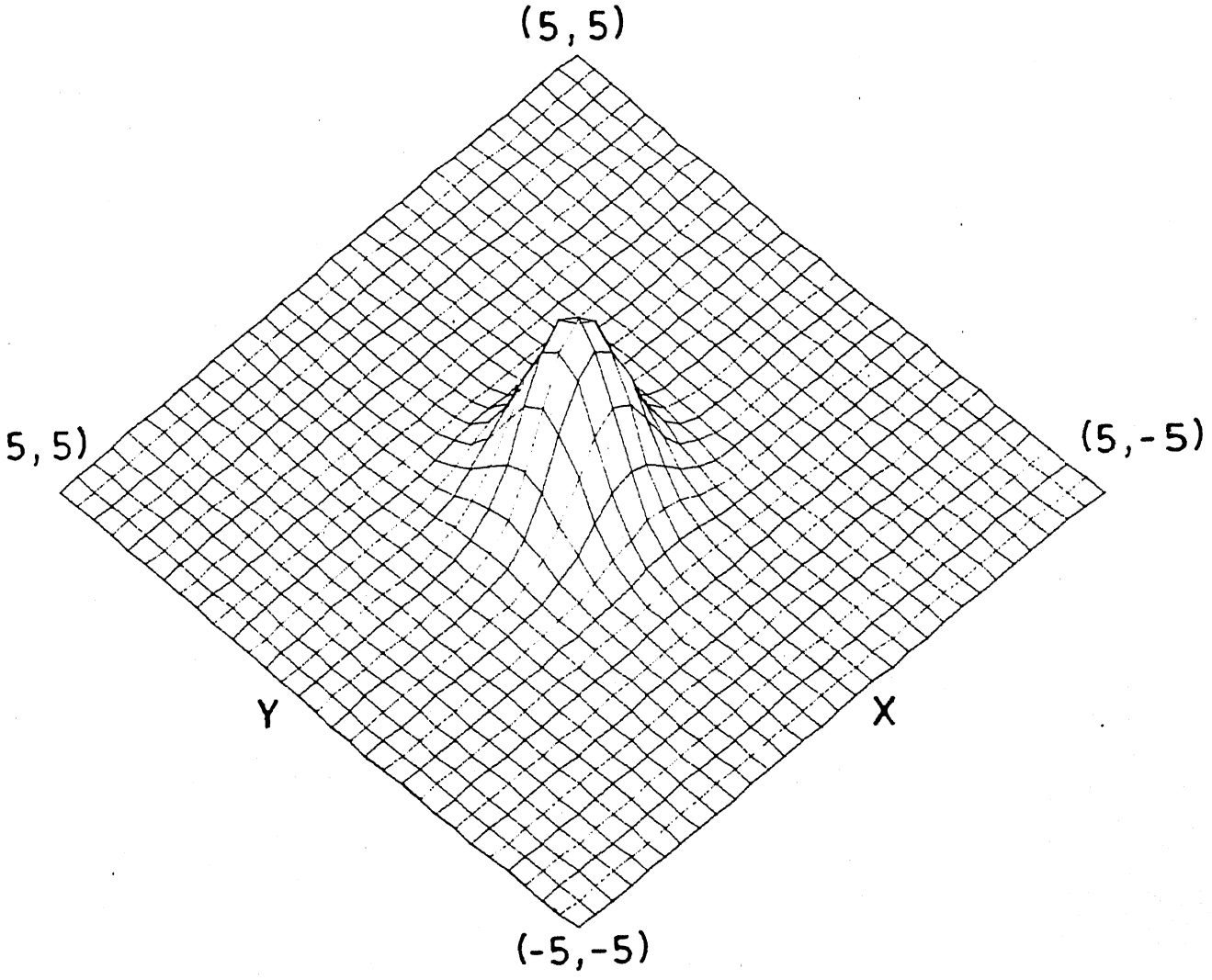

Fig. 2. Plot of the test function $\exp[-(x^2+y^2)]$ with $-5 \leq x \leq 5$ and $-5 \leq y \leq 5$

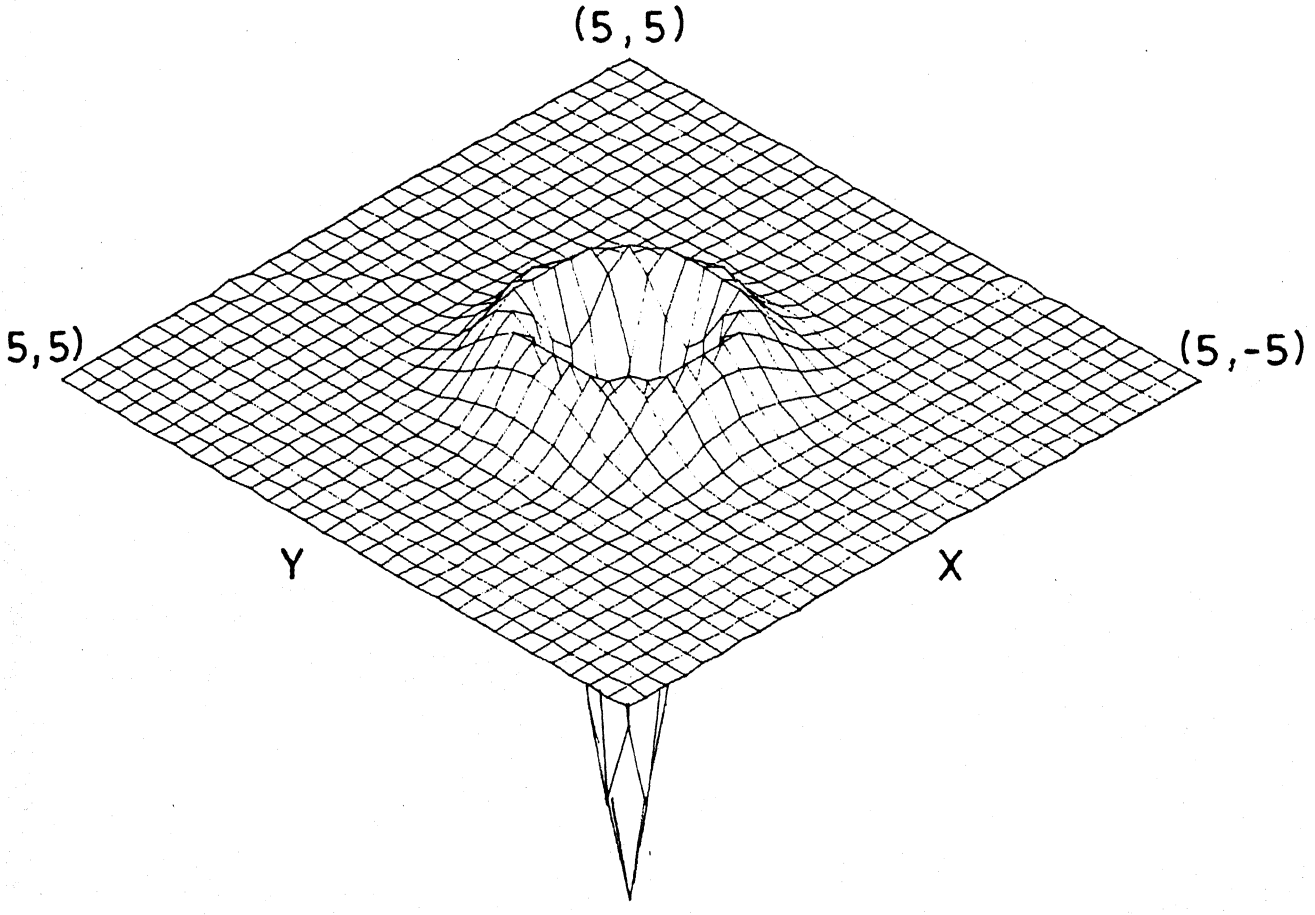

Fig. 3. Laplacian of the test function plotted in Fig. 2

Recently, Bisseling and Kosloff[46] have proposed yet another method for the solution of the TDSE expressed in spherical or polar coordinates. The radial part of the Laplacian has been computed using a Fast Hankel Transform method, based on the FFT algorithm.[43] It has been successfully applied[46] for the collinear reactive system in Delves hyperspherical coordinates.

In order to compute the eigenvalues and eigenfunctions of the Schrödinger equation, Feit et al.[33] have proposed a method, based on the spectral properties of the TDSE. The method requires the computation of a correlation function $\langle \Psi(\vec{r},t_o) | \Psi(\vec{r},t) \rangle$ from a numerical solution of $\Psi(\vec{r},t)$. They have adopted a different strategy to compute $\Psi(\vec{r},t)$, given the initial wavefunction $\Psi(\vec{r},t_o)$.

Since

$$\Psi(\vec{r},t_o + \Delta t) = U(\Delta t)\Psi(\vec{r},t_o) \qquad .. (29)$$

and $$U(\Delta t) = \exp\left[\frac{i\Delta t\hbar \vec{\nabla}^2}{2m}\right]\cdot\exp\left[-\frac{i\Delta t V}{\hbar}\right] \qquad .. (30)$$

$$\Psi(\vec{r},t_o + \Delta t) = \exp\left[\frac{i\Delta t\hbar \vec{\nabla}^2}{2m}\right]\cdot\exp\left[-\frac{i\Delta t V}{\hbar}\right]\Psi(\vec{r},t_o) \qquad .. (31)$$

Similarity transformation of U leads to,

$$\Psi(\vec{r},t_o + \Delta t) = S^{-1}\exp\left[\frac{i\Delta t\hbar \vec{\nabla}^2}{2m}\right]\cdot\exp\left[-\frac{i\Delta t V}{\hbar}\right] S\Psi(\vec{r},t_o) \qquad .. (32)$$

Substitution of

$$S = \exp\left[\frac{i\Delta t\hbar\vec{\nabla}^2}{4m}\right],\ S^{-1} = \exp\left[-\frac{i\Delta t\hbar\vec{\nabla}^2}{4m}\right] \qquad ..(33)$$

in Eq. (32) results in

$$\Psi(\vec{r},t_o+\Delta t) = \exp\left[\frac{i\Delta t\hbar\vec{\nabla}^2}{4m}\right]\exp\left[-\frac{i\Delta tV}{\hbar}\right]\exp\left[\frac{i\Delta t\hbar\vec{\nabla}^2}{4m}\right]\cdot\Psi(\vec{r},t_o) \qquad .. (34)$$

Equation (34) forms the split operator algorithm[33] for advancing the wavefunction by an incremental time Δt.

The operator, $\exp\left[\left(\frac{i\Delta t\hbar}{4m}\right)\vec{\nabla}^2\right]$ applied to $\Psi(\vec{r},t_o)$ is equivalent to solving the free particle wave equation

$$i\hbar\frac{\partial\Psi(\vec{r},t)}{\partial t} = -\frac{\hbar^2}{2m}\vec{\nabla}^2\Psi(\vec{r},t) \qquad .. (35)$$

over a time $\Delta t/2$ with $\Psi(\vec{r},t_o)$ as the initial wavefunction at $t = t_o$. The solution to Eq. (34) is obtained with the help of the band-limited Fourier series representation

$$\Psi(\vec{r},t) = \sum_{j=\frac{-N}{2}+1}^{N/2}\sum_{k=\frac{-N}{2}+1}^{N/2}\sum_{l=\frac{-N}{2}+1}^{N/2}\Psi_{jkl}(t)\exp\left[\frac{2\pi i}{L_o}(j\hat{x}+k\hat{y}+l\hat{z})\right] \qquad .. (36)$$

where $\Psi_{jkl}(t_o+\Delta t) = \Psi_{jkl}(t_o)\exp\left[-\left(\frac{i\Delta t\hbar}{2m}\right)\left(\frac{2\pi}{L_o}\right)^2(j^2+k^2+l^2)\right]$

where L_0 is the length of a side of the computational grid. The RHS of Eq. (34) is thus equivalent to free particle propagation over a half-time increment, a phase change from the action of the potential applied over the whole time increment, and an additional free particle propagation over a half-time increment.

This procedure has been shown to be accurate and efficient when implemented with the help of an FFT algorithm.[43] The sampling interval Δt must be small enough to accommodate atleast the entire spectrum of bound state energy levels for the system. The effectiveness of this spectral method has been demonstrated[33] in the case of a one-dimensional double well potential and for the two dimensional Hénon-Heiles potential. Subsequently its utility has also been tested[50] for practical three-dimensional potentials applicable to SO_2, O_3 and H_2O. It has also been used to time evolve a WP in the Hénon-Heiles potential in order to identify chaotic behaviour of the system.[51]

1.2.1 Stability criteria

A good integrating scheme to solve the TDSE has to be stable to round-off errors in the computation. Yet it has to be general enough to deal with most of the physical potentials and initial wavepackets. Also, the numerical algorithm has to be reasonably fast. The stability criteria to be met by

the choice of steps in time and space for the different methods discussed above have been worked out elsewhere.[28,31,52,53] Only the essential features are outlined below.

If the error $\varepsilon_j^n = \varepsilon^n \exp(iqx_j)$ in Ψ^n is magnified by g times in the next step, that is, $\varepsilon_j^{n+1} = g\,\varepsilon_j^n$, then for the method to be stable, |g| should not exceed unity. The ratio $g = \varepsilon_j^{n+1} / \varepsilon_j^n$ is called the growth factor.

Substituting $\Psi_j^n + \varepsilon_j^n$ and $\Psi^{n\pm1} + (g)^{\pm1}\,\varepsilon_j^n$ for Ψ_j^n and $\Psi_j^{n\pm1}$ in Eq. (19), we obtain

$$g^2 + 2i[2\alpha\{1-\cos(q\Delta x)\} + V_j\Delta t/\hbar]\, g - 1 = 0 \qquad .. (37)$$

where α is defined as in Eq. (14).

The magnitude of each of the two roots of the Eq. (37) would be equal to 1 if the following condition is satisfied:

$$1 \geq |2\alpha[1-\cos(q\Delta x)] + V_j\Delta t/\hbar| \qquad .. (38)$$

As q may have any value, Eq. (38) leads to the following conditions for the stability of the integration:

$$1 \geq 4\alpha \;;\quad \Delta t \leq (1-4\alpha)\hbar/|V_j|_{max} \qquad .. (39)$$

In two dimensions,

$$1 \geq 4\,(\alpha_1 + \alpha_2);\ \Delta t \leq [1 - 4(\alpha_1 + \alpha_2)]\hbar / |V_{jk}|_{max} \qquad .. (40)$$

The TDSE resembles the heat diffusion equation in that it involves a first order temporal derivative and a second order spatial derivative. Yet the former seems more amenable to numerical solution than the latter. The imaginary number i in the TDSE changes the character of the differential equation and results in the corresponding numerical scheme being stable.[31]

The stability conditions of the FT method have been worked out for the case of a free particle system.[32] However, with a knowledge of the physics of the problem, one can come up with optimum values of step size in time and space for cases which deal with either a potential barrier or a potential well.

1.2.2 Choice of initial conditions

To carry out the dynamics of an atom-diatom exchange reaction of the type (R1), if we restrict outselves to collinear collisions, only two coordinates r_1 (the A-B distance) and r_2 (B-C distance) are needed to specify the geometry. It is possible to choose a set of coordinates[54] (q_1, q_2) which reduces the motion of three particles in (r_1, r_2) coordinates to the motion of a single particle. Most of the studies so far have employed the scaled and skewed coordinates (q_1, q_2) which

diagonalize the Hamiltonian

$$H = -(\hbar^2/2\mu_{A,BC})(\partial^2/\partial q_1^2 + \partial^2/\partial q_2^2) + V(q_1, q_2) \quad .. (41)$$

A linear transformation that effects the required diagnolization is

$$q_1 = r_1 + \beta r_2 \sin\theta \quad .. (42)$$

$$q_2 = \beta r_2 \cos\theta \quad .. (43)$$

$$\text{with} \quad \beta = [\{m_C(m_A + m_B)\}/\{m_A(m_B + m_C)\}]^{1/2} \quad .. (44)$$

$$\text{and} \quad \theta = \sin^{-1}[m_A m_C/\{(m_A + m_B)(m_B + m_C)\}]^{1/2} \quad .. (45)$$

where m_A, m_B, m_C denote the masses of the atoms A, B and C, respectively.

The coordinate system is shown schematically in Fig. 4. In such a coordinate system, $\Psi(t = 0)$ is chosen as

$$\Psi(t = 0) = \Psi(q_1, q_2) = \Phi(q_1).X_n(q_2) \quad .. (46)$$

where X_n is the n-th state vibrational eigenfunction of the diatom BC:

$$[-(\hbar^2/2\mu_{BC})\,\partial^2/\partial q_2^2 + V(q_1 = \infty, q_2)]\, X_n(q_2) = E_n X_n(q_2) \quad .. (47)$$

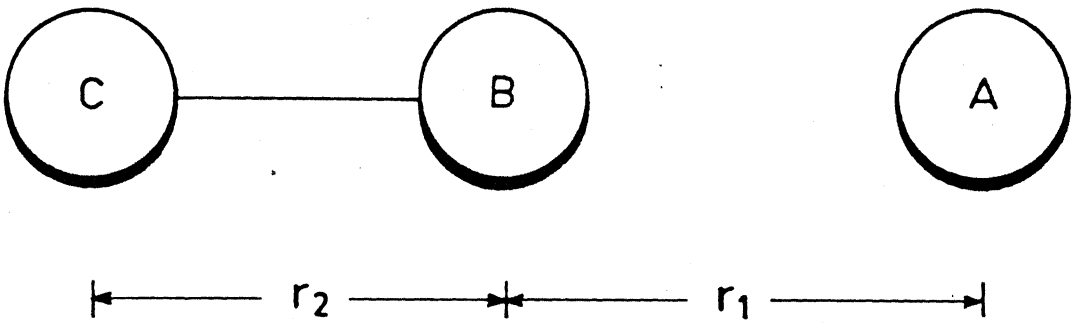

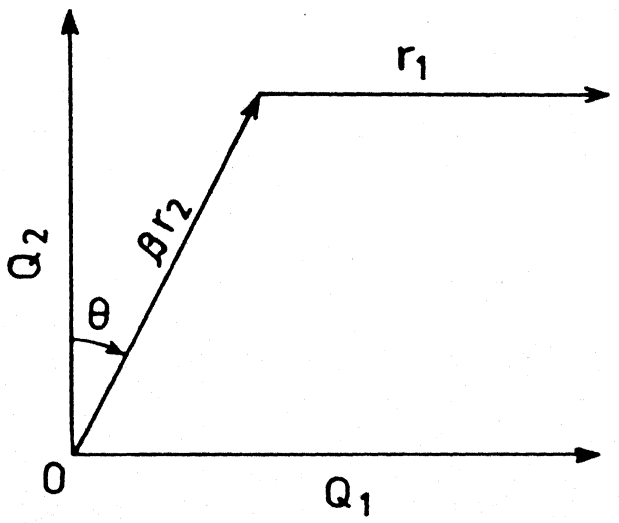

Fig. 4. Coordinate system for collinear A + BC Collisions

For a Morse oscillator, the ground state eigenfunction is given by

$$X_o(q_2) = N_o \exp\left[-\frac{(b+1)}{2}\exp\{-\alpha(q_2-q_2^{\,o})\}\right]\left[(b+1).\exp\{-\alpha(q_2-q_2^{\,o})\}\right]^{b/2} \quad .. (48)$$

where N_o is the normalization constant for the ground vibrational state given below, $b = [(8\mu D)^{1/2}/\alpha\hbar]-1$, μ is the reduced mass of BC, D is the dissociation energy of BC, α is the Morse parameter and $q_2^{\,o}$ is the q_2-space value for the equilibrium internuclear distance of BC. The normalization constant for the n-th vibrational state Morse wavefunction[55] is given by

$$N_n = (1/M_n)^{1/2} \quad .. (49)$$

$$\text{where } M_n = \frac{(n!)^2}{\alpha A^{(A-2n-1)}} \sum_{S=0}^{n} \frac{\Gamma(A-2n+S-1)}{S!} \quad .. (50)$$

where $A = b+1$ and Γ represents the gamma function.

The first vibrational state wavefunction for a Morse oscillator is written as

$$X_1(q_2) = N_1 F_1 F_2 F_3 \quad .. (51)$$

where $F_1 = \exp(-DF)$, $F_2 = F^{((A-2n-1)/2)}$;

$F_3 = Z^n - (A-n-1)nZ^{(n-1)}$; $Z = AF$; $D = A/2$;

$F = \exp[-\alpha(q_2 - q_2^{\,o})]$;

and N_1 is the normalisation constant for the first vibrational state. The first vibrational state wavefunction has a node located at the point $q_2 = q_2^{o}$.

The question of the validity of representing the wavefunction without any concern for the relative phase of the vibrational eigenfunction for the time-dependent WP calculations[27,29,53] has been recently addressed by Agrawal et al.[56] They computed the rate coefficient for the collinear reaction

$$T + HD \longrightarrow TH + D \qquad (R3)$$

using the explicit method,[53] with and without the phase factors of the vibrational eigenfunction being incorporated. The results were identical in both cases, thus providing justification of the earlier approach.

$\Phi(q_1)$ in Eq. (41) is taken to be a WP constructed by superimposing many planewaves to represent the translational motion of the atom A with respect to the center of mass of BC. Typically, it is taken to be a minimum uncertainty Gaussian WP in the momentum (k) space, centered at k_o corresponding to the classical relative translational energy (E_{tr}) of the reactants such that

$$E_{tr} = \hbar^2 k_o^2 / 2\mu_{A,BC}$$

$$\Phi(q_1) = (2\pi\delta^2)^{-1/4} \exp[-(q_1 - q_1^o)^2/4\delta^2 - ik_o q_1] \qquad .. (52)$$

where q_1^o is the center of the WP in the coordinate space, An optimal width (δ) of the WP has to be employed in the computations. In principle, if one chooses a WP whose k space distribution approaches a delta function, then the results can be directly compared to the fixed collision energy results obtained either via QCT or time-independent methods. In practice, however, such a procedure is not feasible since the resulting WP will be completely diffused in the coordinate space. This would result in a non-physical situation, in which even at $t = 0$, the reactants would not be well defined. Hence, the integration of the TDSE has to be carried out over an extensive configuration space grid such that the atom A is separated well from the molecule BC at $t = 0$ requiring a substantial amount of computer time. On the other hand, if the WP has a narrow distribution in the configuration space, it becomes diffused in the k space, thus rendering any determination of the energy dependence of P^R difficult. In most of the studies so far the value of δ has been chosen to be 0.25 a.u.$^{-1}$

If we are interested in a state (v)-selected rate coefficient at a translational temperature T, the following WP has to be chosen:

$$\Phi(q_1) = (\beta/\pi)^{1/2} [\Gamma(3/4)\ {}_1F_1\{3/4, 1/2, -\beta^2(q_1 - q_1^o)^2\} - 2i\Gamma(5/4)(q_1 - q_1^o)\beta\ {}_1F_1\{5/4, 3/2, -\beta^2(q_1 - q_1^o)^2\}] \quad .. (53)$$

where ${}_1F_1$ represents the confluent hypergeometric function and $\beta = (\mu kT/\hbar^2)^{1/2}$. The $\langle E_{tr} \rangle$ of the above WP corresponds to $2\hbar^2\beta^2/\mu$. This WP had been previously utilized by Mazur and Rubin[27] and MW.[29] If an overall rate constant is desired, an appropriate summation over the v states can also be incorporated in the initial wavefunction, in the Eq. (46).

For computational purposes Eq. (46) has to be discretised and the values of the initial wavefunction have to be generated over a set of points in the q_1, q_2 - plane given by $q_1 = (j-1)\Delta q_1 + q_1^o$, $q_2 = (i-1)\Delta q_2 + q_2^o$ where $j = 1, 2, \ldots J$, and $i = 1, 2, \ldots I$, called a grid and q_1^o and q_2^o are convenient starting values for q_1 and q_2, respectively; Δq_1 and Δq_2 are small increments and determine the grid size. Since Ψ is defined throughout the (q_1, q_2) configuration space, the exact grid is of infinite area (I and J would be infinite). The calculation is made feasible by reducing the grid size to a finite range and imposing the boundary condition that the wavefunction is zero in all space not encompassed by the mesh. To reduce the memory requirement, MW[29] started using L-shaped grid enclosing the interaction region. Nowadays, a rectangular grid is used. If the FT method[32] is used to obtain the Laplacian of Ψ, efficiency is maximum if the number of grid points are in powers of 2. Typically 64 or 128 grid points are used. The FD schemes have no such restrictions on the grid size. As a matter of fact, they allow floating grid size, thus reducing

the memory requirement. For reactive scattering, the WP at time t = 0 must be placed in the entry channel, far out from the interaction region (large q_1, small q_2). The complex exponential term of the WP [Eq. (52)] pushes it towards the interaction region. The segments of the boundary in both directions which close off the asymptotic reactant and product channels constitute nonphysical barriers which tend to reflect Ψ back toward the interaction region. Therefore, these boundaries must be placed far out (large q_1, q_2) so that the reaction is essentially over before the interference between the waves reflected from the inner repulsive wall and the outer boundaries becomes significant.

1.2.3 Calculation of reaction probabilities

For a specific eigenstate of BC and a distribution of E_{tr}, $<P^R>$ is computed by obtaining the relative volume of $\Psi^*\Psi$ in the product space P :

$$<P^R> = \int_P \Psi^*(t)\, \Psi(t)\, dq_1\, dq_2 \qquad .. (54)$$

The products are distinguished from the reactants with the aid of a "reasonable" q_2 = constant line. For a symmetric exchange reaction of the type (R2) the dividing line (of the reactants and the products) would pass through the saddle point from the origin diagonally. If the saddle point is located asymmetrically

in the (q_1, q_2) space or if there is no saddle point as in the case of HeH_2^+ system, the dividing line becomes somewhat arbitrary.

The initial wavefunction is time evolved for a "sufficiently long time" and the time evolution is stopped when a plot of $<P^R>$ as a function of time levels off. Another criterion based on the maximisation of entropy principle can be used to terminate the time evolution of Ψ. The information theoretic entropy[57]

$$S = -k\Sigma P_i \ln P_i = -k \int P \ln P \, dP$$
$$= -k \int (\Psi^* \Psi) \ln(\Psi^* \Psi) \, dq_1 \, dq_2 \quad .. (55)$$

can be computed at different time intervals and the time evolution stopped when a plot of S as a function of time levels off. Preliminary results[58] indicate that as time increases, entropy increases and then levels off.

Recently, it has been shown[53] that using the WP

$$\Phi(q_1) = \exp(-ik_o q_1) \sin(\Delta k(q_1 - q_1^o))/((q_1 - q_1^o)(\pi\Delta k)^{1/2}) \quad .. (56)$$

it is possible to obtain $P^R(E)$ for a narrow distribution of energy. For a WP corresponding to $k_o = k_1$ and $\Delta k = \Delta k_1$ let the $<P^R>$ be P_1. For a second WP with $k_o = k_2 = k_1 + \varepsilon$ and $\Delta k = \Delta k_2 = \Delta k_1 + \varepsilon$, let $<P^R>$ be P_2. Since Eq. (56) has a rectangular distribution in k space,

$$P^R(E) = (P_2\Delta k_2 - P_1\Delta k_1)/(\Delta k_2 - \Delta k_1) \quad .. (57)$$

where $P^R(E)$ represents the reaction probability averaged over the energy values in the range $E-\Delta E$ to $E + \Delta E$ with

$$E = \hbar^2(k_1 + \Delta k_1 + \varepsilon)^2/2\mu_{A,BC} \quad .. (58)$$

$$\text{and } \Delta E = \hbar^2\varepsilon(k_1 + \Delta k_1 + \varepsilon)/\mu_{A,BC} \quad .. (59)$$

In principle, ΔE can be made very small so that $P^R(E)$ will approach the time-independent result for a fixed energy.

Leforestier[35] has described how to extract the inelastic ($P^I_{m\to n}$) and reactive ($P^R_{m\to n}$) state-to-state ($m\to n$) probabilities from the final WP. For a collisional eigenstate $\Psi^{(k)}_m$ corresponding to the vibrational state m and to a total energy $E_m = \hbar^2k^2/2\mu_{A,BC} + \varepsilon_m$

$$\Psi^{(k)}_m \simeq \exp(-ikq_1)X_m(q_2) + \sum_n A^{(k)}_{m\to n} \exp(-ik_n q_1)X_n(q_2)$$

$$+ \sum_{n'} A'^{(k)}_{m\to n'} \exp(-ik'_{n'}q'_1)\, X'_{n'}(q_2) + \Psi^{(k)}_{m,diss} \quad .. (60)$$

In the above expression, $\Psi^{(k)}_{m,diss}$ stands for the dissociative contribution to that collisional eigenstate and the primed symbols refer to the products AB + C.

The WP at time t = 0,

$$\Psi_m\,(q_1,q_2) = X_n(q_2) \int_{-\infty}^{\infty} dk\, \Phi(k)\, \exp[-ik(q_1-q_1^{\,o})] \qquad .. (61)$$

can be projected onto the eigenstates defined by Eq. (60), leading to the expression

$$\Psi_m\,(q_1,q_2) = \int_{-\infty}^{\infty} dk\, \Phi(k)\, \Psi_m^{(k)} \qquad .. (62)$$

The above equation has been obtained by neglecting the overlap between the $\Psi(k)\exp[-ik(q_1-q_1^{\,o})]$ function and the $\exp(ik_n q_1)$ or $\exp(ik_n' q_1')$ plane waves. This approximation becomes exact for high-energy collisions such as CID processes because the $\Phi(k)$ distribution function has essentially no components in the negative k plane.

At time T, the WP would have evolved into

$$\Psi_m(q_1,q_2,T) = \int_{-\infty}^{\infty} dk\, \Phi(k)\, \Psi_m^{(k)}\, \exp(-iE_m T/\hbar) \qquad .. (63)$$

If T is sufficiently large, i.e., if the WP is entirely outside the interaction region, one can use the asymptotic evaluation of the collisional eigenstates $\Psi_m^{(k)}$ [Eq. (60)] to rewrite the WP expression as

$$\Psi_m(q_1,q_2,T) = -\sum_n X_n(q_2) \int_{-\infty}^{\infty} dk\, \Phi(k)\, A_{m\to n}^{(k)} \exp(ik_n q_1) \exp(-iE_m T/\hbar)$$

$$-\sum_{n'} X'_{n'}(q_2) \int_{-\infty}^{\infty} dk\, \Phi(k)\, A_{m\to n'}^{(k)} \exp(ik'_{n'} q'_1) \exp(-iE_m T/\hbar)$$

$$- \int_{-\infty}^{\infty} dk\, \Phi(k)\, \Psi_{m,diss}^{(k)} \exp(-iE_m T/\hbar) \qquad .. (64)$$

This last expression, after projection onto the X_n and $X'_{n'}$ eigenfunctions and Fourier transformed yields directly the probability amplitudes $A_{m\to n}^{(k)}$ and $A'^{(k)}_{m\to n'}$

$$A_{m\to n}^{(k)} = -[2\pi\, \Phi(k)]^{-1} \exp(iE_m T/\hbar)(k/k_n) \cdot$$

$$\times \iint dq_1 dq_2\, X_n(q_2) \exp(-ik_n q_1)\, \Psi_m(q_1,q_2,T)$$

$$A'^{(k)}_{m\to n'} = -[2\pi\, \Phi(k)]^{-1} \exp(iE_m T/\hbar)(\mu' k/\mu k'_{n'}) \cdot$$

$$\times \iint dq'_1\, dq'_2\, X'_{n'}(q'_2) \exp(-ik'_{n'} q'_1)\, \Psi_m(q'_1, q'_2, T) \qquad .. (65)$$

From these equations, one can finally obtain the state-to-state probabilities which are defined as the ratio of the outgoing flux in the considered channel to the incoming flux.

$$P^{I}_{m\to n}(k) = \frac{k}{k_n}\frac{1}{4\pi^2|\Phi(k)|^2}\left|\int\int dq_1 dq_2\, X_n(q_2)\exp(-ik_n q_1)\Psi_m(q_1,q_2,T)\right|^2$$

$$P^{R}_{m\to n'}(k) = \frac{\mu' k}{\mu k'_{n'}}\frac{1}{4\pi^2|\Phi(k)|^2}\left|\int\int dq'_1\, dq'_2\, X'_{n'}(q'_2)\exp(-ik'_{n'}q'_1)\Psi_m(q'_1,q'_2,T)\right|^2$$

.. (66)

1.3 Applications

1.3.1 Atom-diatom exchange reactions

By far, the predominant application of the TDQM approach has been in calculating $<P^R>$ for a variety of atom-diatom exchange reactions. A summary of them is presented in Table 1. MW[29] computed the $<P^R>$ at different energies for the reaction (R2) on the Porter-Karplus[30] PES. Agrawal and Raff[53] used the explicit method to compute rate coefficients in the temperature range 1000-3000 K for the collinear reaction (R3) on a London-Eyring-Polanyi-Sato (LEPS) PES. The results were shown to be in good agreement with the time-independent results of Garrett et al.[59] Values of $<P^R>$ computed[37] on the SLTH surface for reaction (R2) also have been shown to be in accord with the time-independent results.[60]

Kellerhals et al.[41] computed $<P^R>$ for the reaction (R1) on a model LEPS surface and studied its dependence on the location of the saddle point. It became clear that $<P^R>$ was sensitive to changes in the PES. Stroud et al.[42] investigated

TABLE 1. Summary of the atom-diatom exchange reactions studied by the TDQM approach, along with a list of numerical methods used

System and PES	Initial conditions v	Initial conditions $\langle E_{tr} \rangle$ eV	Laplacian	Time-evolution	Ref.
$H + H_2$ model^2	0 1	0.14-0.26	3-point FD	FD	27
$H + H_2$ PK	0	0.32-0.51	3-point FD	implicit	29
$H + H_2$ LEPS	0 1 4	3.00-12.00	5-point FD	predictor -corrector	34, 66
$H + H_2$ LEPS	0 2	2.30-4.10	7-point FD	implicit	35
$H + H_2$ SLTH	0 1	0.40-1.00	3-point FD	explicit	37
$H + H_2$ LEPS	0	0.15-1.00	3-point FD	implicit	40-42, 62
$H^+ + H_2$; $D^+ + HD$; $D^+ + H_2$ DIM	0 2 3	E_{tot} =-0.07- -1.17	FT	FD	44
T + HD LEPS	0	0.08-0.21	3-point FD	explicit	53
T + HD SLTH	0	0.08-0.87	3-point FD	explicit	56
$F + H_2$; $F + D_2$ Muckerman	0	0.50-2.00	3-point FD	FD	61
$H + H_2$; H + DH MOEXP^2	0 1 3	0.50-16.00	7-point FD	explicit	67, 68

the influence of v on $\langle P^R \rangle$ and its sensitivity to features of the PES for the reaction

$$He + H_2^+ \longrightarrow HeH^+ + H \qquad (R4)$$

using a diatomics-in-molecules (DIM) and a slightly different spline-fitted <u>ab initio</u> surface. Studies by Zuhrt et al.[61] using three different PESs for the reaction

$$F + H_2 \longrightarrow FH + H \qquad (R5)$$

also showed that $\langle P^R \rangle$ was strongly dependent on the topological features of the PES. Sathyamurthy et al.[62] were able to demonstrate the utility of cubic splines to interpolation of <u>ab initio</u> PESs by showing that results on a spline-fitted surface were identical to those obtained on the original analytic surface. Thareja and Sathyamurthy[63] have recently used the TDQM approach in testing the quality of an analytic fit to the <u>ab initio</u> PES for the reaction (R2). When different fits were obtained for the same original <u>ab initio</u> surface, the fit that led to the same $\langle P^R \rangle$ as on the SLTH surface was taken to be the best.

In addition to yielding P^R at different levels of resolution, the time-evolution method provides valuable insight into the detailed nature of the collision dynamics. Typical 3D perspective plots of $|\Psi|^2$ in configuration space at different

time intervals give a pictorial representation of the reactants transforming into products and the resulting picture can be compared directly with a plot of a family of trajectories. "Structures" in these plots reveal the complexity of the dynamics and are indicative of indirect collisions. Using the FT method[32] Kosloff and Kosloff[44] investigated the conditions for complex formation in $H^+ + H_2$ and its isotopic analogs for which the PES has a deep potential well in it.

From a knowledge of $\Psi(\vec{r},t)$, quantal flux patterns could be drawn, in analogy with the fluid flow in classical hydrodynamics. Plots of the quantal probability flux vector

$$\vec{J}(\vec{r},t) = \frac{\hbar}{\mu} \text{Im}\left[\Psi^*(\vec{r},t)\vec{\nabla}\Psi(\vec{r},t)\right] \qquad .. (67)$$

were made by MW[29] and quantum whirlpools were identified. These have been investigated subsequently by Hirschfelder[64] who described them as quantized vortices around wavefunction nodes.

1.3.2 Spectroscopy of the transition state

Recently, we[37] have made use of the TDQM approach to predict the wings to the Lyman-α line in $H + H_2$ collisions, by obtaining the time-averaged $|\Psi|^2$ values and relating them to absorption intensity. We have made use of the explicit integration scheme[53] to solve the TDSE. Also the same approach has been made use of, in predicting the emission spectrum for the

H_3^* system. The results of our study are presented in detail in Chapters 2 and 3, respectively. Thus, the approach promises to be an effective tool in the emerging area of "spectroscopy of the transition state".

1.3.3 Collision-induced dissociation processes

In contrast to the formidable problems faced by the time-independent approach in studying CID processes, the time-dependent approach is applicable to the CID problem with as much ease as for the exchange reaction. Ford et al.[65] reported the first TDQM results for the reaction of the type

$$A + BC \longrightarrow A + B + C \qquad (R6)$$

using a model potential and the MW algorithm.[29] The fact that the WP represents an average over a momentum distribution can be exploited to extract results for a wide range of energies from a single calculation. In this context, the time-dependent approach is superior to its counterpart, the time-independent approach. Kulander[34] has made use of the TDQM approach in computing the dissociation probabilities (P^D) for the collinear reaction

$$H + H_2 \longrightarrow H + H + H \qquad (R7)$$

on a LEPS surface using the five-point FD scheme to compute the kinetic energy term and a fifth order predictor-corrector method for the time evolution.

Subsequently extensive QCT and quantal WP calculations have been carried out[66] to compare with the earlier reported results.[34] Leforestier et al.[35,67,68] have studied a variety of model CID processes over a wide range of energies. By deconvoluting $\langle P^D \rangle$ to obtain the energy dependence of P^D for a CID process, they have been able to obtain information on the threshold behaviour, vibrational enhancement and inhibition and their dependence on E_{tr}. They have shed further light on the dynamical nature of CID processes by plots of $|\Psi|^2$ and $\vec{J}$ at different time intervals. We have also carried out a study of the CID process in the collinear system (R7) on the accurate SLTH PES over a wide range of E_{tr} and the results will be presented in Chapter 4.

1.3.4 Gas-surface scattering

Atom-surface scattering plays a vital role in the investigation of solid surface properties. The rapid advancement in the recent past on the experimental side of the atom-surface encounters posesa challenge to theoretical models. Time-independent quantal calculations have not become practicable yet. Classical and semiclassical methods have been used extensively in simulating the experimental results. But they are of

limited validity. For the first time Agrawal and Raff[38] showed that the time-dependent approach could be used to study gas-surface scattering by representing an incident atom by a WP and using the explicit integration method[53] for the time evolution of the system. Yinnon and Kosloff[69] have been able to compute scattering intensities, resonance strengths and other attributes using the FT method. Gerber et al.[70,71] have used the same approach to study the scattering of a He atom from a Cu surface with isolated Ar impurities. Kosloff and Cerjan[72] have studied the desorption and scattering of a He atom from W and Pt surfaces using the same method.

Recently, Mowrey and Kouri[73] have shown that by solving the TDSE, molecule-surface scattering processes can also be studied. They have investigated inelastic scattering of H_2 from a flat, rigid surface using a hybrid scheme combining a coupled-channel expansion with a WP formalism.

1.4 Highlights

The TDQM approach scores over the time-independent approach in certain respects, in that there is no need for the construction of channel hamiltonians and matching of the wavefunctions. There is no increase in the complexity of the problem or the computational time requirement with an increase in the total energy of the system. As a matter of fact, there is a reduction

in the computer time with an increase in energy-analogous to the classical approach. In contrast to the time-independent approach in which P^R has to be computed for different E_{tr} and v and averaged over the appropriate distributions in order to calculate state-selected and overall rate constants, the TDQM method could be made to yield them directly by a suitable choice of initial Ψ. Also, the deconvolution methods have made it possible to obtain in a single calculation, P^R (or P^D) over a wide range of E_{tr}.

CHAPTER 2

WINGS TO THE LYMAN-α LINE IN H + H_2 COLLISIONS

It has been recognised in recent years[74-80] that it is possible to obtain the spectrum of the transition state (we use this term in a general sense to refer to all configurations intermediate between reactants and products) for elementary chemical reactions. Arrowsmith et al.[75,76] reported the emission spectrum of the TS for the reaction

$$Na_2 + F \longrightarrow NaF + Na^* \qquad (R8)$$

by monitoring the "wings" to the sodium D-line emission. Polanyi and Wolf[77,78] interpreted the wings as arising from the emission from Na^* while the separating NaF is still in the vicinity. In other words, they concluded that $[FNaNa]^{\ddagger *}$ was the emitter. The emission signals were observed upto ~ 400 Å away from the sodium D-line, in spectral regions where no transitions are known for either reactants or products. Pressures were orders-of-magnitude

too low for the signal to arise from far wing collisional broadening and hence the observed emission must have been due to the TS.

Brooks and coworkers[79] have reported evidence for absorption from the intermediate configurations in the reaction

$$K + HgBr_2 \longrightarrow KBr + HgBr \qquad (R9)$$

Although K and $HgBr_2$ react on nearly every single collision to form KBr and HgBr ($\bar{X}\ ^2\Sigma^+$), the exoergicity is insufficient to yield the electronically excited HgBr*. However, if the system absorbs a photon with $\lambda \sim 590$ nm [no single photon absorptions are known for either reactants or products at this wavelength] the electronically excited HgBr* ($\bar{B}\ ^2\Sigma^+$) state, becomes accessible. And this state is easily detectable from the fluorescence ($\bar{B} \rightarrow \bar{X}$). Thus, it was shown that (R9) is a laser-driven chemical reaction in which the excitation of the reaction complex opens a new channel

$$K + HgBr_2 + h\nu \ (= 595 \text{ nm}) \longrightarrow KBr + HgBr^* \ (\bar{B}\ ^2\Sigma^+) \qquad (R10)$$

$$HgBr^* \ (\bar{B}\ ^2\Sigma^+) \xrightarrow[500 \text{ nm}]{\text{Fluorescence}} HgBr \ (\bar{X}\ ^2\Sigma^+)$$

Recently, Brooks and coworkers[80] have also reported evidence for light absorption by the reaction complex in a similar

reaction

$$K + NaCl + h\nu\ (\backsim 700\ nm) \longrightarrow KCl + Na^*\ (3\ ^2P) \qquad (R11)$$

$$\downarrow \text{Emission } 589\ nm$$

$$Na\ (3\ ^2S)$$

The studies[81,82] on the reaction

$$Xe + Cl_2 + h\nu \longrightarrow XeCl^* + Cl \qquad (R12)$$

also indicate the reaction complex absorbing light.

Spectra of such TSs can provide[83] information on the collision dynamics, complementary to what can be learned from state-to-state studies.[84]

It is of fundamental interest to predict and observe the wings to the Lyman-α line in $H + H_2$ collisions. Polanyi and coworkers[85,86] have computed the absorption spectrum for the TS for the collinear reaction (R2) by determining the probability density distribution for the TS on the chemically accurate SLTH[5] surface using the QCT technique.[87] They assumed vertical transitions from the ground state to one of the low lying excited states, $^2\Pi$ in $D_{\infty h}$ geometry, that correlates with $H^*(2p) + H_2$. For a quick reference, a correlation diagram of a few low lying states of H_3 is presented in Fig. 5. They used model PESs based on the available <u>ab initio</u> data for the upper PES. They studied the effect of increasing relative translational energy of

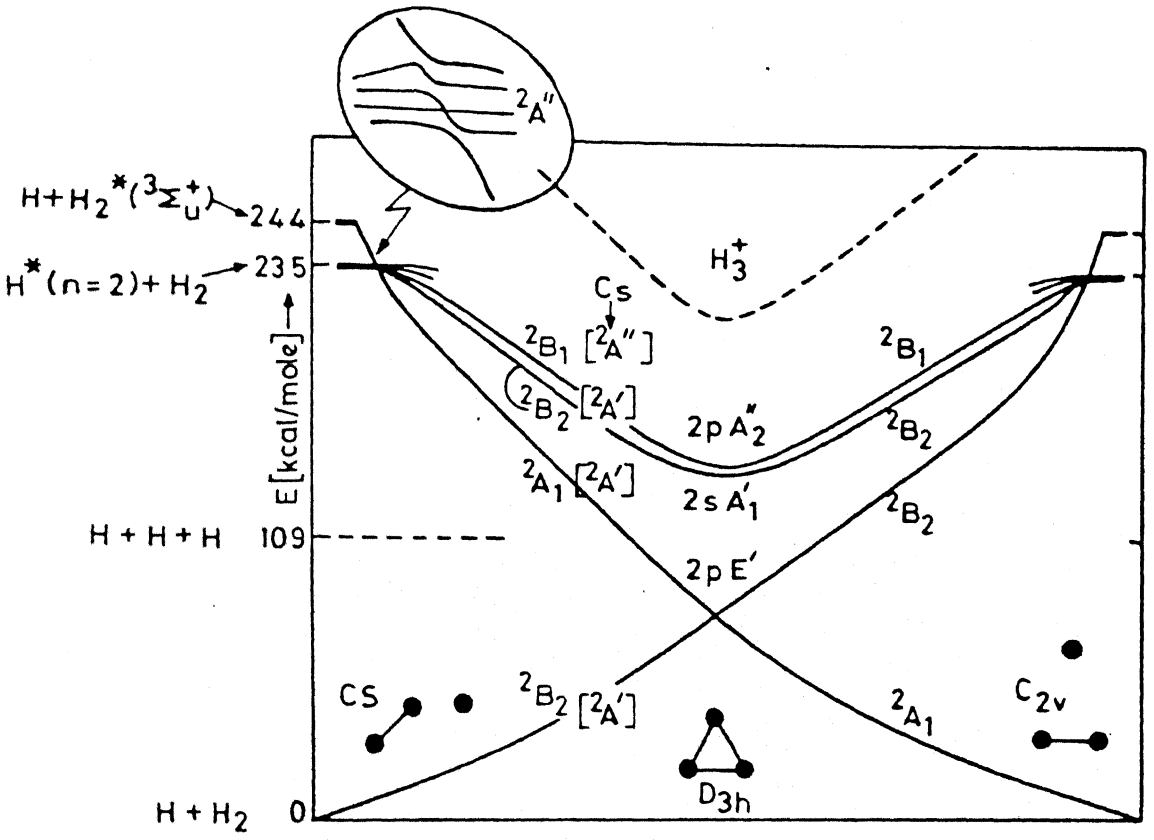

Fig. 5. Correlation energy diagram[88] for the first few lowest potential-energy surfaces of H_3^* together with the ground state surface as a function of nuclear geometry. The lowest excited-state and the ground-state surfaces meet in a conical intersection at D_{3h} geometry

reactants and reagent vibrational excitation on the features of the absorption spectrum. As the collision energy was increased, the intensity of the spectrum diminished and there was a considerable red-shift for the wings to the Lyman-α line. Subsequently, they extended[88] their study to collisions in 3D using a diatomics-in-molecules[89] (DIM) surface for the excited state and concluded that the qualitative features of the spectrum remained while going from collinear geometry to 3D.

Recently, Engel et al.[90] have carried out time-independent QM calculations and predicted the absorption spectrum of the TS for the collinear reaction (R2) for two different vibrational states of the H_2 molecule, at collision energies below the reaction threshold (0.22 eV) using the same ground and upper-state surfaces as Polanyi and coworkers did.[86] They computed the continuum-bound absorption cross section using the relation

$$\sigma(\nu) \sim |\langle \Psi_n^{ex} | \mu | \Psi_{E_{tr}}^{gr} \rangle|^2 \qquad .. (68)$$

where Ψ_n^{ex} denotes the excited state wavefunction describing the n-th bound state and $\Psi_{E_{tr}}^{gr}$, the continuum wavefunction at E_{tr}. They treated the transition moment μ to be a constant (=1) as it was done in earlier studies.[86,88] The bound states, covering 75 per cent of the potential well depth on the upper PES were calculated by expanding the wavefunction in terms of an orthonormal set of vibrational eigenfunctions. The continuum

wavefunction was calculated using three vibrational expansion functions. Their generated spectra agree well with the spectra computed via the QCT method[86] with respect to the basic trends and features. The overall appearance of the absorption spectrum has been interpreted in terms of the amplitude pattern of the continuum wavefunction and the radial extent of the excited state bound level wavefunction. Subsequently they have extended their study[91] to reactive H + H_2 collisions.

Recently a model study has been carried out[92] in our laboratory in which the absorption spectrum for the TS in the collinear reaction (R2) has been predicted, using the time-independent Schrödinger equation for a model consisting of a 1D rectangular potential barrier and a well, at three different collision energies. Results have been shown to be in qualitative agreement with those obtained from a full QM study.[90]

We have also computed[37] the absorption spectrum for the TS for the collinear reaction (R2), but using a TDQM approach. We have used the SLTH[5] PES for the ground state and a DIM surface (described in ref. 88) for the excited state, that correlates with H*(2p) + H_2. The contours of the ground and the excited state PESs are displayed in Fig. 6 and Fig. 7, respectively. The TS spectrum has been predicted for four different $\langle E_{tr} \rangle$ [two of the energies lie below the reaction threshold and the other two well above the threshold] for two different vibrational states (v = 0 and 1) of the H_2 molecule.

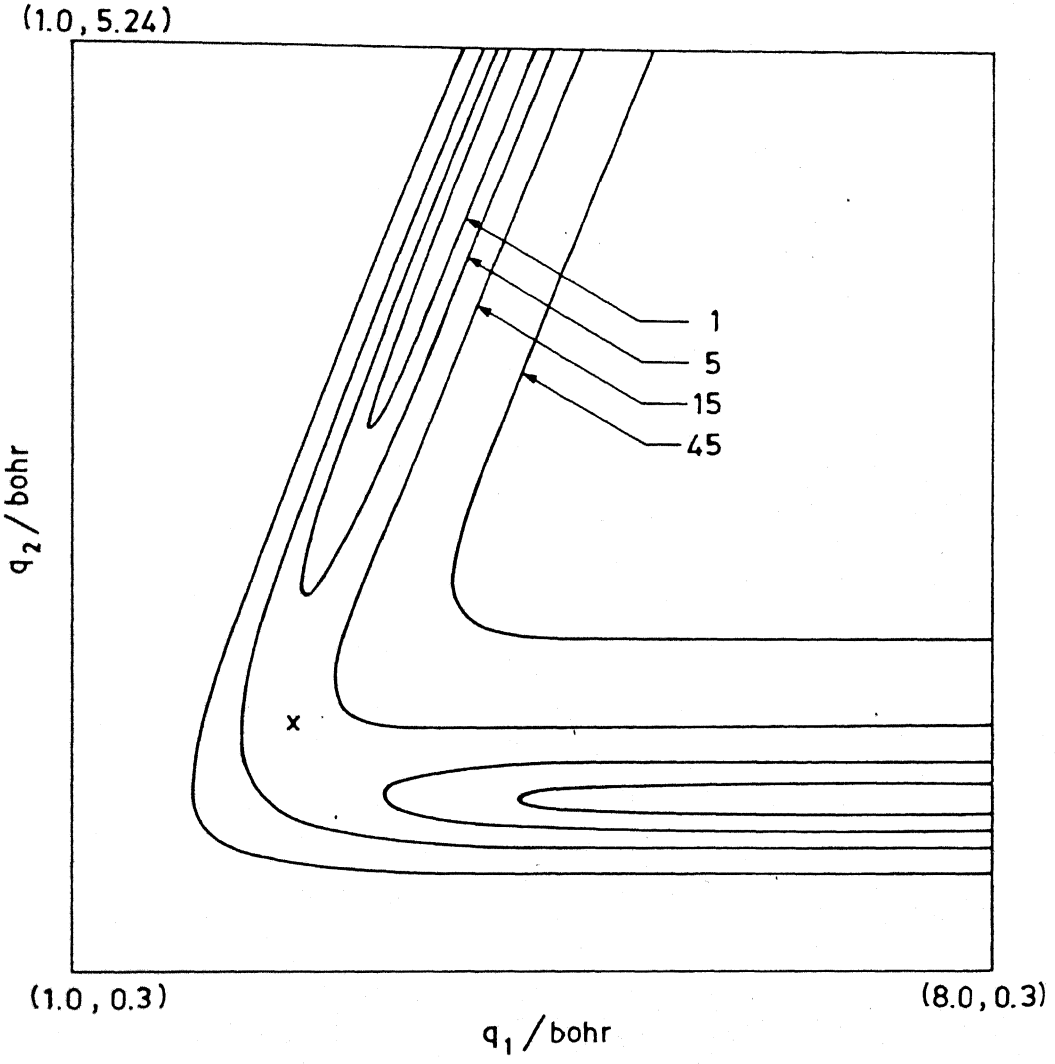

Fig. 6. PE contours for the collinear H_3 in (q_1, q_2) coordinates. The numbers give the values of the contours in kcal/mole relative to the separated H and H_2. X indicates the saddle point

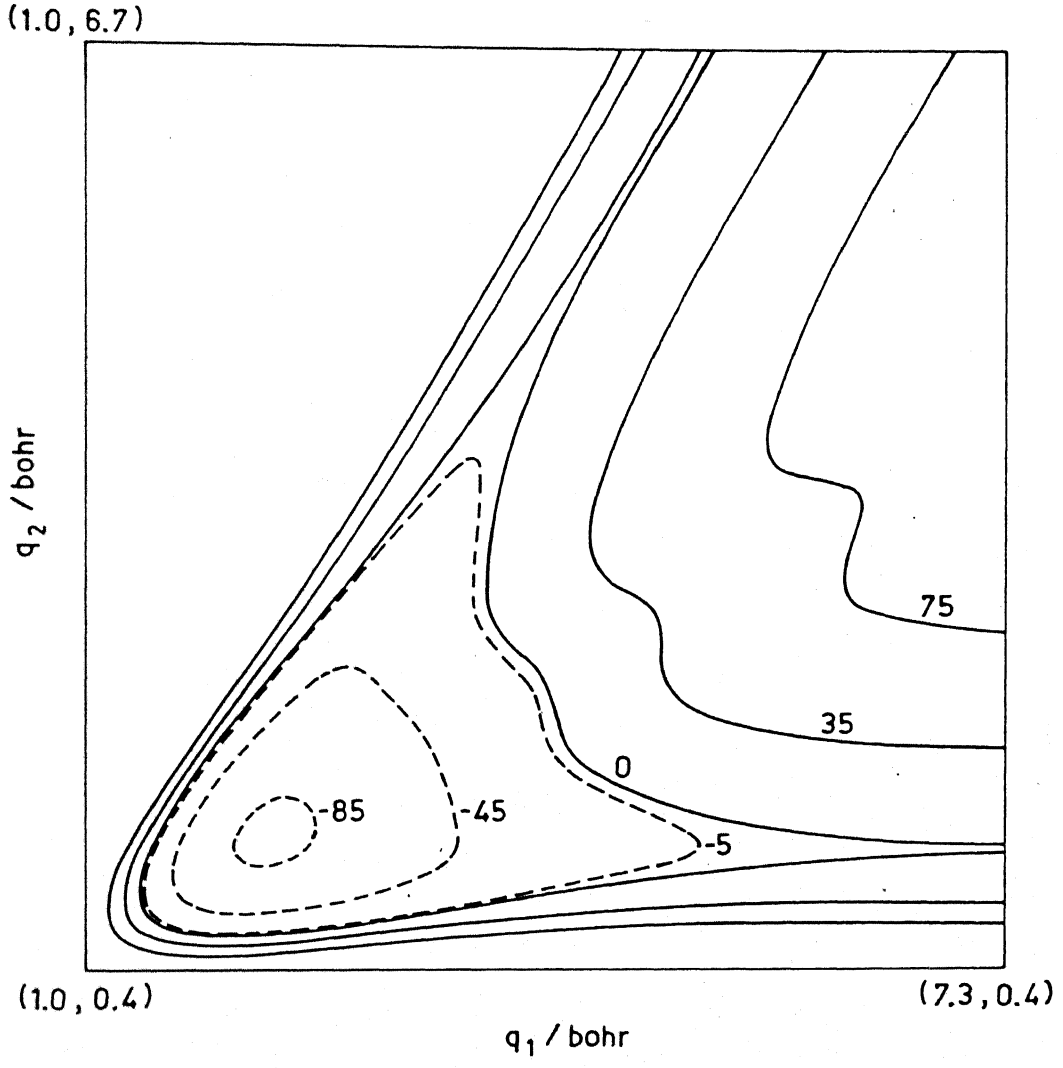

Fig. 7. PE contours of the excited H_3^*. The numbers give the values of the contours in kcal/mole relative to the separated $H^* + H_2$

TS spectra have also been computed for thermal distributions of $H + H_2$, at 300 and 1000 K.

2.1 Computational details

The two dimensional TDSE has been solved by using the explicit integration method.[53] In our earlier work,[37] we had used a 3-point FD scheme to compute the kinetic energy term in Eq. (59). Subsequently, 5-point and 7-point FD schemes and also the FFT algorithm have been used to compute the same. The results are summarised below. A (59 x 45) rectangular grid in the (q_1, q_2) space with $1.7 \leq q_1 \leq 8.08$ a.u. and $0.4 \leq q_2 \leq 5.24$ a.u. has been used. The numerical values for units of distance, time, mass and energy used in our calculations are given in Table 2. The initial WP was located at $q_1^o = 5.5$ a.u. and had a width of $\delta = 0.25$ a.u. The coordinate mesh spacing $\Delta q_1 = \Delta q_2 = 0.11$ a.u. and the time step $\Delta t = 0.01$ were chosen such that they meet the stability criteria for the explicit integration method as discussed in Chapter 1. The initial wavefunction $\Psi(t = 0)$ was set up as in Eqs. (46) and (52) for different $\langle E_{tr} \rangle$ of interest.

The time evolution of the system described by TDSE was terminated at a time when the plot of $\langle P^R \rangle$ as a function of time levelled off as shown in Fig. 8. We have checked the accuracy of our calculation by checking the normalisation condition for Ψ throughout the time evolution of the system.

TABLE 2. Molecular Units

Quantity	Unit
Mass	1 atomic mass unit = 1 a.m.u. = $1.6604345 \times 10^{-24}$ g
Distance	1 atomic unit = 1 a.u. = 0.529167×10^{-8} cm
Energy	1 electron volt = 1 eV = 1.60210×10^{-12} erg
Time	1 time unit = 1 t.u. = $0.5387147 \times 10^{-14}$ sec

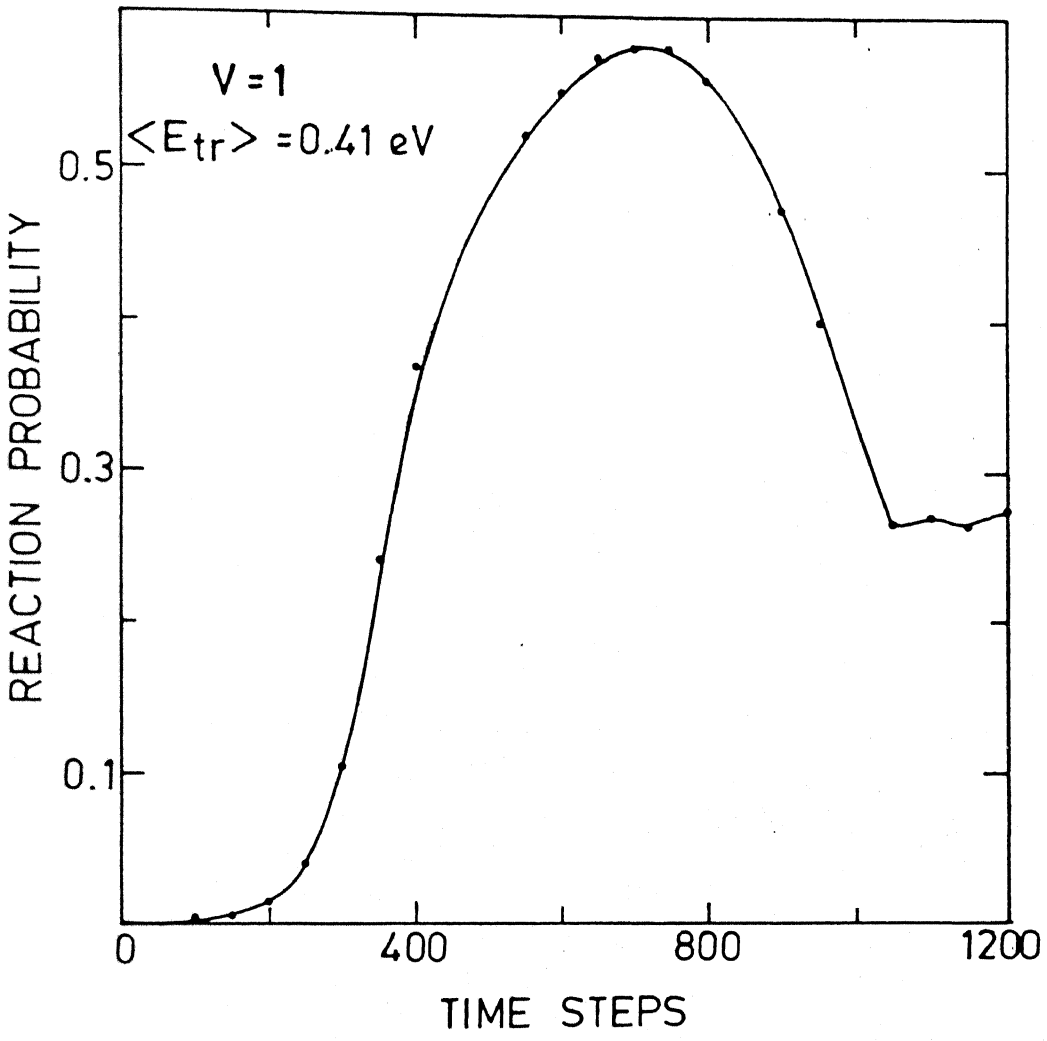

Fig. 8. Reaction probability as a function of time with each time step = 0.53875×10^{-16} s, for a specified initial condition

The accuracy of the method has also been checked by back-evolution technique. That is, the WP is first time evolved from time t_o to $t_o + n\Delta t$. Then, by replacing Δt in Eq. (21) by $-\Delta t$, the wavefunction is "back evolved" n steps to time t_o. Using this technique, we were able to reproduce the initial wavefunction accurately. If the computed $\langle P^R \rangle$ is a converged one, then it should be independent of the number of grid points used and also on the boundary conditions. We have verified that the above statement is true, by computing $\langle P^R \rangle$ with a square computational grid (64 x 64) space (q_1, q_2) with $1.7 \leq q_1 \leq 11.15$ a.u. and $0.4 \leq q_2 \leq 9.85$ a.u. A more stringent test on the accuracy of our calculations would be to compare our computed $\langle P^R \rangle$ to an average of the time-independent reaction probability $P^R(E)$ over the E_{tr} distribution used for the WP, in the following way.

$$\langle P^R \rangle = \frac{\int P(E)\ P^R(E)\ dE}{\int P(E)\ dE} \qquad .. (69)$$

where the weighting function $P(E)$ is given by

$$P(E) = |\Phi(k)|^2 \qquad .. (70)$$

Substituting for $\Phi(k)$ and using the relations

$$k = (2mE)^{1/2}/\hbar$$
$$dk = -(2m)^{1/2}/2\hbar]E^{-1/2}\ dE \qquad .. (71)$$

We get

$$\langle E\rangle = \int_0^{\infty} (2\delta^2/\pi)^{1/2}(m/2)^{1/2}(1/\hbar)\exp[-2\delta^2(2m/\hbar^2)(E^{1/2}-E_o^{1/2})^2] \times E^{-1/2}.E.dE \quad ..(72)$$

Thus,

$$P(E) = (2\delta^2/\pi)^{1/2}(m/2)^{1/2}(1/\hbar)\cdot \exp[-2\delta^2(2m/\hbar^2)(E^{1/2}-E_o^{1/2})^2]E^{-1/2} \quad ..(73)$$

Substituting Eq. (73) and the values of $P^R(E)$ reported in ref. 60 into Eq. (69) and performing the integration, we get the $\langle P^R\rangle$ that is to be compared with our computed results. The results of these comparative studies are presented in Table 3. Since we have computed $\langle P^R\rangle$ for different WPs that correspond to Maxwell-Boltzmann like distribution of relative speeds at temperatures of 300 and 1000 K as well, the corresponding rate coefficients (k) can also be calculated using the relationship

$$k = (k_B T/2\pi\mu)^{1/2} \langle P^R\rangle \quad ..(74)$$

(where k_B = Boltzmann constant) and compared with the results reported in the literature.[60]

We have tested the accuracy of our results obtained by using the 3-point FD scheme to compute the Laplacian of Ψ by repeating the calculations using 5-point and 7-point FD schemes

TABLE 3. Comparison of reaction probabilities and rate coefficients for the collinear reaction $H + H_2 \rightarrow H_2 + H$ as computed from the TDQM approach and its time-independent analog

V	Temp (K)	$\langle E_{tr} \rangle$ (eV)	$\langle p^R \rangle$ (a)	$\langle p^R \rangle$ (b)	k (10^4 cm / sec) (a)	(b)
0	-	0.41	0.561	0.637	-	-
0	-	1.00	0.497	0.490	-	-
0	1000	-	-	-	0.61	0.67
1	1000	-	-	-	2.71	2.98

(a) present calculations

(b) ref. 60

and the FT method[32] based on the FFT algorithm.[43] In the latter cases, norm for Ψ was not conserved when we used the value of $\Delta q = 0.11$ a.u. as was used in the 3-point FD scheme. Therefore, we had to use a larger value of $\Delta q = 0.15$ a.u. In the case of the higher-point FD schemes and the FT method, use of a small value for mesh spacing makes the round-off and the truncation errors dominate and hence spurious results are produced. So the argument that use of a smaller mesh spacing always makes the results to improve, becomes invalid in this context. In fact, only above a critical value of the mesh spacing these formulae for second derivatives become operative and effective as well. We got almost identical results of $\langle P^R \rangle$ in all cases, as it is illustrated in Fig. 9.

For a specified set of initial conditions, $v = 0$ of the H_2 molecule and $\langle E_{tr} \rangle = 0.41$ eV with a 64×64 grid, the mesh space being 0.15 a.u., a run involving the 3-point FD scheme took 12 min of CPU time on the DEC-1090 computer. The corresponding run involving the FT method[32] took 180 minutes. As has already been mentioned in Chapter 1, the number of operations per grid point is larger for the FT method[32] and thus it is 15 times slower than the FD approach.

We solved the TDSE for $H + H_2$ motion on the SLTH surface as described above and obtained $\Psi(t)$ at different time intervals. Then we adopted the following strategy to compute the TS spectrum. The value of $\Psi^*(t)\,\Psi(t)\,dq_1 dq_2$ over each area

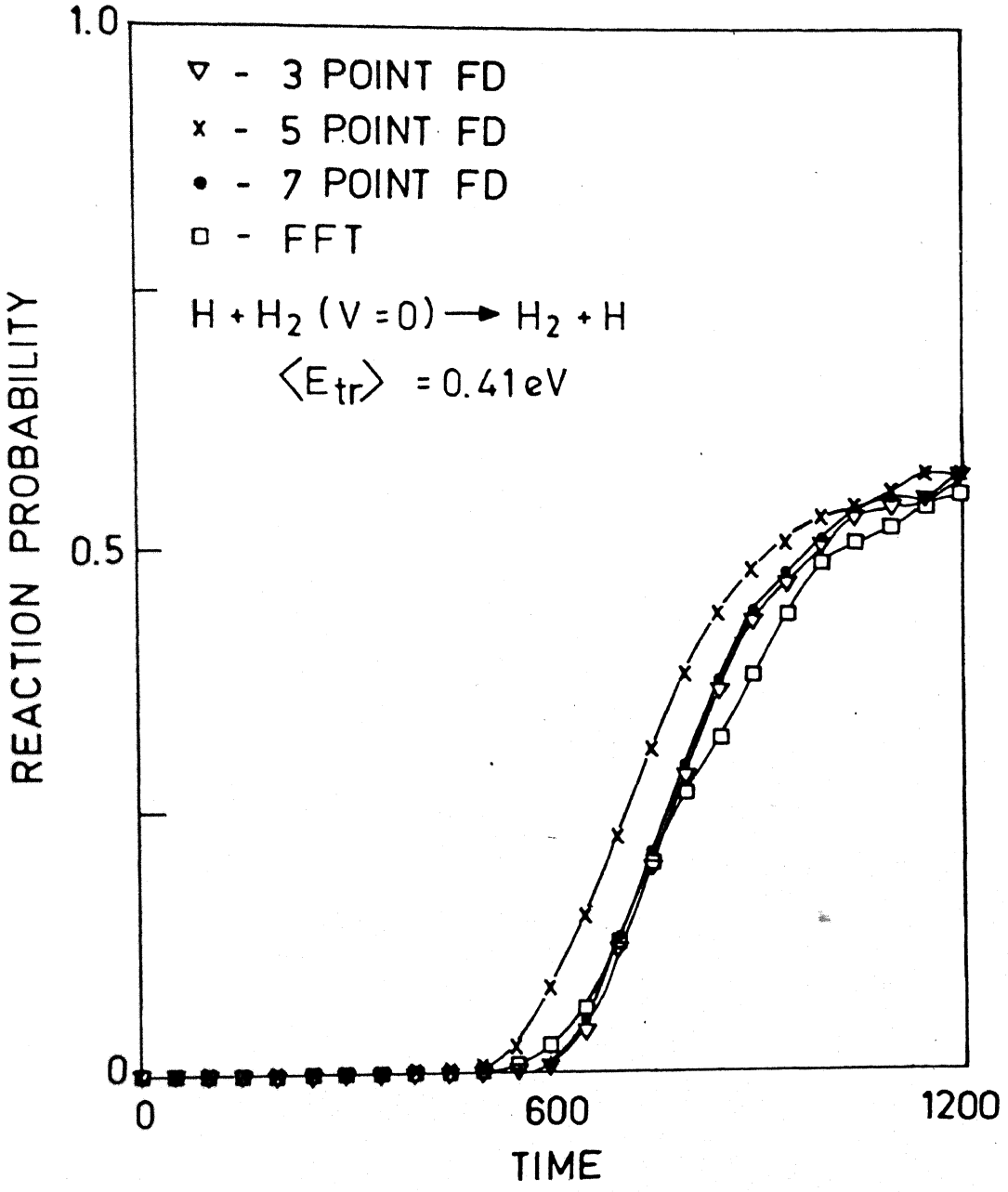

Fig. 9. Reaction probability as a function of time, using different schemes to compute the Laplacian, for a test case

element is taken to be the probability density for the TS in that area element. The time-averaged value of $\Psi^*(t)\,\Psi(t)\,dq_1 dq_2$ over the entire time evolution period for each area element represents the intensity of the transition at an energy equal to the difference between the ground and the excited-state surfaces in that area element. We have used the DIM surface described in ref. 88 for the upper surface. We have assumed constant transition moments as was done by the earlier workers.[86,88,90] We have used a histogram width of 0.2 eV to compute the spectrum.

2.2 Absorption Spectrum for the TS

The resulting absorption spectra for $H_3^{\neq}$ for $\langle E_{tr} \rangle$ ranging from 0.10 to 1.00 eV for v = 0 and 1 are displayed in Fig.10. It is clear that for high energy collisions there are substantial wings to the Lyman-α line at the lower energy region. Two prominent peaks have been identified (at 72,600 and 51,600 cm^{-1}) as a and b. With an increase in the collision energy, the intensity of the peak close to the L_α line decreases and that of the peak in the lower frequency region increases. Similar trends have been reported by earlier workers.[86,88,90]

These results can be understood as follows. We show the comulative value of the probability density function (PDF) over the entire grid, superimposed on the difference potential contours ($\Delta V = V_U - V_L$, the difference in the potential energy

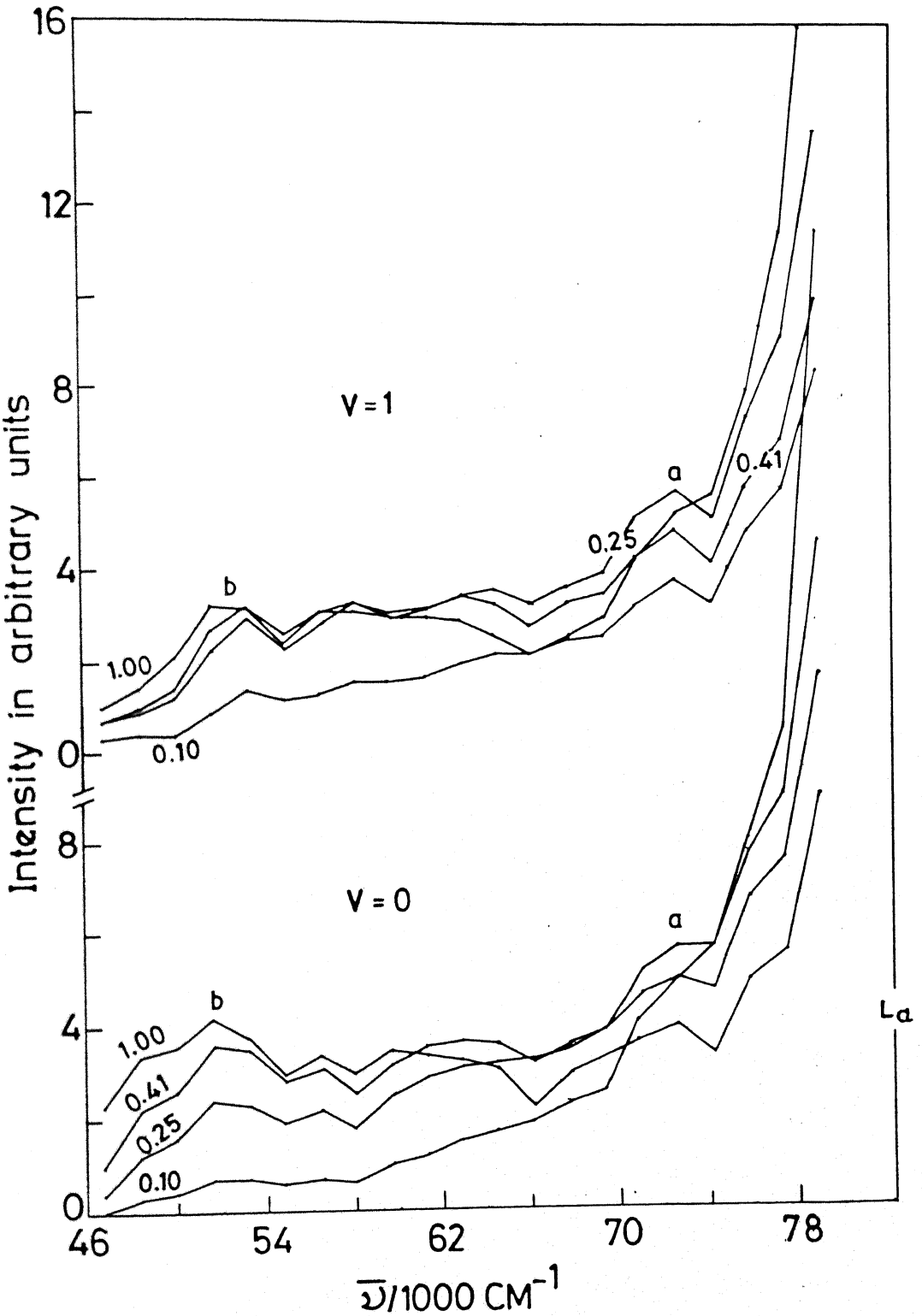

Fig. 10. Absorption spectra for $H_3^{\neq}$ under different initial conditions. Average collision energies are indicated against each spectrum. L_α represents the Lyman-α line.

between the upper and the lower surfaces) in Fig. 11 and 12 for different initial conditions. Hence each point in the configuration space can be read as a spectral frequency ν, corresponding to the energy difference ΔV. The greater the PDF at any particular ΔV, the greater the absorption intensity at the corresponding ν. Thus, the peaks in the absorption spectra can be identified with the accumulation of the PDF at a particular range of ΔV values. At low collision energies (0.10 and 0.25 eV) we do not see substantial wings to the L_α line. At higher collision energies (0.41 and 1.00 eV) two peaks in the lower energy (frequency) regions have been identified as a (71,600 cm^{-1}) and b (51,600 cm^{-1}). These peaks reflect the build up of the PDF near the inner repulsive wall in the PES. Examination of Fig. 11 shows that at low $<E_{tr}>$ PDF is confined to the entry channel indicating that the WP is not able to cross the barrier and hence retrieves back to the reactant valley. As $<E_{tr}>$ is increased, PDF is smeared all over the configuration space and there is a suostantial build up of PDF in particular regions of space. The peak labeled a in Fig. 10 for $<E_{tr}>$ = 0.41 eV is to be identified with the probability density contour (PDC) marked 3 and 5 running parallel to the q_1 axis in the ΔV region between 8 and 9 eV. The peak labelled b is due to the build up of PDF marked 3 near the saddle point. As the collision energy is increased to 1.00 eV, the PDC marked 5 is found to be missing in the ΔV region between 8 and 9 eV

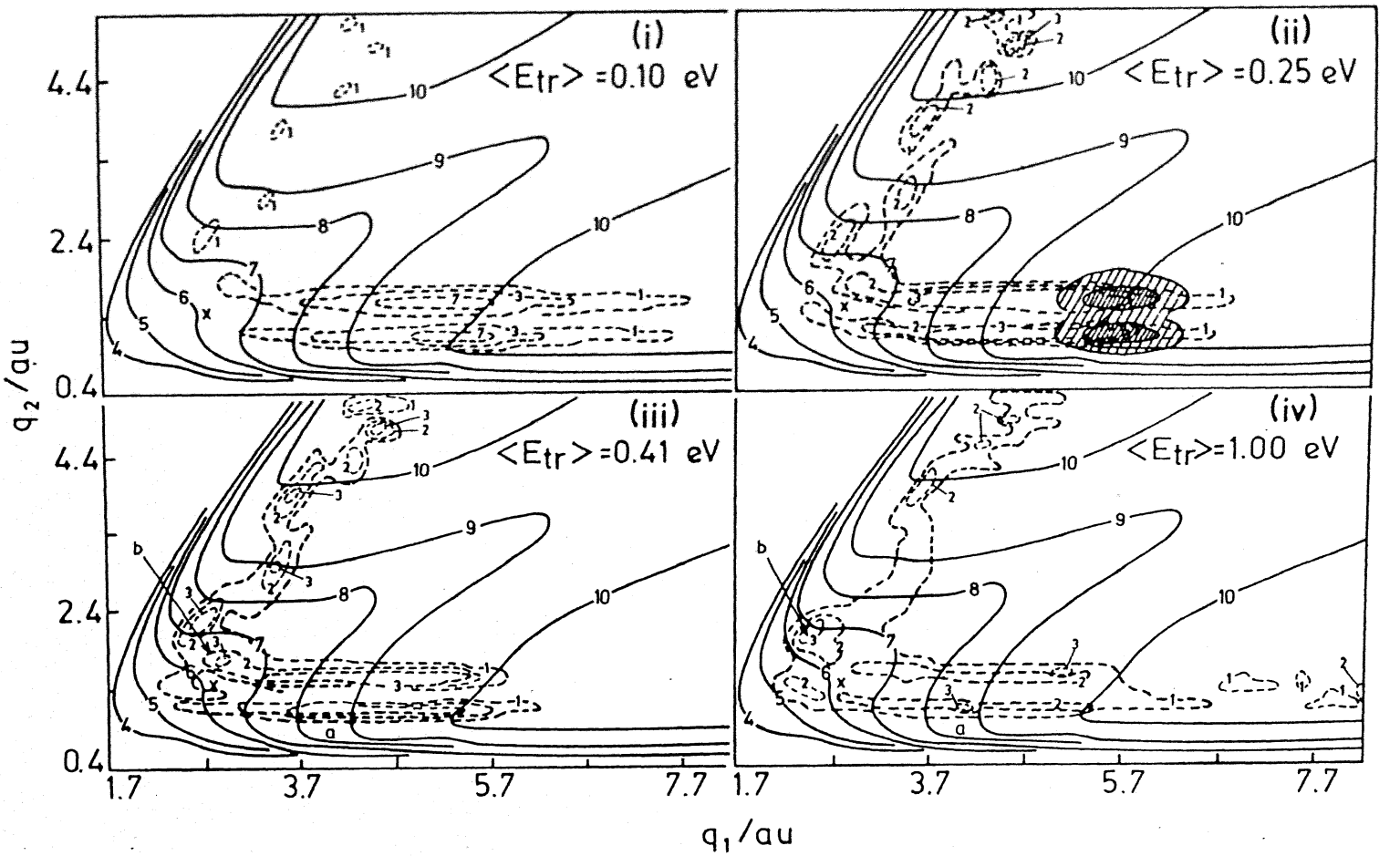

Fig. 11. Cumulative probability density function in the configuration space for $H_2(v=1)+H$ is indicated by dashed lines along with the numbers indicating its relative magnitude. The solid lines represent ΔV contours with numbers indicating the values in eV. The hatched portion in panel (ii) indicates the PDF at time t = 0. a and b indicate the PDF corresponding to the peaks in Fig. 10. X indicates the saddle point

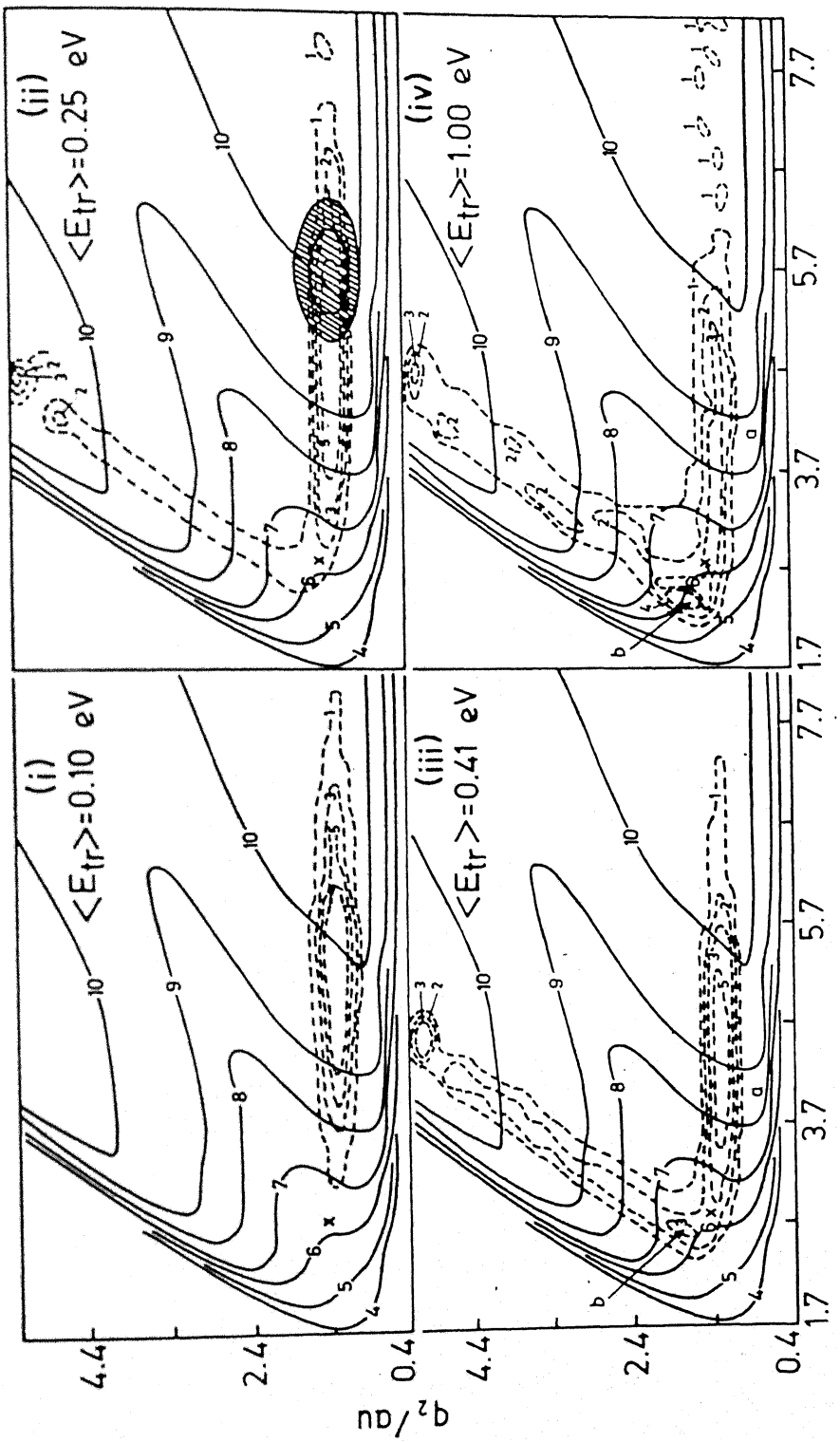

Fig. 12. Same as in Fig. 11 for H_2 (v = 0)

and hence the intensity of the peak " a " falls off. But there is a build up of the PDF marked 4 in the ΔV region between 5 & 6 eV explaining the increase in the intensity of the peak "b" with increase in $\langle E_{tr} \rangle$.

Within the resolution of our spectra, we do not see any significant effect of vibrational effect of H_2 on the spectrum of the TS.

Transition state spectra, computed for thermal distributions of $H + H_2$ at 300 and 1000 K are displayed in Fig. 13. In contrast to the spectra for fixed $\langle E_{tr} \rangle$ (in Fig. 11-12), the spectra in Fig. 13 do not show any significant "far" wing as the $\langle E_{tr} \rangle$ corresponding to T = 300 and 1000 K are only 0.03 and 0.09 eV. The PDF plots in Fig. 14 show that the WP is confined to the entry valley and does not reach upto the inner repulsive wall because of the low $\langle E_{tr} \rangle$. This would explain why the "wings" were not discovered long ago, although atomic spectra have been recorded for a long time. We must add that the shoulder to the Lyman-α line becomes marked with increase in T from 300 to 1000 K in keeping with the observations made for the "fixed" $\langle E_{tr} \rangle$ results.

If the complementary information regarding the emission spectrum becomes available, the analysis of the TS spectrum would become easier. We have computed the emission spectrum of the TS for the same reaction (R2) by carrying out the dynamics on the PES for the excited state of H_3 that correlates with

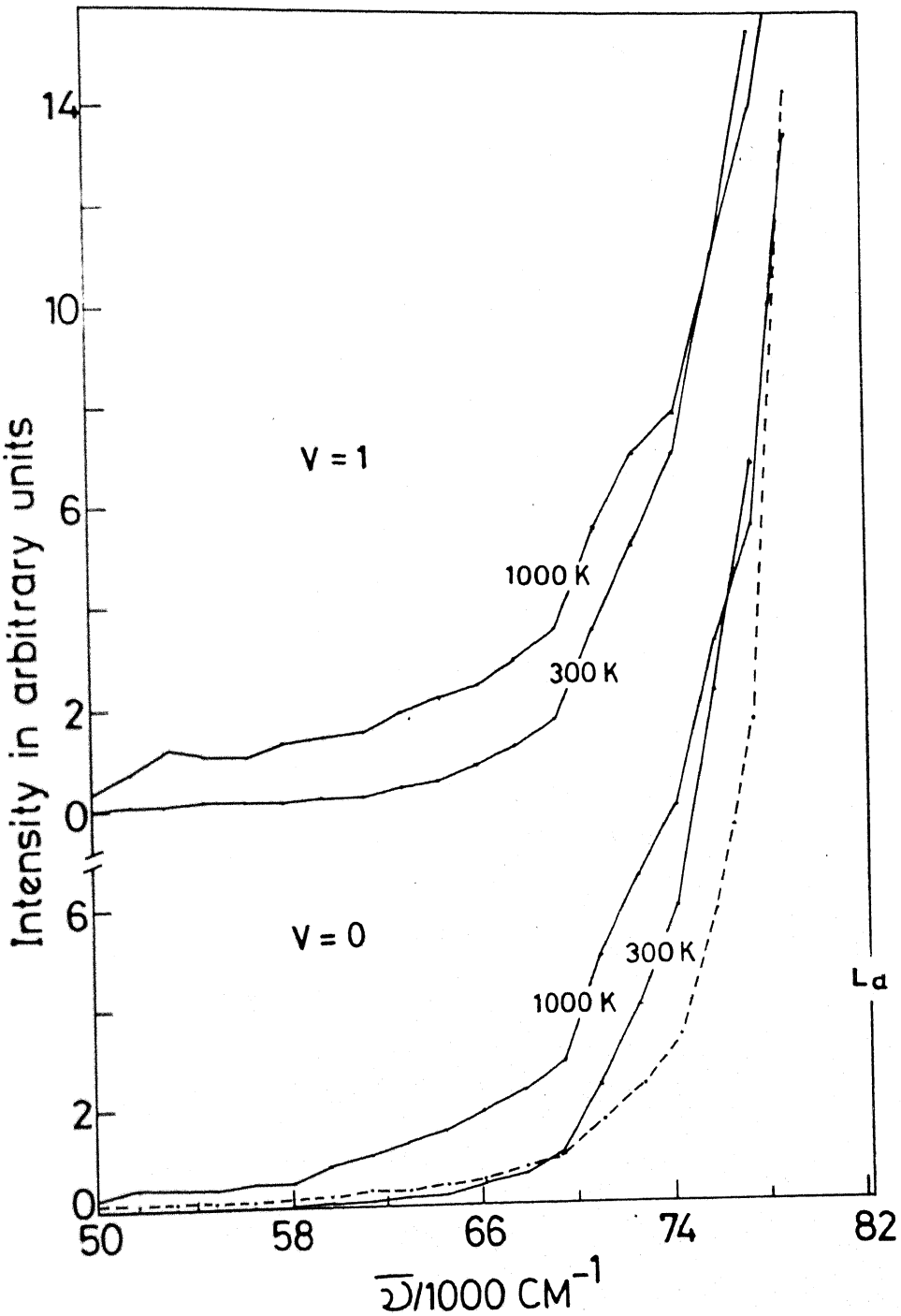

Fig. 13. Absorption spectra for $H_3^{\neq}$ for athermal distribution of H, H_2 (v = 0 and 1) at 300 and 1000 K. The dashed line indicates the spectrum obtained in the absence of any interaction between H and H_2 (at t = 0)

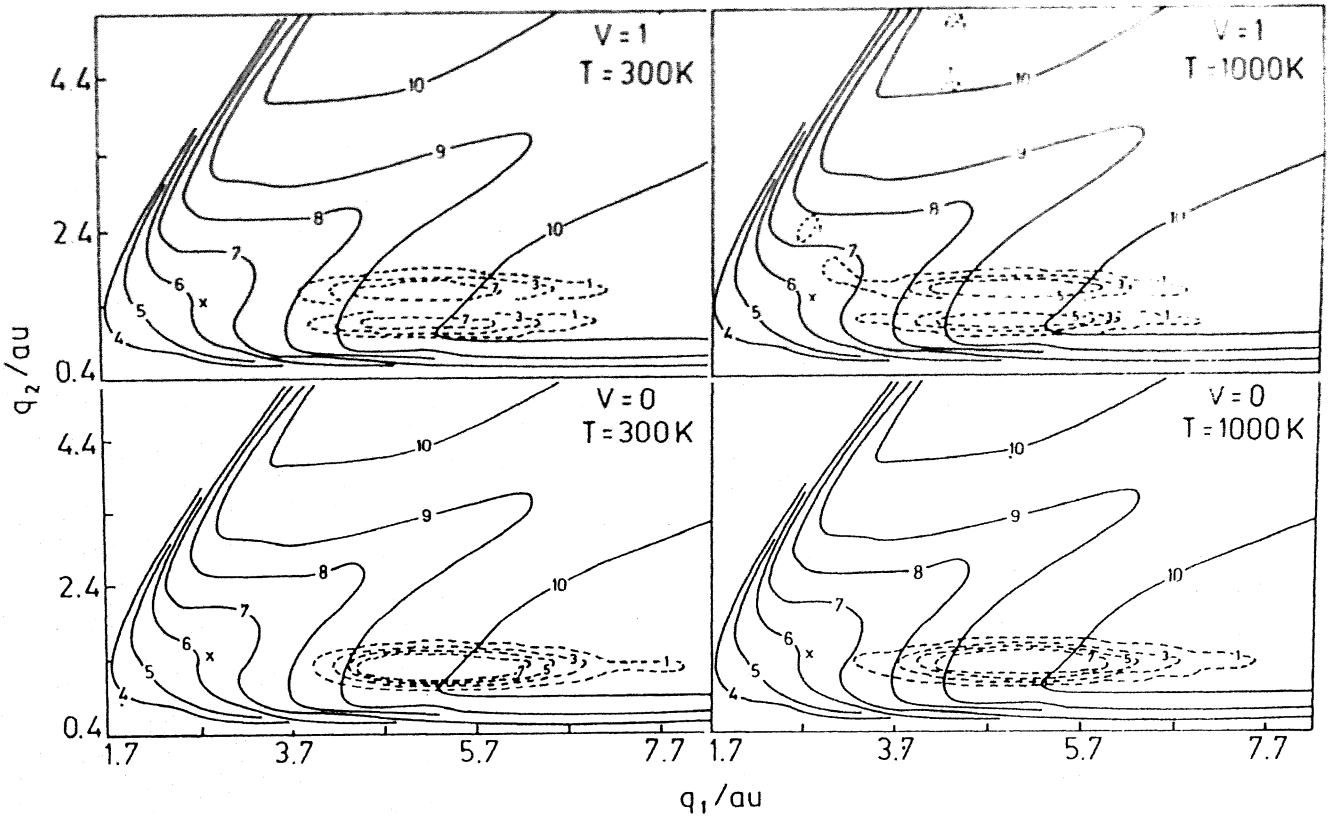

Fig. 14. Same as Fig. 11 but under different thermal distributions as indicated in each panel

$H^*(2p) + H_2$. Details of such a calculation and the results are reported in Chapter 3. The effect of including non-collinear geometries, a variable transition moment and transitions to other low-lying upper electronic states and its implications to an experimental observation of the wings to the Lyman-α line are currently under investigation.

CHAPTER 3

EMISSION SPECTRUM OF THE TRANSITION STATE $H_3^{\neq *}$

By recording the emission spectrum of the transition state for a chemical reaction, one can get a wealth of information about the dynamics of the system. From a knowledge of the total integrated intensity, the breadth and the spectral distribution of the wings, one can learn a great deal regarding the lifetime of the TS, preferred turning points on the PES, bending in the TS and attractive or repulsive character of the PES. That such a link exists between these factors have been demonstrated by preliminary theoretical investigations.[77,78] The TS in a reaction of the type (R1) reveals its existence and the time it spends at successive configurations by emitting radiation of corresponding frequency and intensity as illustrated schematically in Fig. 15.

Emission spectra of dissociating molecules appear to be particularly promising for obtaining detailed information on

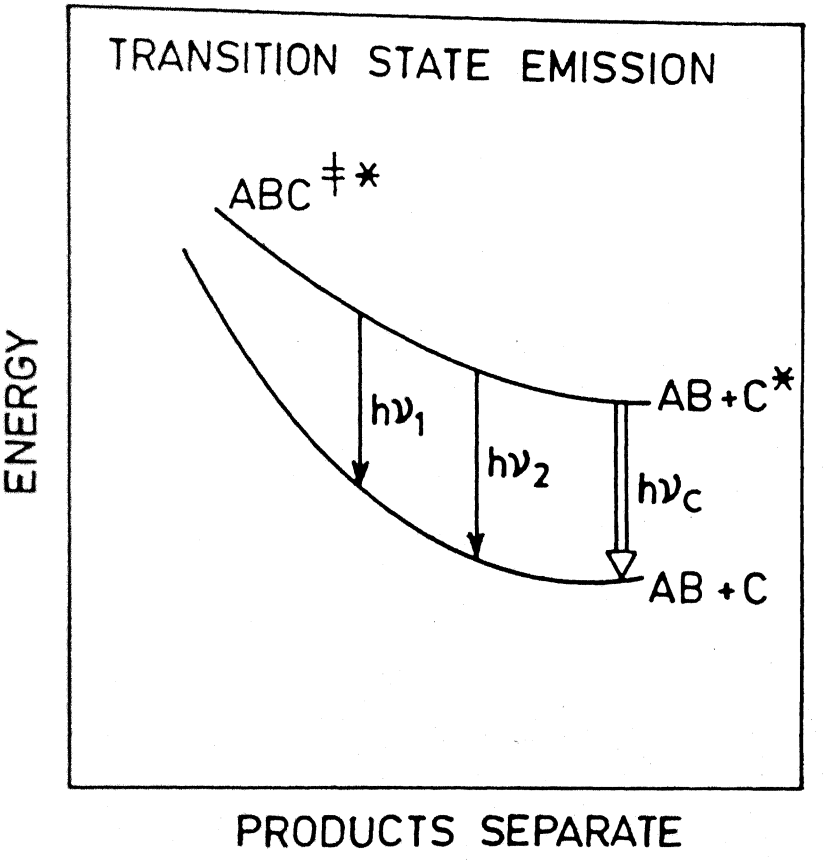

Fig. 15. Schematic diagram of emission from the TS in a typical chemical reaction. Emission from $ABC^{\neq *}$ during separation of products results in "wings" to the atomic transition

the TS for the corresponding bimolecular chemical reaction in the reverse direction.

It has been shown[19] that by recording the photoemission spectrum of (dissociating) polyatomic molecules, the geometry of the upper state PES near its saddle point could be determined and hence the possibility of spectroscopic probing of dynamics has been demonstrated. By his SC approach, Heller[7,12,13] has shown that such problems are amenable to theoretical treatment at present. In this approach, the ground-state initial wave-function (at $t = 0$) is transferred to the electronically excited state and then the time evolution of the WP is governed by the nuclear-motion Hamiltonian whose potential is that of the excited state. A simple Fourier transform in the time domain brings us to the frequency domain. Heller has shown that it is usually unnecessary to follow the complete evolution of the WP on the upper state and that short-time behaviour can be described adequately by simple SC dynamics. He also derived simple formulae to make it possible to infer the characteristics of the upper-state PES directly from the emission spectrum.

Imre and coworkers[19] have recorded the spectrum of O_3^* molecule. Conventional spectroscopic techniques could not be applied to study the excited states of O_3^* owing to their extremely short lifetimes. Some of the electronically excited states are not bound, thus leading to rapid dissociation. From an experimental knowledge of relative intensities of the

fundamental symmetric stretch (ν_1) and the first overtone of the asymmetric stretch (ν_3), they have been able to extract quantitative information regarding the excited state under study. By inserting their data in the relevant equation derived by Heller,[12a] they obtained a negative value for the second derivative of the potential with respect to the Q_3 normal coordinate, indicating that the upper PES has a maximum at the ground-state equilibrium geometry. This result has been vindicated subsequently by ab initio computations.[93]

In an attempt to complement our studies (Chapter 2) on the absorption spectrum of the TS for the reaction (R2), we have carried out a TDQM study to predict the emission spectrum of the TS for the same reaction. We have studied the dynamics on the PES for one of the low-lying excited states of H_3 that correlates with $H^*(2p) + H_2$ and considered the emission to the ground state. The same pair of PESs that were used in predicting the absorption spectrum in Chapter 2 have been used in the emission study.

The potential energy contour of the H_3^* PES has been displayed in Fig. 7. The initial wavefunction $\Psi(t=0)$ has been set up in the same manner as was described in Chapter 2. A 64×64 grid in the (q_1, q_2) space with $1.0 \leq q_1 \leq 7.3$ a.u. and $0.4 \leq q_2 \leq 6.7$ a.u. has been used. Attempts to use 3-point and 5-point FD schemes with $\Delta q = 0.1$ a.u. and $\Delta t = 0.01$ (the values that have been used in the absorption spectrum calculations)

failed. The norm in Ψ was not conserved. Since the PES has a well of about 4 eV [see Fig. 7], in a small range of the interaction region, we faced problems regarding the numerical stability of the solution. Therefore we had to choose a prohibitively small step-size in time, $\Delta t = 0.001$. The 7-point FD scheme with a mesh spacing of $\Delta q = 0.1$ a.u. had been used to compute the Laplacian of Ψ. We found that the norm in Ψ was conserved throughout the collision for the choice of these values of Δt and Δq. We are not surprised that for the choice of a small value of Δq, the 7-point FD scheme was stable (in contrast to the report we have made in Chapter 2). The difference, however, was due to the choice of a small value for Δt. An important factor in integrating partial differential equations [Eq.(1)] is the ratio $(\Delta q/\Delta t)$ and not Δq or Δt alone. Accordingly the ratio of Δq and Δt was adjusted and the deviation of the norm of Ψ from unity was closely followed, to ensure the accuracy of the calculation.

We have considered only collisions with the H_2 molecule in its ground vibrational state and $\langle E_{tr} \rangle = 0.1$ eV. We have used the explicit method (as described in Chapter 2) to time evolve Ψ and the results are shown in the form of contours of $\Psi^*\Psi$ at different time intervals in Fig. 16. It is interesting to note that the WP tends to spend considerable amount of time in the region of the configuration space where the well is located [panel (b) of Fig. 16]. We also obtain a $\langle P^R \rangle$ of 0.4

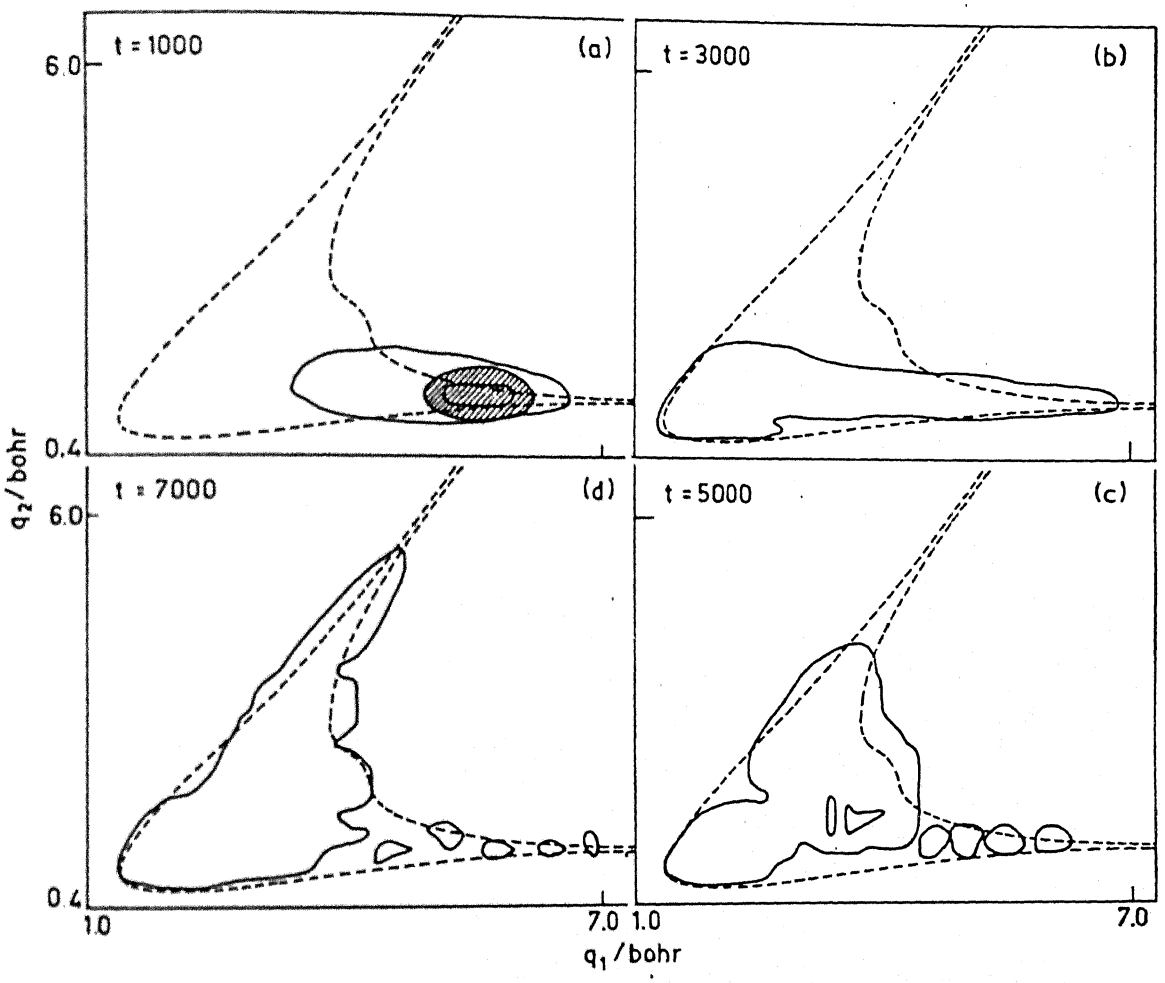

Fig. 16. The probability density of the system at different time intervals. The dashed line indicates the zero kcal/mole PE contour. The hatched region in panel (a) indicates the probability density at time t = 0. The probability density at different time intervals (indicated against each panel) has been shown by solid lines

in reasonable agreement with the quasiclassical trajectory result[94] obtained under identical conditions. At the end of the time evolution of the system, the probability density becomes smeared all over the configuration space [panel (d) in Fig. 16]. The same feature has also been observed in the QCT results.[94]

Using the procedure described in Chapter 2, we have generated the emission spectrum of the TS and the result is displayed in Fig. 17. Three prominent wings labelled "a" (77,500 cm^{-1}), "b" (75,000 cm^{-1}) and "c" (64,000 cm^{-1}) to the Lyman-α line have been predicted. In addition, in the far wing region a hump "d" around 52,500 cm^{-1} is also noticeable. Since the PDF distribution superimposed on the ΔV contours, shown in Fig. 18 is so complicated and since we have the results only for a single collision energy, we have not been able to clearly identify the wings with the build up of PDF in the corresponding region of the configuration space as we could do for the absorption spectrum. A more detailed study to understand the structure of the spectrum is in progress.

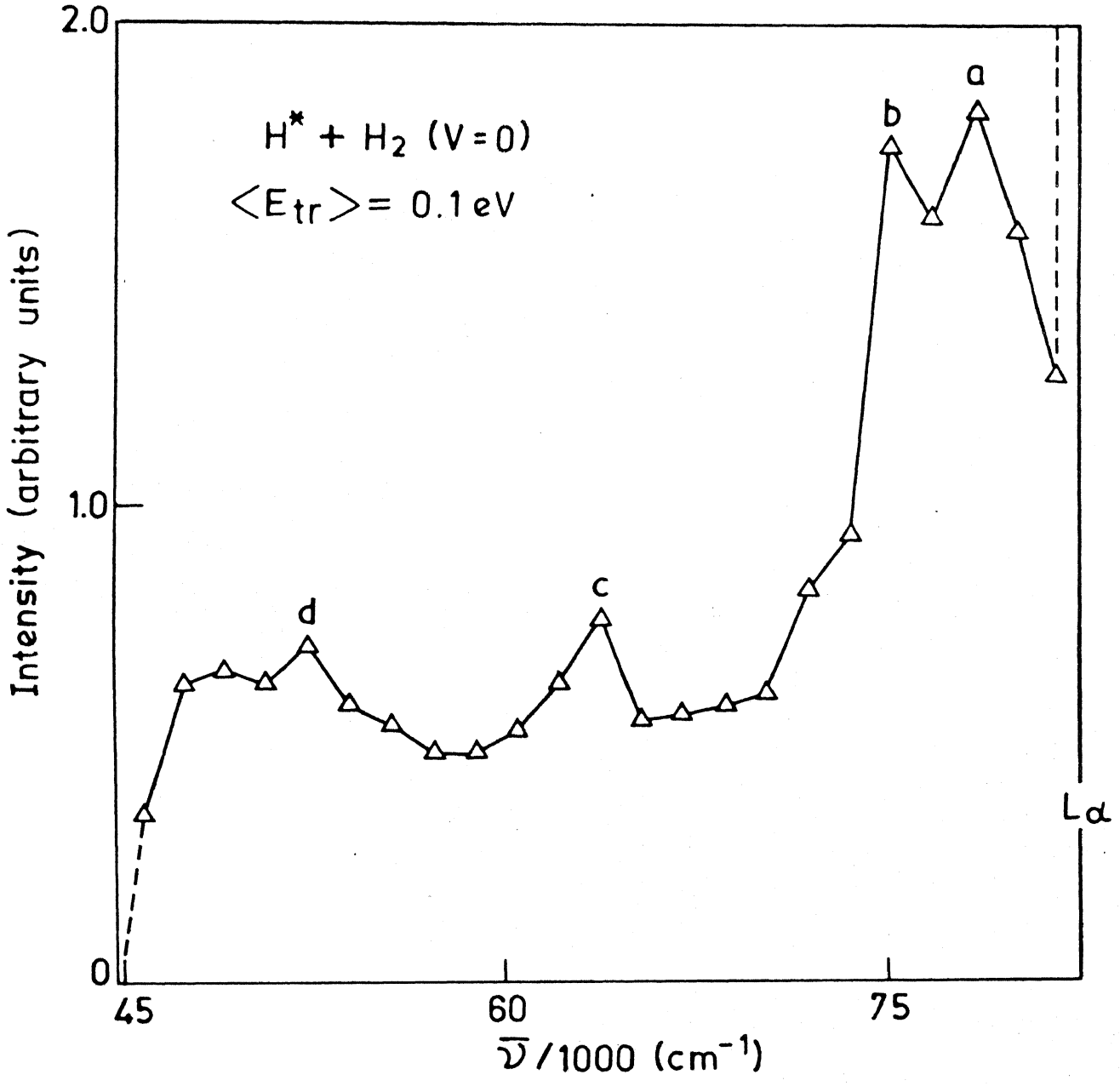

Fig. 17. Emission spectrum for $H_3^{\neq *}$ for a specified initial condition. L_α represents the Lyman-α line

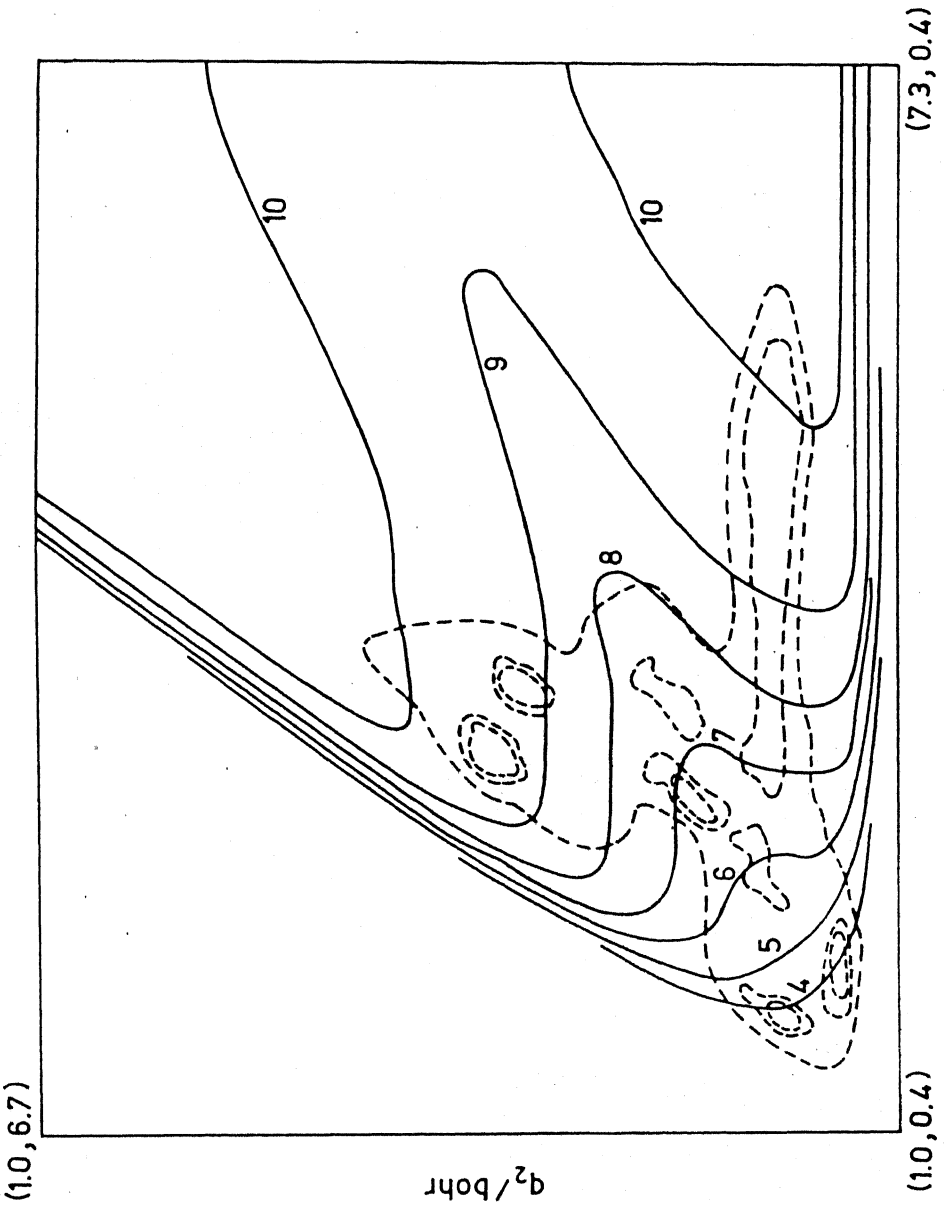

Fig. 18. The dashed line indicate the cumulative probability density in configuration space. The solid lines represent ΔV contours with numbers indicating the values in eV

CHAPTER 4

COLLISION-INDUCED DISSOCIATION IN COLLINEAR $H + H_2$ COLLISIONS

Collision-induced dissociation processes of the type

$$A + BC \longrightarrow A + B + C \qquad (R6)$$

play a vital role in the kinetics of high-temperature systems such as shock tubes and flames. They also have a special relevance in connection with unimolecular decay and three-body recombination processes. CID is also one of the many possible outcomes in high-energy crossed molecular beam reactions, electron attachment and charge transfer processes.

Considerable amount of experimental results on systems exhibiting CID has been available for some time.[95-98] Because of the difficulties associated in computing CID cross sections, this process has received less attention from theorists when compared to elastic, inelastic and exchange reaction processes.

The available theoretical results on CID processes are based on phase-space theory,[99,100] optical model,[101] QCT[102-107] and SC.[108-110] Results of a few time-independent QM calculations restricted to collinear geometries have also been reported.[36,111-113] The major difficulty in the latter approach is the presence of the dissociative continuum preventing a straightforward extension of the methods developed for studying inelastic and exchange reactive scattering processes. A comprehensive review of the close-coupling and QCT methods for CID calculations is given elsewhere.[114,115]

As has been pointed out in Chapter 1 of this thesis, the TDQM approach can be used to study CID processes with as much ease as for the exchange reaction. Very recently, the TDQM method has been used to study CID processes in several systems.[34,35,65-68] Although they have been restricted to collinear collisions, they have provided an insight into the dynamics of CID processes and have helped in assessing the validity of approximate methods.

In real systems, at high energies, the CID process may compete with an exchange process. An accurate quantal method should be able to incorporate such a possibility. The development of such accurate methods have been hindered by the difficulty of representing exchange product bound states in terms of the reagent bound and continuum states.[111,114] As a result, mostly systems in which exchange channel is absent have been

considered in previous studies.[65,112,113] Only recently, studies of systems in which exchange reaction may also occur, have been carried out.[34-36a] The TDQM method was first applied to CID processes by Ford et al.[65] using a model potential. In the TDQM approach the problem associated with a dissociative continuum is circumvented by a completely numerical description of the wavefunction and its time evolution. The disadvantage of the TDQM method is that it requires the solution of the TDSE for evolution of the wavefunction over a long period of time corresponding to the entire collision event. With the advent of fast computing machines, this is not a serious problem anymore.

Kulander[34a] reported the results of a collinear CID calculation for the first time, employing a realistic PES that corresponded to (H, H_2) system. He solved the TDSE for the chosen WPs and projected the time-evolved wavefunction onto the asymptotic eigenstates of the system to extract state-to-state transition probabilities. He used a 5-point FD scheme to compute the Laplacian of Ψ and a fifth order predictor-corrector method to time evolve the system. No exchange reaction was observed around the energetic threshold (E_{th}^{en}) for dissociation. The dynamical threshold (E_{th}^{dy}) for dissociation was substantially larger than the E_{th}^{en} for the ground ($v=0$) and first excited ($v=1$) state of the molecule. However, when the H_2 molecule was excited to $v=4$ state, substantial

dissociation occurred. Gray et al.[106] observed no dissociation for v = 0 and 1 states of the H_2 molecule, when the calculations were carried out using the QCT method for the same system under identical conditions. Subsequently the quantal calculations were repeated[66] to compare quantitatively the quantal results with the QCT results[66] and the same trend was observed. Quantal P^D was only 0.1 for v = 0 and 1 states of the molecule at $\langle E_{tr} \rangle$ as high as 12 eV. QCT results snowed no dissociation at all upto the $\langle E_{tr} \rangle$ considered.

Leforestier et al.[67] have carried out a TDQM study in order to assess the validity of the SC approach[110] to CID processes. Their system consisted of a Morse oscillator interacting through an exponential repulsive potential (MOEXP) and hence did not allow the possibility of an exchange reaction. They used a 7-point FD scheme to compute the Laplacian of Ψ and the explicit method for the time evolution of the system.[31] They found the E_{th}^{dy} to be twice the E_{th}^{en}. More recently, they have extended[68] their study to compute P^D with the molecule under attack in different initial vibrational states. In this study also, they observed the E_{th}^{dy} to be twice the E_{th}^{en}. They attributed it to the collinearity of the model. 3D QCT results[107] suggest that the CID process takes place mainly by non-collinear collisions. The good agreement between quantal and the SC dissociation probabilities showed[67,68] that the latter

had carried out a TDQM study of the CID process in (H,HD) system where inelastic and exchange scattering also occurred simultaneously. He used a modified LEPS surface; a 7-point FD scheme to compute the Laplacian of Ψ and the MW algorithm[29] for the time evolution of the system. Both the E_{th}^{dy} and the E_{th}^{en} coincided with one another. Earlier workers[36a,b] had also obtained a similar result. This effect is attributed to the fact that energy transfer is more efficient in reactive collisions than in inelastic ones.

Recent 3D QCT calculations[116] for three different systems (H,H_2), (He,H_2^+) and (He,H_2) on accurate ab initio PESs indicate the near coincidence of the E_{th}^{dy} for dissociation with that of the E_{th}^{en} for two of the three systems. While (H, H_2) and (He, H_2^+) are potentially reactive systems, (He, H_2) system is not. Hence for the latter system $E_{th}^{dy} \sim 2E_{th}^{en}$. The basic difference between the results for the different systems have been attributed to the difference in the shape of the PES involved. A more comprehensive study is needed to understand the factors governing CID processes.

We have carried out a TDQM study of the CID process in collinear (H, H_2) system over a wide range of energy. We have used the chemically accurate SLTH surface for the system. The molecule has been represented by a Morse oscillator and the classical dissociation energy has a value of 4.75 eV. We have used a 7-point FD scheme to compute the Laplacian and the

explicit method to time-evolve the system. Because of the high collision energies involved, we had to use a small step-size in time, $\Delta t = 0.001$. A 64×64 computational grid in (q_1, q_2) space with $1.0 \leq q_1 \leq 7.3$ a.u. and $0.4 \leq q_2 \leq 6.7$ a.u. and $\Delta q_1 = \Delta q_2 = 0.1$ a.u. has been used. At energies well below the dissociation threshold we observed substantial exchange reaction probability which became zero around E_{th}^{en}. When the molecule was chosen in its ground vibrational state ($v = 0$), no dissociation was found to occur even at $\langle E_{tr} \rangle$ energies as high as 10.0 eV. But when the molecule had been chosen initially in its first excited state ($v = 1$), at the corresponding $\langle E_{tr} \rangle$, the dissociation probability rose to around ten per cent. Thus, the E_{th}^{dy} has been found to be twice the E_{th}^{en} for the first vibrational state, in accord with earlier reported results[106] for the same system but on an LEPS surface using the QCT method. Our results thus agree qualitatively with other quantal results.[34,66]

In confirmity with earlier explanations, we also find that the difference in the dynamical and energetic thresholds arises mainly from the constraint that the three nuclei lie along a straight line. Also, this feature has been attributed to the fact that the exchange reaction probability is identically zero at E_{th}^{en}. We have also observed this behaviour as is illustrated in Fig. 19. Fig. 20 shows the probability densities at different time intervals during the evolution, for v=0 state

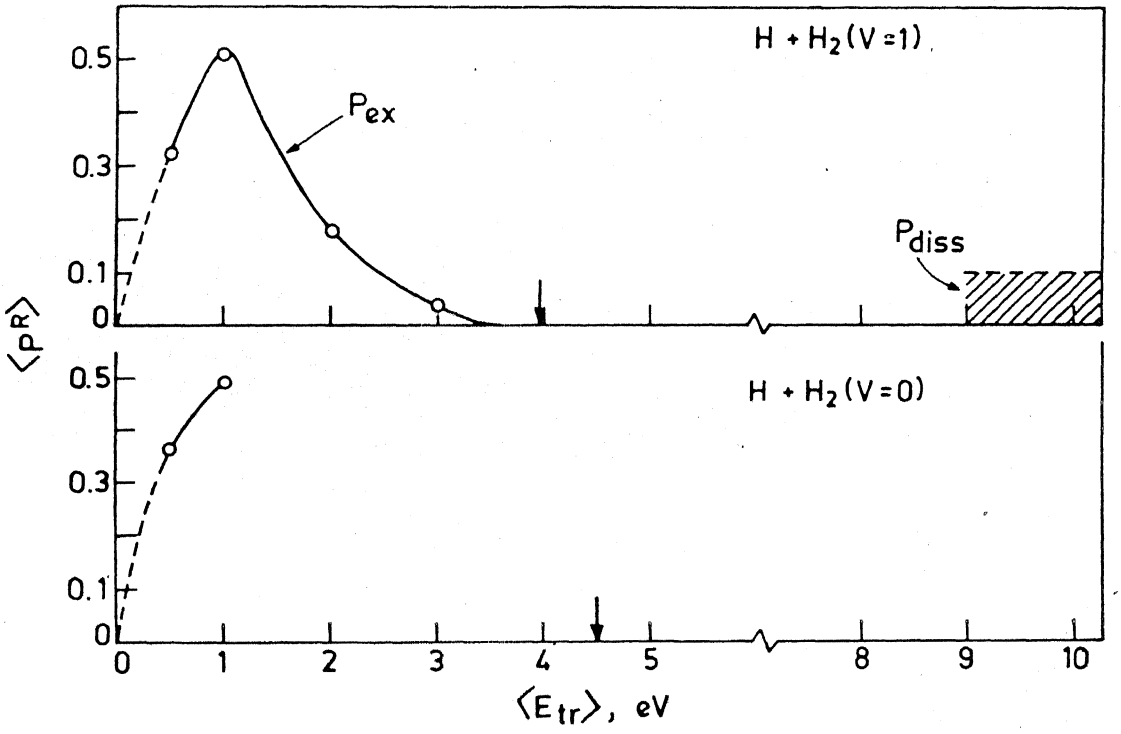

Fig. 19. Exchange and dissociation probabilities as a function of collision energy. The arrows indicate the energetic threshold for dissociation. Note that P^D = 0.0 for v = 0 of H_2 molecule. The hatched portion indicates an upper bound for P^D

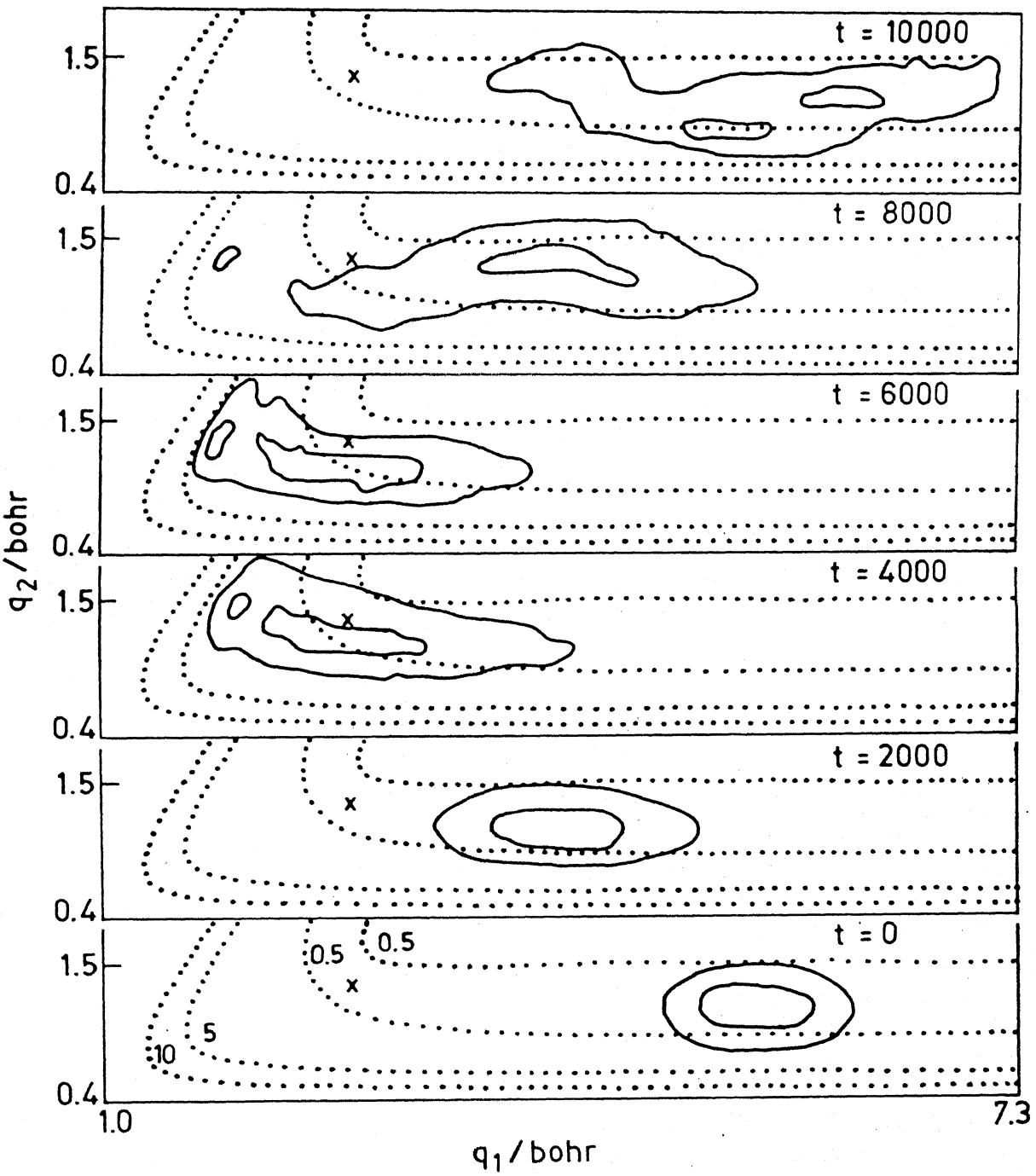

Fig. 20. Probability densities in the configuration space at different time intervals for v = 0, $< E_{tr} >$ = 10.0 eV. The dotted lines are PE contours with values indicated in eV against them. The solid lines are the contours of $\Psi^*\Psi$. X indicates the saddle point.

of the molecule at $\langle E_{tr} \rangle$ = 10.0 eV. It is evident that there is a large amount of elastic scattering. A close inspection of Fig. 20 reveals that the WP is reflected off the repulsive wall of the PES. In Fig. 21, the time evolution of the system with the molecule in its first vibrationally excited state has been depicted. The node in the initial wavefunction is retained even at the end of the collision. Moreover, additional nodal structures become apparent, suggesting a propensity rule for vibrational excitation, $\Delta v = 2$. This observation can be verified if we project the final wavefunction onto the asymptotic eigenstates of the reagents and compute the state-to-state transition probabilities. A more detailed study is in progress.

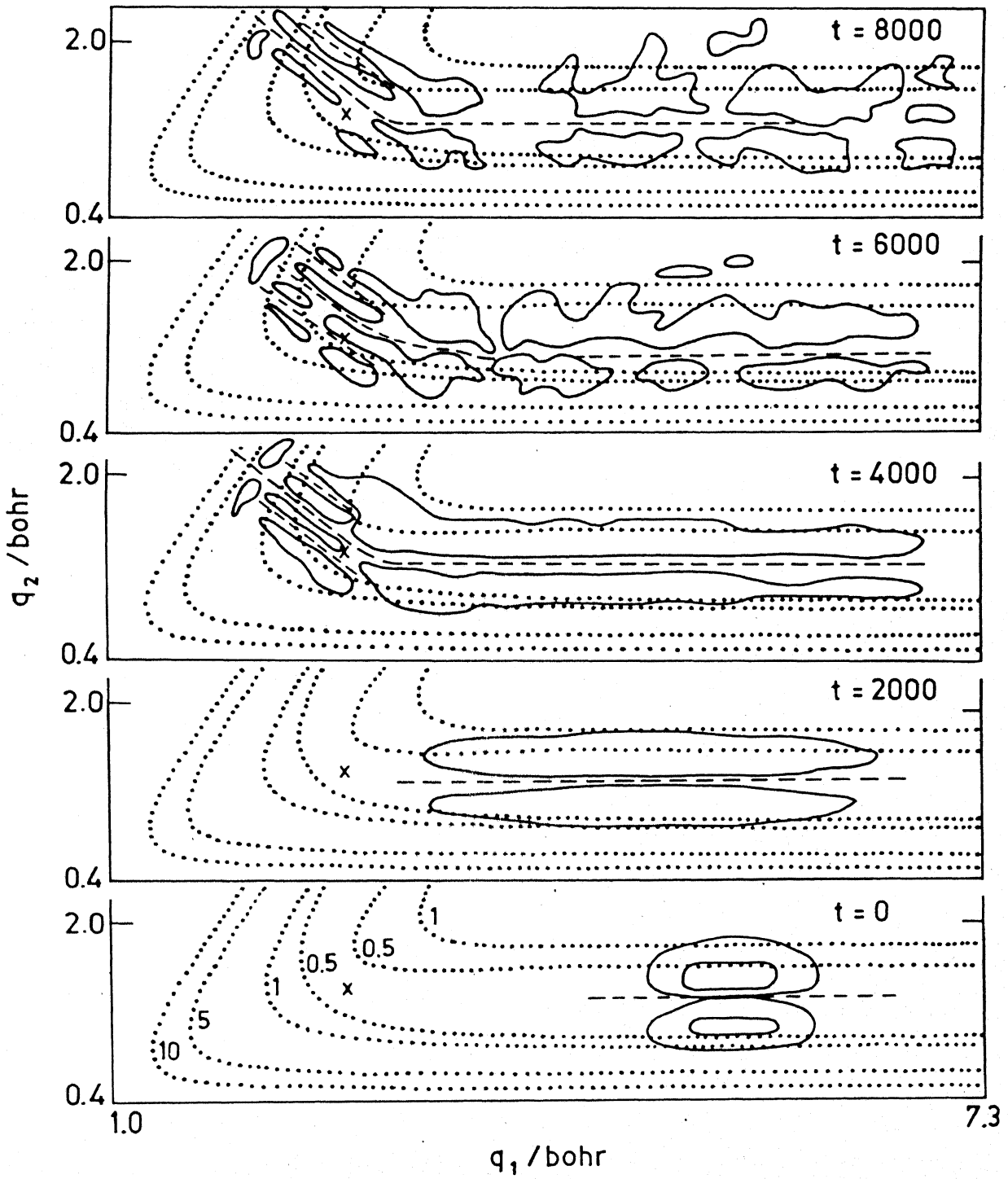

Fig. 21. Same as Fig. 20, for v = 1, $\langle E_{tr} \rangle$ = 10.0 eV. The dashed line indicates the nodal structure in the wavefunction

CHAPTER 5

SUMMARY AND CONCLUSION

We have reviewed the different computational methods that are available till to-date to carry out a study of reactive scattering processes using the TDQM approach and their applications to problems of chemical interest. We have carried out a comparative study of the different algorithms to compute the Laplacian of the wavefunction. Even though the FT method makes use of the accurate nonlocal approximation, it has been shown that it is computationally fifteen times slower than the FD schemes, for the same level of accuracy.

We have predicted the absorption spectrum of the TS for the collinear reaction (R2) by solving the TDSE for nuclear motion on the chemically accurate SLTH PES. We have made use of the explicit method for the time evolution of the system.

For the upper surface, we have used a DIM PES, that corresponds to $H^*(2p)+H_2$. Absorption from the lower (SLTH) PES

to this surface been predicted, assuming constant transition moment. The wings to the Lyman-α line have been interpreted in terms of the build up of the PDF near the inner repulsive wall of the PES. The effect of varying relative translational energy of the reactants and the vibrational state of the molecule have been investigated. As the collision energy is increased, the intensity of the wing close to the Lyman-α line falls off and the intensity of the far wing increases. Vibrational excitation of the molecule does not affect the features of the spectrum. Our results are in agreement with those obtained by using the time-independent QM[90] approach as well as the QCT[86,88] approach. We have computed the TS spectra for thermal distributions of $H + H_2$, at 300 and 1000 K. We did not observe any wings to the Lyman-α line under thermal conditions as $\langle E_{tr} \rangle$ that corresponds to these temperatures is too low to give rise to observable wings.

We have carried out a dynamical study on the H_3^* PES which has a potential well of ~ 4 eV using the TDQM approach. A 7-point FD scheme to evaluate the Laplacian and the explicit method for time evolution of the system have been used. By generating the PDF on this PES, we have predicted the emission spectrum of the TS and it is shown to be complementary to the absorption spectrum results reported in Chapter 2.

We have investigated the CID process in the collinear $H + H_2$ collisions (R6) in detail, on the chemically accurate

SLTH surface, using the TDQM approach. We have computed the exchange and dissociation probabilities over a wide range of $\langle E_{tr} \rangle$ (0.5 - 10.0 eV). No dissociation has been found to occur with the molecule in its ground vibrational state (v = 0) even at the highest $\langle E_{tr} \rangle$ studied. For v = 1 state of the molecule, E_{th}^{dy} has been found to be greater than twice the E_{th}^{en}. This feature, we have attributed (in conformity with the results of earlier workers) to the fact that the exchange reaction probability is zero around E_{th}^{en} for dissociation. Both the dynamical and energetic thresholds have been reported in the literature to coincide with each other for systems wherein the dissociative process is accompanied by the reactive (exchange) process. This feature had been explained in terms of the efficient transfer of energy in reactive in reactive rather than inelastic collisions

Our results are in agreement with other results computed by using TDQM[34,66] and QCT[106] methods. Recent 3D QCT[116] results (on the same PES) for the same system indicate that both the thresholds (E_{th}^{en} and E_{th}^{dy}) agree well with each other. Since experimental results[96] and other 3D QCT[107] calculations on similar systems have also shown that both these thresholds usually match, we have rationalised the difference between the two thresholds we have observed to be an artefact of the collinear model. In addition, careful inspection of the PDF plots of the system with the molecule in its v = 1 state revealed new nodal structures, in addition to the node present in the initial wavefunction. This fact suggests that this collisional process may be governed b

a propensity rule for vibrational excitation to be $\Delta v = 2$. To the best of our knowledge, ours is the first result on the CID process for the collinear (H, H_2) system making use of the accurate ab initio PES. A more detailed study is in progress.

REFERENCES

1. P.A.M. Dirac, Proc. Roy. Soc. (London), 123A, 714 (1929).
2. D.J. Kouri and M. Baer, Chem. Phys. Lett., 24, 37 (1974).
3. a) A. Kuppermann and G.C. Schatz, J. Chem. Phys., 62, 2502 (1975).
   b) G.C. Schatz and A. Kuppermann, J. Chem. Phys., 65, 4668 (1976).
   c) A.B. Elkowitz and R.E. Wyatt, J. Chem. Phys., 62, 2504 (1975); 63, 702 (1975).
4. a) R.B. Walker, E.B. Stechel and J.C. Light, J. Chem. Phys., 69, 2922 (1978).
   b) G.C. Schatz (private communication).
5. a) B. Liu, J. Chem. Phys., 58, 1925 (1973); 80, 581 (1984).
   b) P. Siegbahn and B. Liu, J. Chem. Phys., 68, 2457 (1978).
   c) D.G. Truhlar and C.J. Horowitz, J. Chem. Phys., 68, 2466 (1978); 71, 1514(E) (1979).
6. P.A.M. Dirac, Quantum Mechanics (Oxford Univ. Press, London), 1958.
7. E.J. Heller, J. Chem. Phys., 62, 1544 (1975).
8. E.J. Heller, J. Chem. Phys., 68, 2066 (1978).
9. E.J. Heller, J. Chem. Phys., 68, 3891 (1978).
10. a) K.C. Kulander and E.J. Heller, J. Chem. Phys., 69, 2439 (1978).
    b) S.Y. Lee and E.J. Heller, J. Chem. Phys., 76, 3035 (1982).
11. R.C. Brown and E.J. Heller, J. Chem. Phys., 75, 186 (1981).
12. a) E.J. Heller, R. Sundberg and D. Tannor, J. Phys. Chem., 86, 1822 (1982).
    b) D.J. Tannor and E.J. Heller, J. Chem. Phys., 77, 202 (1982).

13. E.J. Heller, Acc. Chem. Res., 14, 368 (1981).

14. E.J. Heller, J. Chem. Phys., 72, 1337 (1980).

15. E.J. Heller and M.J. Davis, J. Phys. Chem., 85, 307 (1981).

16. M.J. Davis and E.J. Heller, J. Chem. Phys., 75, 246 (1981).

17. G. Drolshagen and E.J. Heller, J. Chem. Phys., 79, 2072 (1983).

18. G. Drolshagen and E.J. Heller, Surf. Sci., 139, 260 (1984).

19. D.G. Imre, J.L. Kinsey, R.W. Field and D.H. Katayama, J. Phys. Chem., 86, 2564 (1982).

20. D. Imre, J.L. Kinsey, A. Sinha and J. Krenos, J. Phys. Chem., 88, 3956 (1984).

21. R.D. Coalson and M. Karplus, Chem. Phys. Lett., 90, 301 (1982).

22. a) R.D. Coalson and M. Karplus, J. Chem. Phys., 79, 6150 (1983).
    b) B. Jackson and H. Metiu, J. Chem. Phys., 82, 5707 (1985).

23. R. Heather and H. Metiu, Chem. Phys. Lett., 118, 558 (1985).

24. S. Sawada, R. Heather, B. Jackson and H. Metiu, J. Chem. Phys., 83, 3009 (1985).

25. a) R.T. Skodje and D.G. Truhlar, J. Chem. Phys., 80, 3123 (1984).
    b) R.T. Skodje, Chem. Phys. Lett., 109, 227 (1984).

26. R. Heather, B. Jackson and H. Metiu (to be published).

27. J. Mazur and R.J. Rubin, J. Chem. Phys., 31, 1395 (1959).

28. H.F. Harmuth, J. Math. Phys., 36, 269 (1957).

29. E.A. McCullough and R.E. Wyatt, J. Chem. Phys., 51, 1253 (1969); 54, 3578 (1971); 54, 3592 (1971).

30. R.N. Porter and M. Karplus, J. Chem. Phys., 40, 1105 (1964).

31. A. Askar and C.S. Cakmak, J. Chem. Phys., 68, 2794 (1978).

32. D. Kosloff and R. Kosloff, J. Comput. Phys., 52, 35 (1983).

33. M.D. Feit, J.A. Fleck Jr. and A. Steiger, J. Comput. Phys., 47, 412 (1982).

34.a) K.C. Kulander, J. Chem. Phys., 69, 5064 (1978).

b) K.C. Kulander, Nucl. Phys. A., 353, 341 (1981).

35. C. Leforestier, Chem. Phys., 87, 241 (1984).

36. a) J.A. Kaye and A. Kuppermann, Chem. Phys. Lett., 78, 546 (1981).

b) J. Manz and J. Römlet, Chem. Phys. Lett., 77, 172 (1981).

37. P.M. Agrawal, V. Mohan and N. Sathyamurthy, Chem. Phys. Lett., 114, 343 (1985).

38. P.M. Agrawal and L.M. Raff, J. Chem. Phys., 77, 3946 (1982).

39. J.L. Jackson, Ph.D. Thesis, The University of Texas, Austin, USA, 1971.

40. G.E. Kellerhals, Ph.D. Thesis, Oklahoma State University, Stillwater, US.A., 1974.

41. G.E. Kellerhals, N. Sathyamurthy and L.M. Raff, J. Chem. Phys., 64, 818 (1976).

42. C. Stroud, N. Sathyamurthy, R. Rangarajan and L.M. Raff, Chem. Phys. Lett., 48, 350 (1977).

43. H.J. Nussbaumer, Fast Fourier Transform and Convolution Algorithms, 2nd edition, Springer, Berlin, 1982.

44. R. Kosloff and D. Kosloff, J. Chem. Phys., 79, 1823 (1983).

45. H. Tal-Ezer and R. Kosloff, J. Chem. Phys., 81, 3967 (1984).

46. R.H. Bisseling and R. Kosloff, J. Comput. Phys., (to be published).

47. R.H. Bisseling, R. Kosloff, J. Manz and H.H.R. Schor, Ber. Bunsenges. Phys. Chem., 89, 270 (1985).

48. R.H. Bisseling, R. Kosloff and J. Manz, J. Chem. Phys., 83, 993 (1985).

49. T. Joseph and J. Manz, Mol. Phys.,(to be published).

50. M.D. Feit and J.A. Fleck Jr, J. Chem. Phys., 78, 301 (1983).

51. M.D. Feit and J.A. Fleck Jr., J. Chem. Phys., 80, 2578 (1983).

52. R.J. Rubin, J. Chem. Phys., 70, 4811 (1979).

53. P.M. Agrawal and L.M. Raff, J. Chem. Phys., 74, 5076 (1981).

54. P.J. Kuntz, in Modern Theoretical Chemistry, Vol. 2, ed. W.H. Miller (Plenum Press, New York), 1976.

55. G.D. Brabson, J. Chem. Ed., 50, 397 (1973).

56. P.M. Agrawal, N.C. Agrawal, R. Viswanathan and L.M. Raff, J. Chem. Phys., 80, 760 (1984).

57. R. Baierlein, Atoms and Information Theory, W.H. Freeman, San Francisco, 1970.

58. S.P. Gejji and N. Sathyamurthy (unpublished results).

59. B.C. Garrett, D.G. Truhlar, R.S. Grev and R.B. Walker, J. Chem. Phys., 73, 235 (1980).

60. D.K. Bondi, D.C. Clary, J.N.L. Connor, B.C. Garrett, and D.G. Truhlar, J. Chem. Phys., 76, 4896 (1982).

61. Ch. Zhurt, T. Kamal and L. Zülicke, Chem. Phys. Lett., 36, 396 (1975).

62. N. Sathyamurthy, G.E. Kellerhals and L.M. Raff, J. Chem. Phys., 64, 2259 (1976).

63. S. Thareja and N. Sathyamurthy, Mol. Phys., (to be published).

64. J.O. Hirschfelder and K.T. Tang, J. Chem. Phys., 64, 760 (1976).

65. L.W. Ford, D.J. Diestler and A.F. Wagner, J. Chem. Phys., 63, 2019 (1975).

66. G.C. Gray, G.A. Fraser, D.G. Truhlar and K.C. Kulander, J. Chem. Phys., 73, 5726 (1980).

67. C. Leforestier, G. Bergeron and P.C. Hiberty, Chem. Phys. Lett., 84, 385 (1981).

68. G. Bergeron, P.C. Hiberty and C. Leforestier, Chem. Phys., 93, 253 (1985).

69. A.T. Yinnon and R. Kosloff, Chem. Phys. Lett., 102, 216 (1983).

70. R.B. Gerber, A.T. Yinnon and R. Kosloff, Chem. Phys. Lett., 105, 523 (1984).

71. A.T. Yinnon, R. Kosloff and R.B. Gerber, Chem. Phys., 87, 441 (1984).

72. R. Kosloff and C. Cerjan, J. Chem. Phys., 81, 3722 (1984).

73. R.C. Mowrey and D.J. Kouri, Chem. Phys. Lett., 119, 285 (1985).

74. a) J.C. Polanyi, Faraday Discussion Chem. Soc., 67, 129 (1979).
b) H.F. Foth, J.C. Polanyi and H.H. Telle, J. Phys. Chem., 86, 5027 (1982).

75. P. Arrowsmith, F.E. Bartoszeck, S.H.P. Bly, T. Carrington Jr., P.E. Charters and J.C. Polanyi, J. Chem. Phys., 73, 5895 (1980).

76. P. Arrowsmith, S.H.P. Bly, P.E. Charters and J.C. Polanyi, J. Chem. Phys., 79, 283 (1983).

77. J.C. Polanyi and R.J. Wolf, J. Chem. Phys., 75, 5951 (1981).

78. T. Carrington Jr., J.C. Polanyi and R.J. Wolf, in: Physics of Electronic and Atomic Collisions, ed. S. Datz (North Holland, Amsterdam), 1982, p. 393.

79. P. Hering, P.R. Brooks, R.F. Curl Jr., R.S. Judson and R.S. Lowe, Phys. Rev. Lett., 44, 687 (1980).

80. T.C. Maguire, P.R. Brooks and R.F. Curl Jr., Phys. Rev. Lett., 50, 1918 (1983).

81. H.P. Grieneisen, H. Xue-Jing and K.L. Kompa, Chem. Phys. Lett., 82, 421 (1981).

82. B.E. Wilcomb and R.E. Burnham, J. Chem. Phys., 74, 6784 (1981).

83. P.R. Brooks, R.F. Curl Jr., and T.C. Maguire, Ber. Bunsenges. Phys. Chem., 86, 401 (1982).

84. R.B. Bernstein, Chemical Dynamics via Molecular Beam and Laser Techniques (Oxford Univ. Press, London), 1982.

85. H.J. Foth, H.R. Mayne, R.A. Poirier, J.C. Polanyi and H.H. Telle, Laser Chemistry, Vol. 2 (Harwood, New York), 1983, p. 229.

86. H.R. Mayne, R.A. Poirier and J.C. Polanyi, J. Chem. Phys., 80, 4025 (1984).

87. R.N. Porter and L.M. Raff, in: Dynamics of Molecular Collisions, Part B, ed. W.H. Miller (Plenum Press, New York), 1976.

88. H.R. Mayne, J.C. Polanyi, N. Sathyamurthy and S. Raynor, J. Phys. Chem., 88, 4064 (1984).

89. S. Raynor and D.R. Herschbach, J. Phys. Chem., 86, 1214 (1982).

90. V. Engel, Z. Bačić, R. Schinke and M. Shapiro, J. Chem. Phys., 82, 4844 (1985).

91. V. Engel and R. Schinke, Chem. Phys. Lett., 122, 103 (1985).

92. S. Sinha, N. Sathyamurthy and K. Banerjee, Proc. Ind. Acad. Sci., 96, 215 (1986).

93. P.J. Hay, R.T Pack, R.B. Walker and E.J. Heller, J. Phys. Chem., 86, 862 (1982).

94. A. Singhal, M.Sc. Project Report, Indian Institute of Technology, Kanpur, 1985.

95. W.A. Chupka, J. Berkowitz and M.E. Russell, VI ICPEAC,, ed. I. Amdur, MIT Press, 1969, p. 71.

96. F.P. Tully, Y.T. Lee and R.S. Berry, Chem. Phys. Lett., 9, 80 (1971).

97. E.K. Parks, N.J. Hansen and S. Waxler, J. Chem. Phys., 58, 5489 (1973); 58, 5502 (1973).

98. J. Schöttler and J.P. Toennies, Chem. Phys., 2, 137 (1973); 4, 24 (1974).

99. a) T.F. Moran and D.C. Fullerton, J. Chem. Phys., 54, 5231 (1971).
b) R. Huber and H.G. Weber, Chem. Phys., 35, 461 (1978).
c) V. Havemann, V. Pacák, Z. Herman, F. Schneider, Ch. Zuhrt and L. Zulicke, Chem. Phys., 28, 147 (1978).

100. C. Rebick and R.D. Levine, J. Chem. Phys., 58, 3942 (1973).

101. R.D. Levine and R.B. Bernstein, Chem. Phys. Lett., 11, 552 (1971).

102. S.W. Benson and G.C. Berend, J. Chem. Phys., 40, 1289 (1964).

103. H. Fan, J. Chem. Phys., 55, 4628 (1971).

104. W.H. Wong and G. Burns, 62, 1712 (1975).

105. R.E. Howard, R.E. Roberts and M.J. DelleDonne, J. Chem. Phys., 65, 3067 (1976).

106. J.C. Gray, G.A. Fraser and D.G. Truhlar, Chem. Phys. Lett., 68, 359 (1979).

107. T. Lehr and J.W. Birks, J. Chem. Phys., 70, 4843 (1979).

108. L.L. Johnson and R.E. Roberts, Chem. Phys. Lett., 7, 480 (1970).

109. R.D. Levine, Chem. Phys. Lett., 11, 109 (1971).

110. a) I. Rusinek and R.E. Roberts, J. Chem. Phys., 65, 872 (1976).

b)I.Rusinek and R.E. Roberts, J. Chem. Phys., 68, 1147 (1978).

c) I. Rusinek, J. Chem. Phys., 72, 4518 (1980).

111. G. Wolken Jr., J. Chem. Phys., 63, 528 (1975).

112. E.W. Knapp, D.J. Diestler and Y.W. Lin, Chem. Phys. Lett., 49, 379 (1977).

113. E.W. Knapp and D.J. Diestler, J. Chem. Phys., 67, 4969 (1977).

114. D.J. Diestler in: Atom-Molecule Collision Theory, ed. R.B. Bernstein (Plenum Press, New York), 1979.

115. P.J. Kuntz in: Atom-Molecule Collision Theory, ed. R.B. Bernstein (Plenum Press, New York), 1979.

116. J.E. Dove, M.E. Mandy, N. Sathyamurthy and T. Joseph, Chem. Phys. Lett (in press).

117. Numerical Algorithms Group, Mark 8 Library, Daresbury Laboratory, U.K.

APPENDIX A

The Fourier transform $F(w)$ of a function $f(x)$ is given by

$$F(w) = \int_{-\infty}^{\infty} f(x)\ e^{-iwx}\ dx \qquad ..(A1)$$

we evaluate the integral numerically, we consider the discrete Fourier transform (DFT):

$$F(w) \cong \sum_{n=0}^{N-1} f(n\Delta x)\ e^{-iw(n\Delta x)}\Delta x \qquad ..(A2)$$

where Δx is the sampling interval (mesh spacing). For equi-distant sampling points, Eq. (A2) becomes,

$$F(m\Delta w) = \Delta x \sum_{n=0}^{N-1} f(n\Delta x)\ e^{-i(m\Delta w)(n\Delta x)} \qquad .. (A3)$$

Standard softwares like the NAG[117] depend only on the summation indices and not the nature of the independent variable Therefore we rewrite Eq. (A3) in order for it to be compatible with the NAG[117] subroutine C06FCF as follows:

$$F_m = \Delta x \sum_{n=0}^{N-1} f_n\ e^{-i2\pi mn/N} \qquad .. (A4)$$

where $\Delta w\ \Delta x = 2\pi/N$; $0 \leqslant m \leqslant N-1$ .. (A5)

$$F_m = F(m\Delta w) \text{ and } f_n = f(n\Delta x) \qquad .. (A6)$$

In two dimensions Eq. (A4) becomes

$$F_{m_1,m_2} = \Delta x \sum_{n_1=0}^{N-1} e^{-im_1n_1 2\pi/N} \; \Delta y \sum_{n_2=0}^{N-1} f(n_1,n_2)\, e^{-im_2n_2 2\pi/N} \qquad ..(A7)$$

We have to evaluate the DFTs along the columns and with this result, subsequently evaluate the DFTs along the rows. This approach is called the row-column method because it can be viewed as equivalent to organising the input data into sets of row and column vectors in an array and performing the computation.

If the values of the function are known from the point $-N/2$ to the point $N/2 - 1$ at equidistant points, Eq. (A3) becomes

$$F(m\Delta w) = \Delta x \sum_{n=-N/2}^{N/2-1} f(n\Delta x)\, e^{-i(m\Delta w)(n\Delta x)} \qquad ..(A8)$$

where $-N/2 \leqslant m \leqslant N/2-1$

Change of indices

$$k = m + N/2 \quad ; \quad l = n + N/2 \qquad ..(A9)$$

leads to

$$F[(k-N/2)\Delta w] = \Delta x \sum_{l=0}^{N-1} f[(l-N/2)\Delta x]\, e^{-i(k-N/2)(l-N/2)2\pi/N} \qquad ..(A10)$$

which on simplification yields:

$$F[(k-N/2)\Delta w] = e^{i(k-N/2)\pi} \Delta x \sum_{l=0}^{N-1} (-1)^l f[(l-N/2)\Delta x] \cdot e^{-i2\pi kl/N} \quad ..(A11)$$

The second derivative of the function f(x) can be obtained using the properties of Fourier transform. The inverse Fourier transform of Eq. (A1) is

$$f(x) = \frac{1}{2\pi} \int_{-\infty}^{\infty} F(w)\, e^{iwx}\, dw \quad ..(A12)$$

The second derivative of f(x) with respect to x is

$$f''(x) = \frac{1}{2\pi} \int_{-\infty}^{\infty} -w^2 F(w)\, e^{iwx}\, dw \quad ..(A13)$$

Discretising Eq. (13) we obtain

$$f''(x) \cong \frac{1}{2\pi} \sum_{m=0}^{N-1} -(m\Delta w)^2 F(m\Delta w)\, e^{i(m\Delta w)x}\, \Delta w \quad ..(A14)$$

$$\cong \frac{-(\Delta w)^3}{2\pi} \sum_{m=0}^{N-1} m^2 F(m\Delta w)\, e^{i(m\Delta w)x} \quad ..(A15)$$

$$f''(n\Delta x) \cong \frac{-(\Delta w)^3}{2\pi} \sum_{m=0}^{N-1} m^2 F(m\Delta w)\, e^{i(m\Delta w)(n\Delta x)} \quad ..(A16)$$

$$f_n'' = -\frac{(\Delta w)^3}{2\pi} \sum_{m=0}^{N-1} m^2 F_m e^{imn2\pi/N} \qquad ..(A17)$$

In order to compute the second derivative, first the set $\{F_m\}$ has to be calculated using Eq. (4) with a knowledge of the set $\{f_n\}$. We have made use of the subroutine C06FCF of NAG[117] to compute $\{F_m\}$. The result has to be multiplied by $-m^2$, where m is defined as in Eq. (A5). Then we have to perform an inverse Fourier transform. For this, we have made use of the subroutine C06GCF of NAG[117] in conjunction with the subroutine C06FCF. The result when multiplied by the constants as in Eq. (A17), gives the desired second derivative.

In two dimensions Eq. (A17) becomes

$$f''(m\Delta x, n\Delta y) = \frac{\Delta w_x}{2\pi} \sum_{k=0}^{N-1} e^{i(k\Delta w_x)(m\Delta x)} \left[\frac{-(\Delta w_y)^3}{2\pi}\right] \times \sum_{l=0}^{N-1} (k^2 + l^2) F_{k,l} e^{i(l\Delta w_y)(n\Delta y)} \qquad ..(A18)$$

APPENDIX B

TIME-DEPENDENT WAVE MECHANICAL STUDY OF THE WINGS TO THE LYMAN-α LINE IN H + H_2 REACTIVE COLLISIONS

P.M. AGRAWAL [1], V. MOHAN [2] and N. SATHYAMURTHY
Department of Chemistry, Indian Institute of Technology, Kanpur-208016, India

Received 2 January 1985; in final form 24 January 1985

We have predicted the absorption spectrum of the transition state configurations for the collinear reaction $H + H_2 \rightarrow H_3^{\ddagger} \rightarrow H_2 + H$ by solving the time-dependent Schrödinger equation for the nuclear motion. The spectral features have been interpreted in terms of the build up of the probability density function in the inner repulsive wall of the potential-energy surface.

1. Introduction

It has been recognized in recent years [1] that it is possible to obtain the spectrum of the transition state $(TS)^{\ddagger}$ for elementary chemical reactions. Arrowsmith et al. [2,3] reported the emission spectrum of the TS for the reaction

$$Na_2 + F \rightarrow NaF + Na^* \qquad (R1)$$

by monitoring the "wings" to the sodium D-line emission. Polanyi and Wolf [4,5] interpreted the wings as arising from the emission from Na^* while the separating NaF is still in the vicinity. Brooks and co-workers [6–8] have reported evidence for absorption from the intermediate configurations in the reactions

$$K + HgBr_2 \rightarrow KBr + HgBr\,, \qquad (R2)$$

$$K + NaCl \rightarrow KCl + Na\,. \qquad (R3)$$

Such TS spectra can provide information on the collision dynamics complementary to what can be learned from state-to-state studies [9].

It is of fundamental interest to predict and observe the wings (if any) to the Lyman-α absorption (emission) line in $H + H_2$ collisions. Polanyi and co-workers [10,11] have computed the absorption spectrum for the TS for the collinear reaction

$$H + H_2 \rightarrow H_2 + H \qquad (R4)$$

by determining the probability density distribution for the TS on the chemically accurate Siegbahn–Liu–Truhlar–Horowitz (SLTH) [12,13] ab initio potential-energy surface (PES) using the quasiclassical trajectory (QCT) technique [14]. They assumed vertical transitions from the ground state to one of the low-lying excited states $^2\Pi$ in $D_{\infty h}$ geometry that correlates with $H^*(2p) + H_2$. A correlation diagram of different states for H_3 is presented in fig. 1 of ref. [15]. They used model PESs based on the available ab initio data for the upper PES. They studied the effect of increasing relative translational energy of reactants and reagent vibrational excitation on the features of the absorption spectrum. As the collision energy increased, the intensity of the spectrum diminished and there was a considerable red-shift for the wings to the Lyman-α line. Subsequently, they extended [15] their study to collisions in three dimensions (3D) using a diatomics-in-molecules [16] (DIM) surface for the upper state and concluded that the qualitative features of the spectrum remained while going from collinear geometry to 3D.

Recently, Engel et al. [17] have carried out time-independent quantum mechanical (QM) calculations

[1] Permanent address: School of Studies in Physics, Vikram University, Ujjain, Madhya Pradesh, India.

[2] In partial fulfillment of the requirements for the degree of Doctor of Philosophy.

[‡] We use the term transition state in a general sense to refer to all configurations intermediate between reactants and products.

and predicted the absorption spectrum for the collinear reaction (R4) for two different vibrational states ($v = 0$ and 1) of the hydrogen molecule and at collision energies below the reaction threshold (0.22 eV) using the same ground- and upper-state surfaces as Polanyi and co-workers did [11]. The QM and the QCT results agree with each other in the basic features and trends in the spectrum.

In this Letter, we report the results of a time-dependent wave mechanical calculation of the absorption spectrum for the same collinear reaction (R4) for $v = 0$ and 1, at two different collision energies, 0.41 and 1.00 eV, that are well above the reaction threshold, thus complementary to the results of ref. [17].

2. Computational method

The two-dimensional time-dependent Schrödinger equation

$$[(-\hbar^2/2\mu)(\partial^2/\partial q_1^2 + \partial^2/\partial q_2^2) + V(q_1, q_2)]\Psi = i\hbar\,\partial\Psi/\partial t\,, \quad (1)$$

where q_1 and q_2 are the scaled and skewed coordinates [18], has been solved using the explicit integration method described elsewhere [19]. An L-shaped box in the (q_1, q_2) space, $1.7 \leqslant q_1 \leqslant 8.19$ au and $0.4 \leqslant q_2 \leqslant 5.35$ au, enclosing the interaction region has been divided into a larger number of mesh points. The values of the time step Δt ($= 0.53875 \times 10^{-16}$ s) and the mesh spacing Δq ($\Delta q_1 = \Delta q_2 = 0.11$ au) have been chosen such that they meet the stability criterion for the explicit integration method [19]. The initial wavefunction $\Psi(t = 0)$ was chosen as

$$\Psi(t = 0) = \Psi(q_1, q_2) = \phi(q_1)\, X_n(q_2)\,, \quad (2)$$

where X_n is the nth state Morse oscillator wavefunction for the hydrogen molecule. $\phi(q_1)$ is the minimum uncertainty Gaussian wavepacket representing the relative translational motion, given by

$$\phi(q_1) = (2\pi\delta^2)^{-1/4} \times \exp[-(q_1 - q_{10})^2/4\delta^2 - ik_0 q_1]\,. \quad (3)$$

The momentum space distribution is given by its Fourier transform:

$$F(k) = (2\delta^2/\pi)^{1/4} \times \exp[-(k - k_0)^2\delta^2 + iq_{10}(k - k_0)]\,. \quad (4)$$

The average kinetic energy of this packet is

$$\langle E\rangle = (\hbar^2/2\mu)(k_0^2 + 1/4\delta^2)\,. \quad (5)$$

We have chosen $\delta = 0.25$ au; $q_{10} = 5.50$ au; and $k_0 = 5.75$ and 9.27 au for $\langle E\rangle = 0.41$ and 1.00 eV, respectively. The time evolution of the system on the SLTH surface described by eq. (1) was terminated at the time when the plot of the reaction probability as a function of time levelled off, as shown in fig. 1. We have checked the accuracy of our calculation by checking the normalization condition for Ψ throughout the time evolution of the system. In addition, we find that an average of the time-independent collinear reaction probability [20] over the translational energy distribution used for the wavepacket is in agreement with our reaction probability value for $v = 0$ at $\langle E\rangle = 0.41$ and 1.00 eV to within 10%.

The value of $\Psi^*\Psi\, dq_1\, dq_2$ over each area element represents the probability of the TS in that area element. The cumulative value of $\Psi^*\Psi\, dq_1\, dq_2$ over the entire time evolution period for each area element represents the intensity of the transition at an energy equal to the energy difference between the ground- and the excited-state surfaces in that area element.

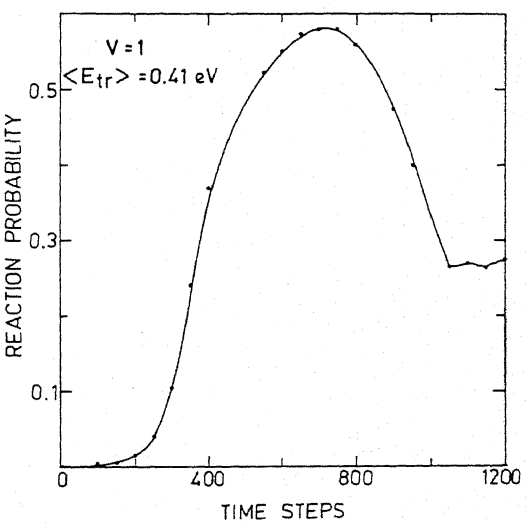

Fig. 1. Reaction probability as a function of time with each time step = 0.53875×10^{-16} s, for a specific initial condition.

We have used the DIM surface described in ref. [15] for the upper surface. We have assumed a constant electronic transition moment as was done by the earlier workers [11,15,17]. We have used a histogram width of 0.2 eV in reporting the spectrum.

3. Results and discussion

The resulting absorption spectra for $H_3^{\neq}$ for $\langle E \rangle$ = 0.41 and 1.00 eV for $v = 0$ and 1 are reported in fig. 2. It is clear that there are substantial wings to the Lyman-α line at the lower energy region. Two prominent peaks have been identified as a and b. With an increase in collision energy, the intensity of the peak close to the L_α line decreases and that of the peak in the lower-frequency region increases. Similar trends have also been reported by the earlier workers [11,15,17].

In fig. 3, the cumulative value of the probability density function (PDF) over the entire grid is superimposed over the difference potential contours ($\Delta V = V_U - V_L$, the difference in the potential energy between the ground- and the excited-state surfaces). Hence each configuration can be read as a spectral frequency ν, corresponding to the energy difference ΔV. The greater the PDF at any particular ΔV, the greater the absorption intensity at the corresponding ν. Thus the peaks in the absorption spectra can be identified with the accumulation of the PDF at a particular range of ΔV values. The peak labelled "a" (at

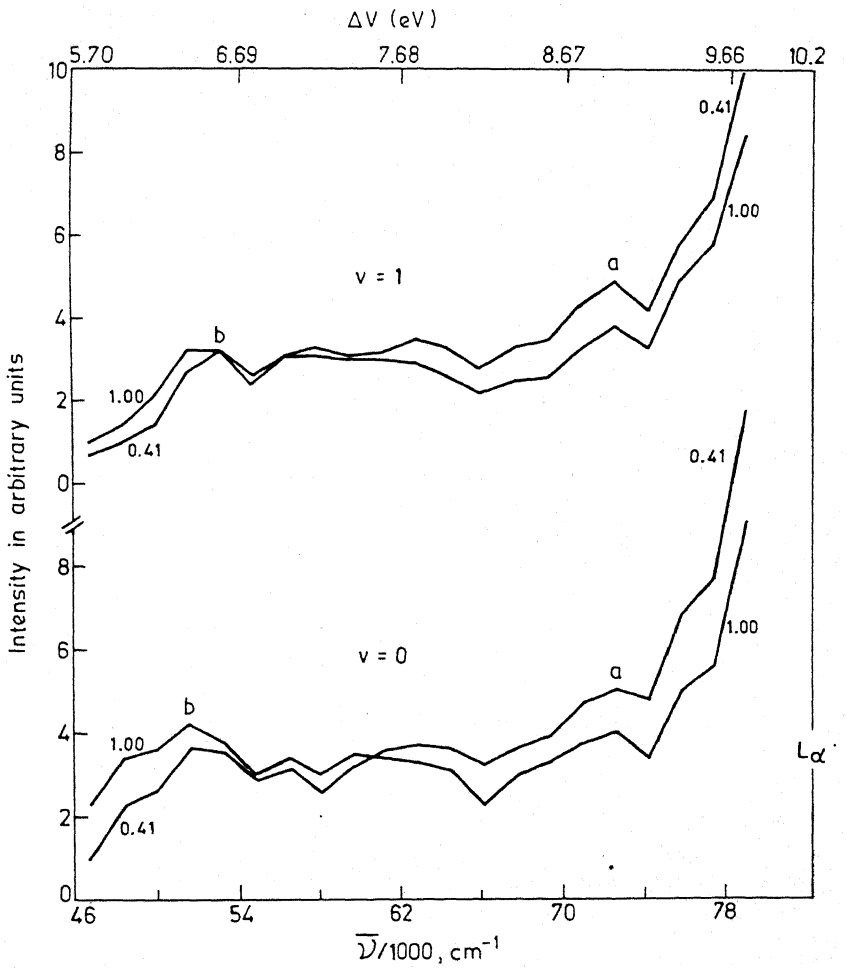

Fig. 2. Absorption spectra for $H_3^{\neq}$ under different initial consitions. Average collision energies are indicated against each spectrum. L_α represents the Lyman-α line.

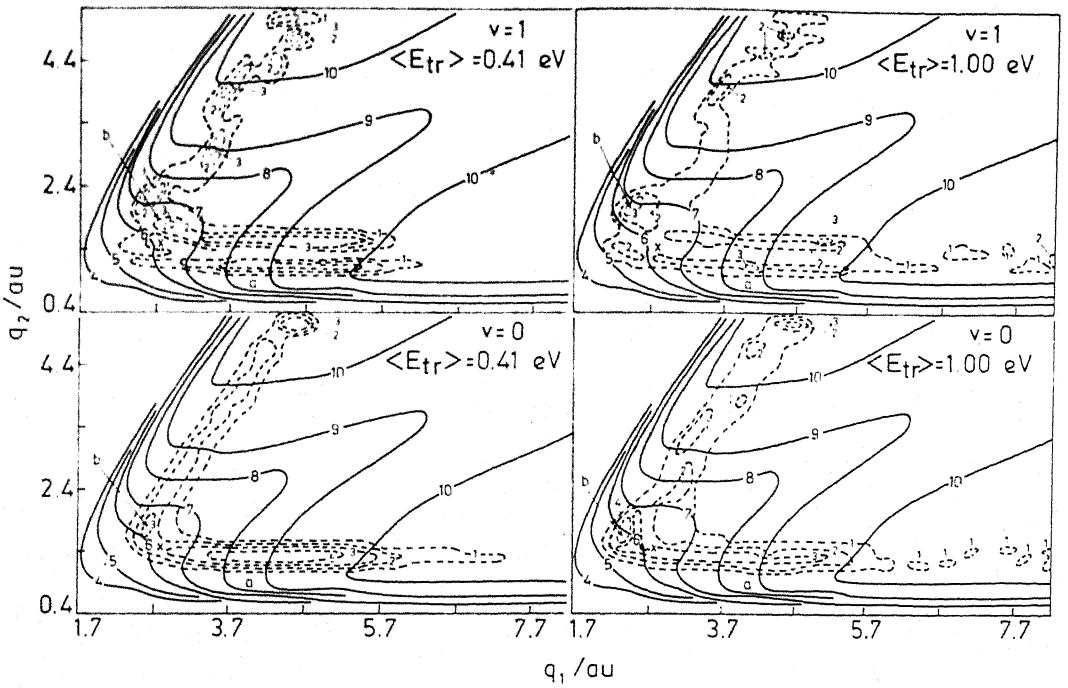

Fig. 3. Cumulative probability density function in the configuration space is indicated by dashed lines, along with numbers indicating its relative magnitude in different regions. The solid lines represent ΔV contours with the numbers indicating the values in eV. a and b indicate the PDF corresponding to the peaks in fig. 2. × indicates the saddle point.

72600 cm^{-1}) in fig. 2 for $\langle E \rangle$ = 0.41 eV arises due to the probability density contour (PDC) marked 3 and 5 running parallel to the q_1 axis in the ΔV region between 8 and 9 eV. The peak labelled "b" in the lower wave number region of the spectrum (at 51600 cm^{-1}) arises due to the build up of the PDF marked 3 near the saddle point. As the collision energy is increased to 1 eV, the PDC marked 5 is found to be missing in the ΔV region between 8 and 9 eV and hence the intensity of the peak "a" falls off. But there is a build up of the PDF marked 4 in the ΔV region between 5 and 6 eV explaining the increase in the intensity of the peak "b" with increase in $\langle E \rangle$.

It is interesting to note that increase in v from 0 to 1 does not affect the shape of the wings to any significant extent as was found by the earlier workers [11,15,17].

4. Conclusion

We have predicted the absorption spectrum for the TS for the collinear reaction (R4) using the SLTH surface for the ground state and a DIM surface for one of the upper states that correlates with $H^*(2p) + H_2$, using a constant electronic transition moment. Two prominent peaks have been identified and interpreted in terms of the build up of the PDF in the configuration space. The effect of including non-collinear collisions, a variable transition moment, and transition to the other low-lying upper electronic states and its implications to an experimental observation of the wings to the Lyman-α line are currently under investigation.

Acknowledgement

Calculations reported herein were carried out on the DEC-1090 computer at the Indian Institute of Technology, Kanpur. This study was supported in part by a grant from the Department of Science and Technology, New Delhi. We thank Professors John Polanyi and Howard Mayne for helpful correspondence and discussions.

References

[1] J.C. Polanyi, Faraday Discussions Chem. Soc. 67 (1979) 129.

[2] P. Arrowsmith, F.E. Bartoszeck, S.H.P. Bly, T. Carrington Jr., P.E. Charters and J.C. Polanyi, J. Chem. Phys. 73 (1980) 5895.

[3] P. Arrowsmith, S.H.P. Bly, P.E. Charters and J.C. Polanyi, J. Chem. Phys. 79 (1983) 283.

[4] J.C. Polanyi and R.J. Wolf, J. Chem. Phys. 75 (1981) 5951.

[5] T. Carrington Jr., J.C. Polanyi and R.J. Wolf, in: Physics of electronic and atomic collisions, ed. S. Datz (North-Holland, Amsterdam, 1982) p. 393.

[6] P. Hering, P.R. Brooks, R.F. Curl Jr., R.S. Judson and R.S. Lowe, Phys. Rev. Letters 44 (1980) 687.

[7] P.R. Brooks, R.F. Curl Jr. and T.C. Maguire, Ber. Bunsenges. Physik. Chem. 86 (1982) 401.

[8] T.C. Maguire, P.R. Brooks and R.F.Curl Jr., Phys. Rev. Letters 50 (1983) 1918.

[9] R.B. Bernstein, Chemical dynamics via molecular beam and laser techniques (Oxford Univ. Press, London, 1982).

[10] H.J. Foth, H.R. Mayne, R.A. Poirier, J.C. Polanyi and H.H. Telle, Laser chemistry, Vol. 2 (Harwood, New York, 1983) p. 229.

[11] H.R. Mayne, R.A. Poirier and J.C. Polanyi, J. Chem. Phys. 80 (1984) 4025.

[12] P. Siegbahn and B. Liu, J. Chem. Phys. 68 (1978) 2457.

[13] D.G. Truhlar and C.J. Horowitz, J. Chem. Phys. 68 (1978) 2466; 71 (1979) 1514 (E).

[14] R.N. Porter and L.M. Raff, in: Dynamics of molecular collisions, Part B, ed. W.H. Miller (Plenum Press, New York, 1976).

[15] H.R. Mayne, J.C. Polanyi, N. Sathyamurthy and S. Raynor, J. Phys. Chem. 88 (1984) 4064.

[16] S. Raynor and D.R. Herschbach, J. Phys. Chem. 86 (1982) 1214.

[17] V. Engel, Z. Bačić, R. Schinke and M. Shapiro, J. Chem. Phys., submitted for publication.

[18] E.A. McCullough Jr. and R.E. Wyatt, J. Chem. Phys. 51 (1969) 1253; 54 (1971) 3592.

[19] P.M. Agrawal and L.M. Raff, J. Chem. Phys. 74 (1981) 5076.

[20] D.K. Bondi, D.C. Clary, J.N.L. Connor, B.C. Garrett and D.G. Truhlar, J. Chem. Phys. 76 (1982) 4986.

APPENDIX C

Reprinted from *Current Science*, February 5, 1986, Vol. 55, No. 3, pp 115-119

TIME-DEPENDENT QUANTUM MECHANICAL APPROACH TO REACTIVE SCATTERING

V. MOHAN* and N. SATHYAMURTHY
Department of Chemistry, Indian Institute of Technology, Kanpur 208016, India.

ABSTRACT

There has been a renewed interest in the time-dependent quantum mechanical approach to reactive scattering in the last few years. The different computational methods and applications that have created such an interest are reviewed here.

1. INTRODUCTION

ALTHOUGH it was realised more than fifty years ago that, in principle, any chemical problem could be solved by an appropriate formulation of it in quantum-mechanical terms[1], in practice, developments in that direction had to await the arrival of modern electronic computers. In the early seventies one could calculate reaction probabilities (P^R) readily for exchange reactions of the type

$$A + BC \rightarrow AB + C \qquad \text{(R1)}$$

in collinear geometries by solving the time-independent Schrödinger equation for the nuclear motion, given the electronic energy (for example, see ref. 2). That exact (converged) solutions to the problem in three dimensions (3D) also could be obtained was demonstrated in 1975 when Kuppermann and Schtaz[3a, 3b] and Elkowitz and Wyatt[3c] published their results for the reaction

$$H + H_2 \rightarrow H_2 + H \qquad \text{(R2)}$$

at low energies, making full use of the symmetry of the system. There has not been any report on results of similar accuracy for any other reactive system in the past ten years. Even for the reaction (R2), some converged results have become available[4] only recently on the chemically accurate Siegbahn-Liu-Truhlar-Horowitz[5] (SLTH) potential-energy surface (PES) for the ground and the first excited vibrational states (v = 0.1) of the reactant. While some progress can be expected in the next few years, thanks to the supercomputers/parallel processors becoming available, yet the enormity of the problem remains. In a parallel development, Mazur and Rubin[6a] showed that the time-dependent Schrödinger equation (TDSE) could be solved for a reaction of the type (R1) using a model potential based on Harmuth integration scheme[6b]. McCullough and Wyatt[7] (MW) did an elaborate study in which they solved the TDSE for the reaction (R2) in collinear geometries using a realistic PES[8]. Unfortunately their approach could not be used readily for many systems as (i) the computer memory and time requirements were large (ii) the resolution of the state-to-state P^R information was poor and (iii) there was very little hope of the method being extended to three dimensions. In the last few years, however, the situation has changed dramatically. Newer methods[9,10] of solving the TDSE have become available and they are an order of magnitude faster than that one used by MW. Thus there is a renewed hope of studying 3D atom-diatom exchange reactions quantum mechanically. Also Kulander[11] and Leforestier[12] have shown that it is possible to deconvolute the average reaction probabilities ($\langle P^R \rangle$) that result from a time-dependent quantum mechanical (TDQM) study. They have also shown that the TDQM approach can be used successfully in studying collision-induced dissociation (CID) processes – an area where the time-independent approach has been carried out successfully only for a model system[32] because of the continuum

* In partial fulfilment of the requirements for the degree of Doctor of Philosophy.

problem. There are also other attractions offered by the time-dependent approach. It is analogous to classical trajectories in that a pictorial representation of the chemical reaction is possible—giving us a "feel" for the molecular collision. It has been shown[7] that flux patterns could be obtained for a chemical reaction on a PES and the whirlpools in the resulting picture can provide insight into reactive scattering resonances. Very recently we have also shown[13] that by solving the TDSE, we can construct the probability density function and predict the absorption spectrum for the transition state of the collinear reaction (R2). Gas-surface scattering problems have also been shown[14] to be amenable to solution via the TDSE. Because of the renewed interest in the area, we present here a review of the existing methodology and applications of the TDQM approach to a study of reactive scattering processes.

2. METHODOLOGY

Mazur and Rubin[6] solved the TDSE

$$H\Psi = i\hbar\frac{\partial\Psi}{\partial t}$$

by separating the real and imaginary parts in Ψ. Letting $\Psi = u + iv$, the equation becomes

$$Hu = -\hbar\frac{\partial\Psi}{\partial t}$$

$$Hv = \hbar\frac{\partial u}{\partial t}.$$

They approximated the spatial derivative in the hamiltonian and the temporal derivative by second order and first order finite differences respectively. Subsequent workers could deal with the complex wavefunction directly. Kulander[11] used a five-point finite difference formula for the spatial derivative and a fifth order predictor-corrector method for propagating the wavefunction in time. Kosloff and Kosloff[10] have shown recently that the second order spatial derivative can be evaluated by a fast fourier transform (FFT) of the wavefunction accurately. They used a second order finite difference formula for evaluating $\partial\Psi/\partial t$.

The time-evolution of the wavefunction can be expressed elegantly in terms of a time evolution operator U as

$$\Psi(t) = U\Psi(t_0)$$

with $U = \exp[-iH(t-t_0)/\hbar]$. For practical reasons, this exponential operator has to be truncated. It was represented by MW as

$$U = [1 - iH(t-t_0)/\hbar]/[1 + iH(t-t_0)/\hbar]$$

which is unitary as is the untruncated U. But using it for determining the time evolution of a chemical system, involves inverting a very large matrix. Therefore the method is computationally expensive and it requires a large computer memory. As a result it has been applied to a few systems only[15,16].

Askar and Cakmak[9] have proposed an explicit method in which U was truncated after the linear term. By combining the forward and the backward evolution operators, they could devise an algorithm which was an order of magnitude faster than the implicit method of MW.

The first order explicit-method proposed by Askar and Cakmak[9] is equivalent to the second order finite difference in time used by Kosloff and Kosloff[10]. It also turns out that the first order explicit is identical to a second order explicit method. (As a matter of fact, truncation upto an odd order in time is equivalent to truncation upto the next higher order.) Therefore, the errors are of third order. The stability criteria to be met by the choice of steps in time and space for the method have been worked out elsewhere[17a].

The above methods have been applied to different *collinear* triatomic systems. The only exception is the study of Jackson and Wyatt[14] who studied the time evolution of a *planar* H_3 system. The speed of the explicit method gives us the hope of extending it to atom-diatom exchange reactions in *three dimensions* in the very near future.

In solving the TDSE for an atom-diatom exchange reaction, the initial wavefunction is represented by a product of the eigen-function for the v^{th} vibrational state of the diatom (say, a

Morse oscillator) and a translational wavepacket which is gaussian in the momentum (k) space, centered at k_0 corresponding to the classical relative translational energy of the reactants. The width (δ) of the gaussian is chosen to be 'optimal' (= 0.25 a.u. in our studies). Such a wavefunction, when time evolved, would yield an average probability $\langle P^R \rangle$ for reaction into all the available product vibrational (v') states. If we are interested in a state (v)–selected rate coefficient at a translational temperature T, the wavepacket can be chosen accordingly[17b]. If an overall rate constant is desired, an appropriate summation over the v states can also be incorporated in the initial wavefunction. Recently, it has been shown that the $\langle P^R \rangle$ can be deconvoluted to obtain the dependence of P^R on the translational energy E_{trans} and also the product state specified reaction probability $\langle P^R \rangle_{v'}$[11, 12].

3. APPLICATIONS

3.1 *Atom-diatom exchange reactions*

By far the predominant application of the TDQM approach has been to calculate $\langle P^R \rangle$ for a variety of atom-diatom exchange reactions. MW[7] computed the $\langle P^R \rangle$ at different energies for the reaction (R2) on the Porter-Karplus[8] PES. Agrawal and Raff[17b] used the explicit method to compute rate coefficients for the reaction

$$T + HD \rightarrow TH + D \qquad (R3)$$

on a London-Eyring-Polanyi-Sato (LEPS) surface. The results were shown to be in good agreement with the time-independent results of Garrett *et al*[19]. Values of $\langle P^R \rangle$ computed[13] on the SLTH surface also have been shown to be in accord with the time-independent results[20].

Kellerhals *et al*[15] computed $\langle P^R \rangle$ for the reaction (R1) on a model LEPS surface and studied its dependence on the location of the saddle point. It became clear that $\langle P^R \rangle$ was sensitive to changes in the PES. Stroud *et al*[16] investigated the influence of v on $\langle P^R \rangle$ and its sensitivity to features of the PES for the reaction

$$He + H_2^+ \rightarrow HeH^+ + H \qquad (R4)$$

using a diatomics-in-molecules and a slightly different spline-fitted ab initio surface. Studies by Zuhrt *et al*[21] using three different PESs for the reaction

$$F + H_2 \rightarrow FH + H \qquad (R5)$$

also showed that $\langle P^R \rangle$ was strongly dependent on the topological features of the PES. Sathyamurthy *et al*[22] were able to demonstrate the utility of cubic splines to interpolation of ab initio PESs by showing that results on a splinefitted surface were identical with those obtained on the original analytic surface. Thareja and Satyamurthy[23] have recently used the TDQM approach in testing the quality of an analytic fit to the ab initio PES for the reaction (R2). When different fits were obtained for the same original ab initio surface, the fit that led to the same $\langle P^R \rangle$ as on the SLTH was taken to be the best.

In addition to yielding P^R at different levels of resolution, the time-evolution method provides a valuable insight into the detailed nature of the collision dynamics. Typical 3D perspective plots of $|\Psi|^2$ in configuration space at different time intervals give a pictorial representation of the reactants transforming into products and the resulting picture can be compared directly with a plot of a family of trajectories "Structures" in these plots reveal the complexity of the dynamics and are indicative of indirect collisions. Using the FFT algorithm, Kosloff and Kosloff[24] investigated the conditions for complex formation in $H^+ + H_2$ and its isotopic analogs for which the PES has a deep potential well in it.

From a knowledge of $\Psi(\mathbf{r}, t)$, quantal flux patterns could be drawn, in analogy with the fluid flow in classical hydrodynamics. Plots of the quantal probability flux vector

$$\mathbf{j}(\mathbf{r}, t) = \frac{\hbar}{\mu} \operatorname{Im}[\Psi^*(\mathbf{r}, t)\, \nabla \Psi(\mathbf{r}, t)]$$

were made by MW[7] and quantum whirlpools were identified. These have been investigated subsequently by Hirschfelder[25] who described them as quantized vortices around wavefunction nodes.

3.2 *Collision-induced dissociation processes*

In contrast to the formidable problems faced by the time-independent approach in studying CID processes, the time-dependent approach is applicable to the CID problem with as much ease as for the exchange reaction. Ford *et al*[26] reported the first TDQM results for the reaction of the type

$$A + BC \rightarrow A + B + C \qquad \text{(R6)}$$

using a model potential. Subsequently Kulander[11] reported the results for the reaction

$$H + H_2 \rightarrow H + H + H \qquad \text{(R7)}$$

on a LEPS surface. Leforestier *et al*[12,27,28] have studied a variety of model CID reactions over a wide range of energies. By deconvoluting $\langle P^R \rangle$to obtain the energy dependence of P^R for a CID process, they have been able to obtain information on the threshold behaviour, vibrational enhancement and inhibition and their dependence on E_{trans}. They have shed further light on the dynamical nature of CID processes by plots of $|\Psi|^2$ and **j** at different time intervals.

3.3 *Spectroscopy of the transition state*

Recently, we[13] have made use of the TDQM approach to predict the wings to the Lyman-α absorption line in $H + H_2$ collisions by obtaining the time averaged $|\Psi|^2$ values and relating them to absorption intensity. Work is in progress in using this approach in predicting the emission spectrum for the H_3^* system and spectra of transition states for a few other systems. The approach thus promises to be an effective tool in the emerging area of 'spectroscopy of the transition state'.

3.4. *Gas-surface scattering*

Atom-surface scattering plays a vital role in the investigation of solid surface properties. The rapid advancement in the recent past on the experimental side of the atom-surface encounters pose a challenge to theoretical models. Time-independent quantal calculations have not become practicable yet. Classical and semi-classical methods have been used extensively in simulating the experimental results. But they are of limited validity. For the first time Agrawal and Raff[14] showed that the time-dependent approach could be used to study gas-surface scattering by representing an incident atom by a wavepacket and using the explicit integration method for the time evolution of the system. Yinnon and Kosloff[29] have been able to compute scattering intensities, resonance strengths and other attributes using the FFT algorithm. Gerber *et al*[30] have used the same approach to study the scattering of He atom from a Cu surface with isolated Ar impurities. Kosloff and Cerjan[31] have studied the desorption and scattering of a He atom from W and Pt surfaces using the same method.

4. CONCLUDING REMARKS

The TDQM approach to reactive scattering has been receiving considerable attention, of late. It scores over the time-independent approach in that there is no need for construction of channel hamiltonians and matching of the wavefunctions. There is no increase in the complexity of the problem or the computational time requirement with an increase in the total energy of the system. As a matter of fact, there is a reduction in the computer time with an increase in energy-analogous to the classical approach. In contrast to the time-independent approach in which P^R has to be computed for different E_{trans} and v and averaged over the appropriate distributions in order to calculate state-selected and overall rate constants, the TDQM method could be made to yield them directly by a suitable choice of initial Ψ. Also, the deconvolution methods have made it possible to obtain in a single calculation P^R over a wide range of E_{trans}.

The time is not far off when the time-dependent approach could be used with much more ease than its time-independent analog in predicting rate observables for reactions in three dimensions.

ACKNOWLEDGEMENTS

This study was supported in part by a grant from the Department of Science and Technology,

New Delhi. We thank Professor C. N. R. Rao for giving us an opportunity to contribute this article.

25 June 1985

1. Dirac, P. A. M., *Proc. R. Soc.* (*London*), 1929, **123A,** 714.
2. Kouri, D. J. and Baer, M., *Chem. Phys. Lett.*, 1974, **24,** 37.
3. (a) Kuppermann, A. and Schatz, G. C., *J. Chem. Phys.*, 1975, **62,** 2502.
   (b) Schatz, G. C. and Kuppermann, A., *J. Chem. Phys.*, 1976, **65,** 4668.
   (c) Elkowitz, A. B. and Wyatt, R. E., *J. Chem. Phys.*, 1975, **62,** 2504; 1975, **63,** 702.
4. (a) Walker, R. B., Stechel, E. B. and Light, J. C., *J. Chem. Phys.*, 1978, **69,** 2922.
   (b) Schatz, G. C., (Private communication).
5. (a) Liu, B., *J. Chem. Phys.*, 1973, **58,** 1925; 1984, **80,** 581.
   (b) Siegbahn, P. and Liu, B., *J. Chem. Phys.*, 1978, **68,** 2457.
   (c) Truhlar, D. G. and Horowitz, C. T., *J. Chem. Phys.*, 1978, **68,** 2466; 1979, **71,** 1514 (E).
6. (a) Mazur, J. and Rubin, R. J., *J. Chem. Phys.*, 1959, **31,** 1395.
   (b) Harmuth, H. F., *J. Math. Phys.*, 1957, **36,** 269.
7. McCullough, E. A. and Wyatt, R. E., *J. Chem. Phys.*, 1969, **51,** 1253; 1971, **54,** 3578 and 3592.
8. Porter, R. N. and Karplus, M., *J. Chem. Phys.*, 1964, **40,** 1105.
9. Askar, A. and Cakmak, C. S., *J. Chem. Phys.*, 1978, **68,** 2794.
10. Kosloff, D. and Kosloff, R., *J. Comput. Phys.*, 1983, **52,** 35.
11. Kulander, K. C., *J. Chem. Phys.*, 1978, **69,** 5064.
12. Leforestier, C., *Chem. Phys.*, 1984, **87,** 241.
13. Agrawal, P. M., Mohan, V. and Sathyamurthy, N., *Chem. Phys. Lett.*, 1985, **114,** 343.
14. Agrawal, P. M. and Raff, L. M., *J. Chem. Phys.*, 1982, **77,** 3946.
15. Kellerhals, G. E., Sathyamurthy, N. and Raff, L. M., *J. Chem. Phys.*, 1976, **64,** 818.
16. Stroud, C., Sathyamurthy, N., Rangarajan, R. and Raff, L. M., *Chem. Phys. Lett.*, 1977, **48,** 350.
17. (a) Rubin, R. J., *J. Chem. Phys.*, 1979, **70,** 4811.
    (b) Agrawal, P. M. and Raff, L. M., *J. Chem. Phys.*, 1981, **74,** 5076.
18. Jackson, J. L., Ph.D. Thesis, The University of Texas, Austin, USA, 1971.
19. Garrett, B. C., Truhlar, D. G., Grev, R. S. and Walker, R. B., *J. Chem. Phys.*, 1980, **73,** 235.
20. Bondi, D. K., Clary, D. C., Connor, J. N. L., Garrett, B. C. and Truhlar, D. G., *J. Chem. Phys.*, 1982, **76,** 4986.
21. Zuhrt, Ch., Kamal, T. and Zülicke, L., *Chem. Phys. Lett.*, 1975, **36,** 396.
22. Sathyamurthy, N., Kellerhals, G. E. and Raff, L. M., *J. Chem. Phys.*, 1976, **64,** 2259.
23. Thareja, S. and Sathyamurthy, N., (to be published).
24. Kosloff, R. and Kosloff, D., *J. Chem. Phys.*, 1983, **79,** 1823.
25. Hirschfelder, J. O. and Tang, K. T., *J. Chem. Phys.*, 1976, **64,** 760.
26. Ford, L. W., Diestler, D. J. and Wagner, A. F., *J. Chem. Phys.*, 1975, **63,** 2019.
27. Leforestier, C., Bergeron, G. and Hiberty, P. C., *Chem. Phys. Lett.*, 1981, **84,** 385.
28. Bergeron, G., Hiberty, P. C. and Leforestier, C., *Chem. Phys.*, 1985, **93,** 253.
29. Yinnon, A. T. and Kosloff, R., *Chem. Phys. Lett.*, 1983, **102,** 216.
30. Gerber, R. B., Yinnon, A. T. and Kosloff, R., *Chem. Phys. Lett.*, 1984, **105,** 523.
31. Kosloff, R. and Cerjan, C., *J. Chem. Phys.*, 1984, **81,** 3722.
32. Kaye, J. A. and Kuppermann, A., *Chem. Phys. Lett.*, 1981, **78,** 546.